Valorization of bio-based alcohols using catalytic technology

Kumalaputri, Angela Justina

Valorization of Bio-based Alcohols using Catalytic Technology

Angela Justina Kumalaputri

Paranymphs: Dr. Idoia Hita
Dr. Sanne W. L. Palstra

The research reported in thesis was partly supported by the EDGAR research program (Energy Delta Gas Research), as a part of the AGATE (Advanced Green Gas Technology) project. The Indonesian Directorate General of Higher Education (DIKTI) is acknowledged for providing a scholarship to AJK.

Cover design: Angela Justina Kumalaputri & Stephen Surya
Layout & Printing: Lovebird design
www.lovebird-design.com
ISBN (printed version): 978-94-034-0140-9
ISBN (digital version): 978-94-034-0139-3

university of groningen

Valorization of Bio-based Alcohols using Catalytic Technology

PhD thesis

to obtain the degree of PhD at the
University of Groningen
on the authority of the
Rector Magnificus Prof. E. Sterken
and in accordance with
the decision by the College of Deans.

This thesis will be defended in public on

Friday 22 December 2017 at 14.30 hours

by

Angela Justina Kumalaputri

born on 06 February 1985
in Cirebon, Indonesië

Supervisors
Prof. H. J. Heeres
Prof. K. Barta

Co-supervisor
Dr. P. J. Deuss

Assessment Committee
Prof. A. A. Broekhuis
Prof. F. Picchioni
Prof. K. Seshan

dedicated to Papi (†) & Mami (†)

Contents

Chapter 1

Introduction

1.1 Background – Biomass-based vs fossil resources

The global demand for energy has been steadily growing in the last decades. The major drivers for this trend are a growth in global population and higher welfare levels. The main sources for primary energy generation are fossil-based ones, like coal, oil and gas, see Figure 1 for details.

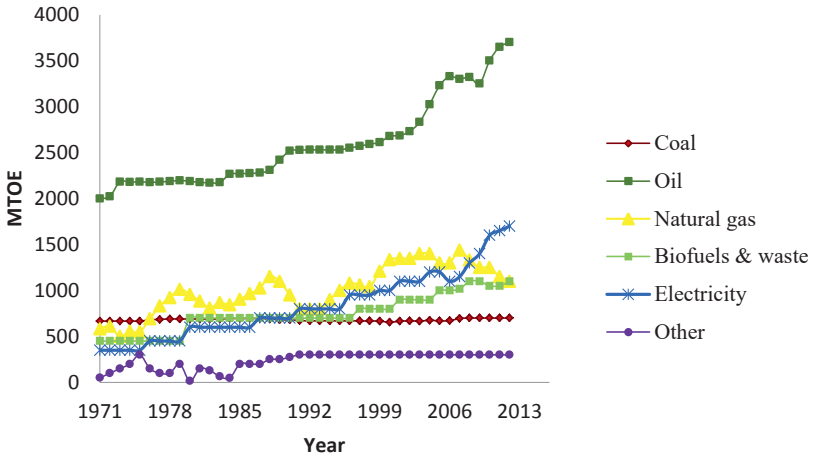

Figure 1. Total energy consumption in the world [1]

Due to the anticipated depletion of fossil resources and concerns about the environment due to CO_2 emissions, there is a huge interest in the generation of renewable energy. Examples of renewable resources are solar, wind, geothermal, hydropower and tidal energy. However, the estimated share of renewables in the total energy slate is still below 20 % (Figure 2). Biomass is expected to play a major role, for instance for heat and power generation and for the production of biofuels. However, besides conventional biomass burning for cooking and heating, the use of biomass in advanced power and heat generation and for biofuels is at the moment still limited. [2]

In the context of bioenergy, biomass refers to organic material from plants and animals. It is abundantly available on earth. About a decade ago, the steady growth in biofuels triggered a discussion whether it was ethical to use food products like wheat, soy, corn and vegetable oils for biofuels generation (food versus fuel debate). As a result, the focus has now shifted to the use of non-food biomass like

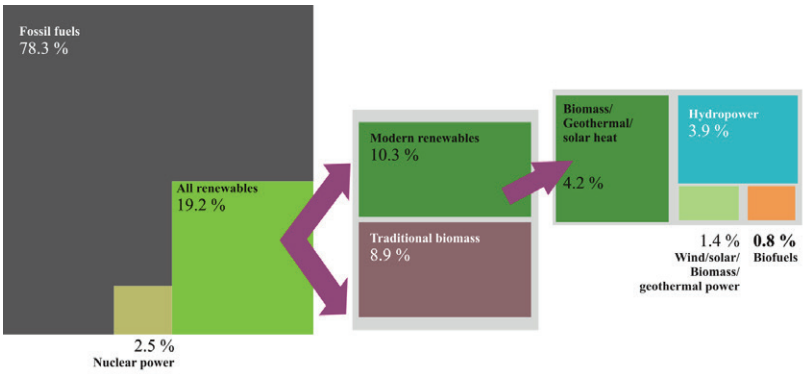

Figure 2. Estimated renewable energy share of global final energy consumption [2]

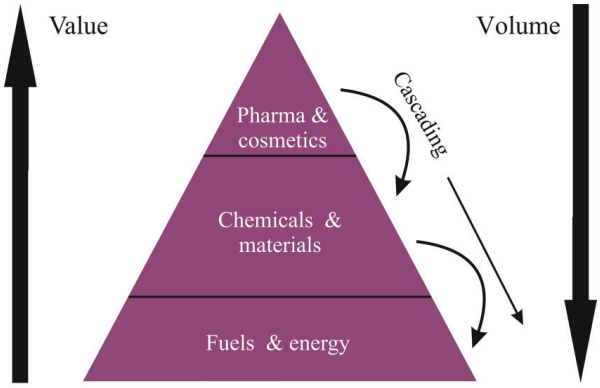

Figure 3. Bio-based product pyramid [6]

agricultural residues, residues from forestry, pulp and paper industry and municipal waste. Examples are second generation biofuels like bioethanol from lignocellulosic biomass and pyrolysis liquids. [3,4,5]

1.1.1 Biomass for chemicals

Besides the use for heat and power generation and biofuels production, biomass is expected to play an important role in the future chemical industry and particularly for the production of carbon-based products like many organic polymers (polyethylene, polypropylene and polystyrene). As the available global biomass sources are limited,

particularly when only considering non-food biomass, smart choices need to be made regarding the best possible use of biomass. To select the best option(s), the use of the so called value pyramid is useful (Figure 3). Here, the application sectors are grouped according to price and volume, with high volume-low price applications (heat and power) at the base and high value-low volume applications at the top. [6]

A highly advocated option involves the use of biomass primarily for bio-based chemicals production, rationalised by the fact that other renewable alternatives are not suitable for the production of the current carbon-based chemicals. In this scenario, by-products from bio-based chemicals production are used for energy generation.

When using biomass for bio-based chemicals production, two options may be considered, namely i) the production of existing bulk chemical products derived from fossil resources like olefins (butadiene, ethylene, propylene) and aromatics (benzene, toluene, xylene) and ii) the production of novel chemicals with high derivatization potential. The latter are also known as platform chemicals: biomass derived chemicals with a high application potential that can be produced in high yields. These platform chemicals may be viewed as the biomass-based alternatives for the base chemicals (ethylene, propylene, aromatics) in the petrochemical value chain. [6,7]

1.2 Bio-based platform chemicals

In 2004, the US Department of Energy (DOE) published a top 12 of bio-based platform chemicals, see Figure 4 for details. Initially, more than 300 compounds were selected and evaluated based on selection criteria like estimated costs of the raw materials, ease of processing, selling price, technical complexity, market potential, the possibility for direct replacement and novel properties. [7]

In 2010, an updated version was published, see Figure 5. Compared to the original list in Figure 4, ethanol, furfural, 5-hydroxymethylfurfural, isoprene and lactic acid were added and a number of organic acids (fumaric acid, malic acid, aspartic acid, glucaric acid, glutamic acid and itaconic acid) as well as 3-hydroxybutyrolactone were removed. The list was updated by considering additional criteria, such as the potential for near-term deployment, anticipated (high) market volume and value, market maturity, feedstock flexibility, the potential for integration with hydrocarbon conversion pathways, competition with natural gas-derived petrochemicals and the possibility to

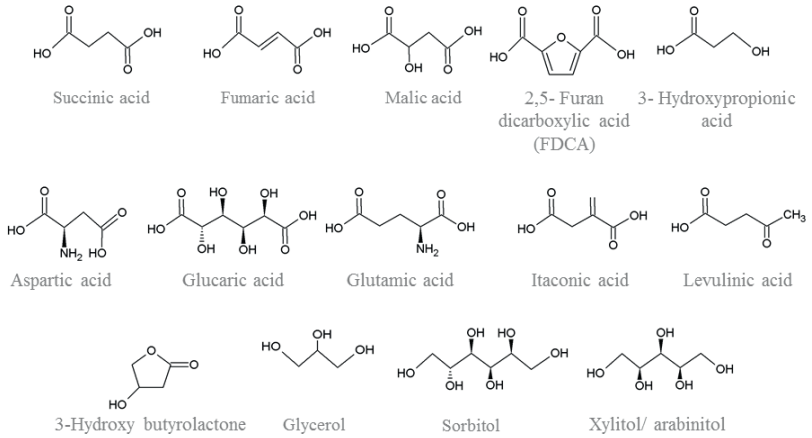

Figure 4. Top 12 sugar-derived building blocks [7]

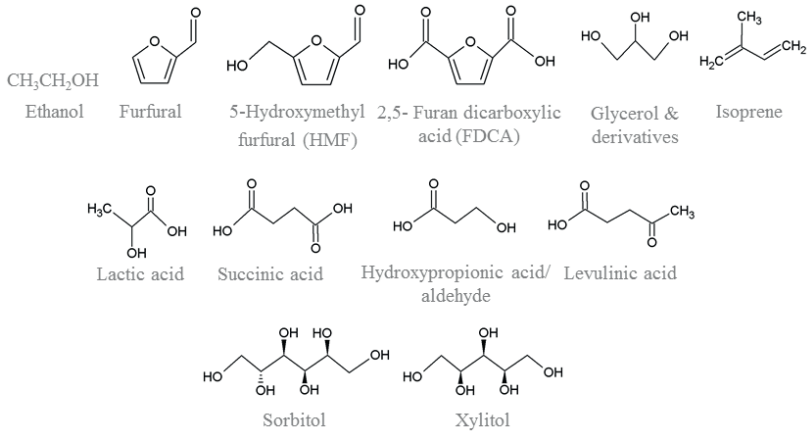

Figure 5. Top 10+4 bio-based chemicals [8]

be synthesized at a lower cost from biomass versus petroleum-based, anticipated growth, market pull and favorable life cycle analysis. [8]

Recently the National Renewable Energy Laboratory (NREL) made an updated version of the top list (see Figure 6). [9] The ranking was modified by considering additional selection criteria like the existence of extensive recent literature, multiple product applicability, possibility for direct substitution, potential market, platform potential and ease for industrial scale-up. [8] Compared to the older versions of the list, a number of the components are existing bulk chemicals derived from fossil resources and manufactured in million tons per

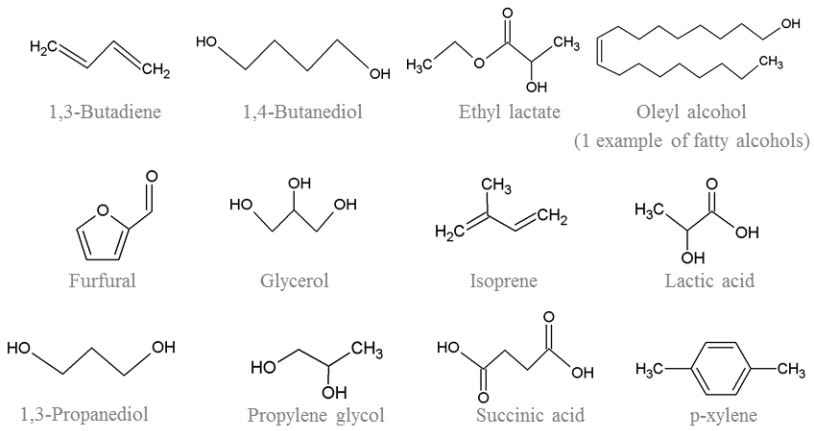

Figure 6. Updated top 12 chemical building blocks from biomass [9]

year. As such, it appears that the drop in approach is getting more attention, at the expense of new chemicals. [9]

1.3 Selected platform chemicals for study in this thesis

In this thesis, experimental studies will be reported on two main platform chemicals from biomass, HMF and glycerol, with the objective to convert them to interesting derivatives using catalytic methodology. In the case of HMF, the emphasis will be on the synthesis of reduced components like FDM, DMF as well as on the formation of BTO and for glycerol it will be on green gas. As such, this introduction will focus on the state-of-the-art regarding these transformations. Literature overviews of the various catalytic systems will be provided, reported and reviewed.

1.3.1 5-Hydroxymethylfurfural (HMF)

Lignocellulosic biomass is a good starting material for the production of C5 (xylose and arabinose) and C6 sugars (fructose, glucose, mannose and galactose). The C6 sugars can be converted into 5-hydroxymethylfurfural (HMF), a versatile furan-type compound. [10] As one of the top 10+4 bio-based chemicals, HMF is an interesting precursor for bulk chemicals to be applied for polymer synthesis, solvents and

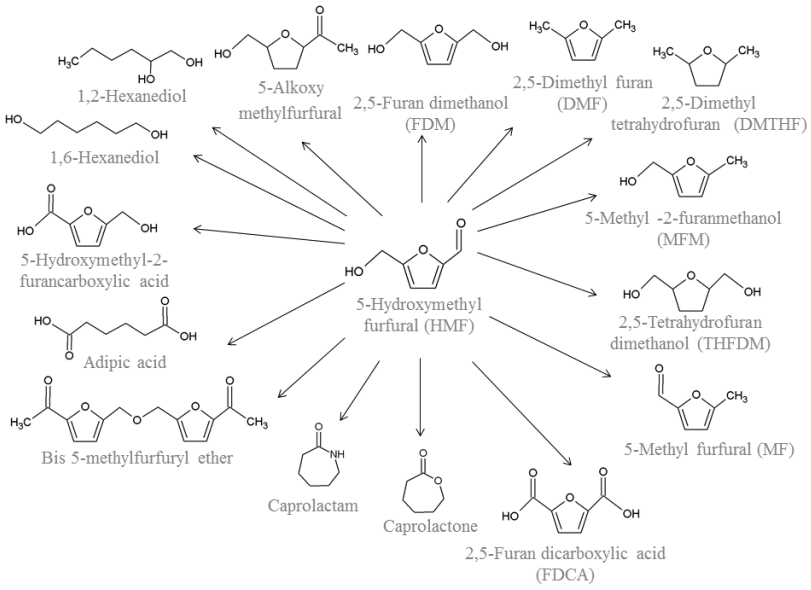

Figure 7. HMF derivatives [12,13]

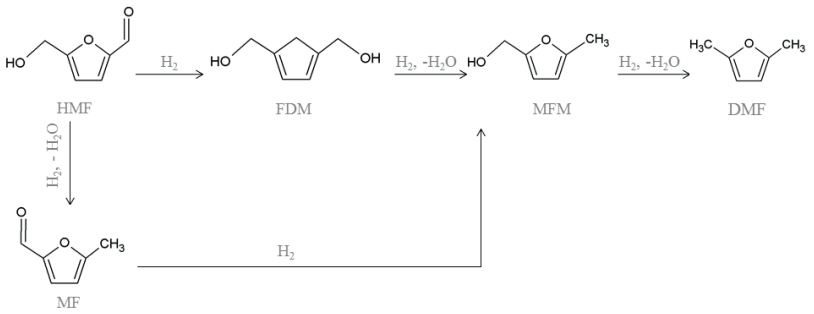

Figure 8. Possible products of HMF by reductive routes [16,17]

other interesting intermediates and pharmaceuticals. [8,11] For example, catalytic reduction of HMF allows the synthesis of 2,5-furan dimethanol (FDM), 2,5-dimethyl furan (DMF), 2,5-dimethyl tetrahydrofuran (DMTHF), 5-methyl-2-furanmethanol (MFM), 2,5-tetrahydrofuran dimethanol (THFDM) and 5-methyl furfural (MF), see Figure 7. [12,13]

HMF can also be (catalytically) oxidized to 5-hydroxymethyl-2-furancarboxylic acid (HMFCA), 2,5-diformylfuran (DFF) and 2,5-furandicarboxylic acid (FDCA). [14] The latter is being commercialized by Avantium at the moment since it is an important monomer for the

production of polyethylene furanoate (PEF), a renewable polyethylene terephthalate (PET) derivative.[15] The studies described in this thesis are among others centered around the catalytic reduction of HMF derivatives and as such the state-of-the-art regarding some of the major derivatives will be described in the following paragraphs.

1.3.2 2,5-Furandimethanol (FDM)

One of the most interesting HMF derivatives is 2,5-furan dimethanol (FDM), see Figure 7 for details. Typically, it may be obtained from HMF through catalytic reduction (Figure 8). FDM can be used as a building block for polyesters, resins, polyurethanes, and drug synthesis.[16,17] FDM can also be further hydrogenated to 2,5-tetrahydrofuran dimethanol (THFDM), which may also be used for polymer synthesis. It has been shown that THFDM can be catalytically converted to 1,6-hexanediol, which may be converted to caprolactam, the monomer for nylon-6 synthesis. Near quantitative yields of THFDM were reported by Buntara *et al.* using 10 wt % Raney-Ni catalyst at 100 °C and 90 bar H_2 pressure for 14 h. THFDM was further hydrogenated to 1,2,6-hexanetriol in high selectivity (97 % at 21 % THFDM conversion).[13]

A large number of studies have been reported on the synthesis of FDM through catalytic hydrogenation using heterogeneous (Table 1) and homogeneous catalysts (Table 2). Typically the studies are highly exploratory and batch reactors were used to assess activity and selectivity.

For the heterogeneous catalysts, molecular hydrogen was used as the reductant. Relatively mild conditions were applied, for instance temperatures between 30–160 °C and pressures between 8 and 28 bar. Mostly, supported noble metal catalysts were used (Ru, Pd, Pt) with Al_2O_3 as the most common support. Water and water/ 1-butanol were used as the solvents. Full conversion and near quantitative yields (99 %) of FDM were obtained when using Pt/MCM-41 in water at mild conditions (35 °C and pressure of 8 bar H_2)[17]. Ir-ReOx/SiO_2 also gave nearly full conversion of HMF (>99 %) and close to quantitative yields of FDM (>99 %) at 30 °C and a hydrogen pressure of 8 bar.

Three papers have been reported using continuous reactor set-ups. The use of a Raney-Co catalyst, gave full conversion of HMF and 97 % FDM yield at 60 °C and a pressure of 35 bar for a LHSV (Liquid Hourly Space Velocity) of 1 h^{-1}. A Co-based catalyst (Co/SiO_2) was tested at the same conditions using a LHSV of 4 h^{-1} and led to a full conversion of

Table 1. Overview of FDM synthesis from HMF using heterogeneous catalysts

Catalyst	Solvent	T (°C)	P H_2 (bar)	t (h)	HMF Conversion (%)	Yield of FDM (%)	Mode	Ref
Ru/CeOx	1-Butanol – water	130	28.5	2	100	81	Batch	19
Ru/Mg-Zr	1-Butanol – water	130	28.5	2	100	93	Batch	19
Ru/γ-Alumina	1-Butanol – water	130	28.5	2	92	75	Batch	19
Pd/Al_2O_3	Water	140	38	4	100	20	Batch	20
Ag/Al_2O_3	Water	140	38	4	5	5	Batch	20
Ir-ReOx/SiO_2 -1	Water	30	8	6	>99	>99	Batch	21
Pt/MCM-41	Water	35	8	2	100	99	Batch	17
Pt/Al_2O_3	Water	130–160	38	4	100	0	Batch	20
Cu/Al_2O_3	Water	140	38	4	0	0	Batch	20
Pt/Al_2O_3	Water	60	35	2	94	92	Continuous	18
Co/SiO_2	Water	60	35	4[a]	100	96	Continuous	18
Raney/Co	Water	60	35	1[a]	100	97	Continuous	18

[a]LHSV in h^{-1}

Table 2. Overview of FDM synthesis from HMF using homogeneous catalysts [a,b]

Catalyst	Solvent	T (°C)	P H_2 (bar)	t (h)	HMF Conversion (%)	Yield of FDM (%)	Mode	Ref
Ru(TsDPEN-H)	Methanol	40	-	2	n.d.	99	Batch	14
Cp*Ir (TsDPEN-H)	THF	40	-	2	100	99	Batch	14
Cp*Ir ($NHCPh_2C_6H_4$)	Methanol)	40	-	1	90	99	Batch	14
Cp*Ir (TsDACH)	Methanol	40	-	1	83	99	Batch	14
Cp*Ir (TsDPEN-H)	Methanol	40	-	16	80	99	Batch	14

[a] TsDPEN=H2NCHPhCHPhNTs; Cp*=C_5Me_5; Ts=tosyl; [b] Formic acid as the hydrogen donor

HMF and a FDM yield of 96 %. At about similar reaction conditions (60 °C, 35 bar, LHSV of 2 h^{-1}), Pt/Al_2O_3 resulted in a slightly lower HMF conversion (94 %) and FDM yield (92 %). [18]

The use of homogeneous catalysts for FDM synthesis has received by far less attention compared to the heterogeneous analogues. Cp*Ir catalysts have been investigated in detail using formic acid as the hydrogen donor and methanol or THF as the solvent. Good results were obtained at mild conditions (100 % HMF conversion and 99 % FDM yield) of 40 °C for 2 h in a batch reactor, which is similar to the data reported for the heterogenous Pt/MCM-41 catalyst. [14]

1.3.3 2,5-Dimethylfuran (DMF)

2,5-dimethylfuran (DMF) is attainable from HMF by a catalytic hydrodeoxygenation route (Figure. 8). DMF has been identified as a second generation biofuel/biofuel additive as it has a 40 % higher energy density than ethanol (31.5 MJ/L vs 23 MJ/L), which is actually close to that of gasoline (35 MJ/L). Compared to ethanol, DMF is immiscible with water, which is a major advantage when using it for blending in gasoline. DMF has a high octane number (RON=119) and a higher boiling point compared to ethanol (92 °C vs 78 °C).[4,22,23]

A number of catalytic hydro(deoxy)genation systems have been developed (Table 3). Most of them use hydrogen as the reductant, though the use of an alternative hydrogen donor in the form of formic acid has also been reported. Typically, the catalytic hydrodeoxygenation reaction is carried out in a temperature range between 70–280 °C, though most studies are reported in the 180–220 °C range. In by far

Table 3. Overview of DMF synthesis from HMF

Catalyst	Solvent	T (°C)	P H_2 (bar)	t (h)	Conversion of HMF (%)	Yield of DMF (%)	Mode	Ref
Ru/C	2-Propanol [a]	190	n.d.	6	100	80	Batch	25
Ru/C	THF [a]	190	n.d.	6	92	60	Batch	25
Ru/C	Isopropanol [a]	190	n.d.	6	100	81	Batch	25
Ru/C	1-Butanol	260	n.d.	1.5	100	60	Batch	26
Ru/Co_3O_4	THF	130	7	24	>99	93	Batch	27
Pd	Ethanol [b]	140	-	21	>99	16	Batch	28
Pd/C	Water-SC CO_2	80	100 (CO_2)	2	100	100	Batch	17
Pd/C	EMIMCl and acetonitrile	120	62	1	47	15	Batch	23
Pd/C	THF [c]	70	-	15	100	>95	Batch	14
Pd/C	Dioxane [b]	120	-	15	n.d.	>95	Batch	29
PtCo/AC & PtCo/GC	1-Butanol	180	10	2	100	98	Batch	24
CuRu/C	1-Butanol [d]	220	6.8	10	100	71	Batch	22
CuRu/C	1-Butanol	220	6.8	10	n.d.	49	Batch	30
$CuCrO_4$	1-Butanol [d]	220	6.8	10	100	61	Batch	22
$CuCrO_4$	1-Butanol	220	6.8	n.d.	100	61	Batch	22
Cu–PMO	Methanol	260	n.d.	3	100	48	Batch	31
Ni–W carbide	THF	180	40	3	100	96	Batch	32
RaNi	1,4-Dioxane	180	15	15	100	89	Batch	33
Pd/Fe_2O_3	2-Propanol	180	25	5/12[e]	100	72	Continuous	34
CuRu/C	1-Butanol	220	17	2[e]	100	79	Continuous	22

[a] 20 bar N_2 [b] plus formic acid [c] plus formic acid and H_2SO_4 [d] plus NaCl [e] residence time

the most cases, supported noble metal catalysts are used (Ru, Pd, Pt), either as a monometallic catalyst or in combination with a second metal (e.g. Cu). The most used support is carbon. A wide range of polar organics solvents have been explored, mainly in the form of low carbon alcohols, likely due to the good solubility of the substrate-product in these solvents. Most experiments were carried out in batch reactor set-ups, and only two papers reported the use of a continuous reactor.

HMF conversions in batch are typically close to quantitative, with DMF yields ranging from 15 to close to quantitative. Best results were obtained using a Pd/C catalyst in THF and dioxane (>95 % DMF yield) and bimetallic Pt catalysts (PtCo/AC and PtCo/GC) in 1-butanol (100 % HMF conversion and 98 % DMF yield).[24] A recent interesting finding involves the use of supercritical CO_2 in combination with water. Near quantitative yields of DMF were reported in batch using Pd/C (80 °C and 100 bar CO_2 for 2 h).[17]

1.3.4 1,2,4-Benzenetriol (BTO)

A 'forgotten' derivative from HMF is 1,2,4-benzenetriol (BTO). It has been reported as a byproduct in several studies on particularly HMF conversions in water and has potentially interesting applications such as the use as precursor for pharmaceuticals and agrochemicals.[16,35] BTO is typically formed from HMF at relatively harsh conditions (e.g. sub- and supercritical water).[36–45] A reaction mechanism has been proposed involving the hydrolysis of the HMF furan ring, followed by an electrolytic rearrangement to hexatriene and further dehydration to form BTO (Figure 9).[36,37]

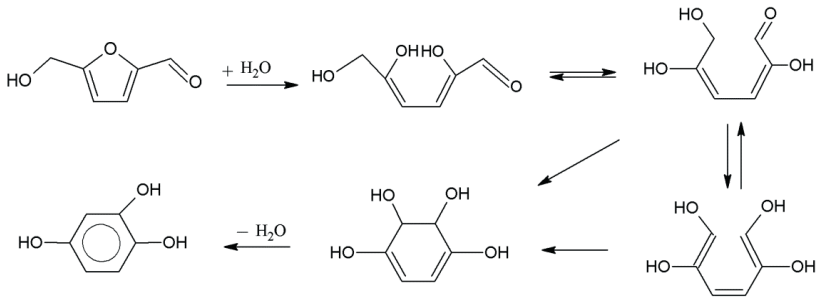

Figure 9. Proposed mechanism of BTO formation from HMF[36,37]

A limited number of studies have been reported for BTO synthesis (Table 4). Several substrates were tested including D-fructose, D-glucose, HMF and cellulose, though the reported BTO yields are generally low (max. 25 %). Best results, *viz*. 25 % BTO yield at 50 % HMF conversion were obtained using an aqueous HMF (0.05 M) solution as the substrate, without any catalysts, at temperatures between 300 and 350 °C and a pressure of 280 bar using a residence time of 250 s in a continuous setup. [36,37]

Table 4. Overview of studies for BTO production from (monomeric) C6 sugars and HMF

Feed	T (°C)	P (bar)	t (s)	Yield of BTO	Mode	Ref
Cellulose	250	n.d	1800	n.d.	Batch	42
D-glucose	300–400	250	70	4	Batch	41
HMF	175–350	250	80–400	n.d.	Batch	41
HMF	350–450	250	0–3000	5	Batch	43
D-fructose	330	280	185	9	Continuous	36, 37
D-glucose	340	275	25–204	6	Continuous	39
D-glucose	350–400	400	0.2–1.5	6	Continuous	40
HMF	330 & 350	280	250[a]	25	Continuous	36, 37

[a] residence time

1.3.5 Glycerol

Glycerol is mentioned in all versions of the published top bio-based chemicals. [7,8,9] Glycerol is an excellent building block for 1,3-propanediol, epichlorohydrin, hydrogen, methanol and mixtures of di- and tri-isobutyl ethers. [46] A well-known example is the large scale production of epichlorohydrin from glycerol by Solvay (Epicerol process), which can be used for the production of epoxy resins, paper chemicals, surfactants, elastomers and chemicals for water treatment. [47] Besides, glycerol may also be used for syngas generation and the synthesis of green methane.

Glycerol is the main byproduct of biodiesel production and generated in about 10 wt % on plant-oil intake. The amount of glycerol is expected to grow substantially in the future due to the anticipated growth of the global biodiesel industry (Figure 10). [18,19]

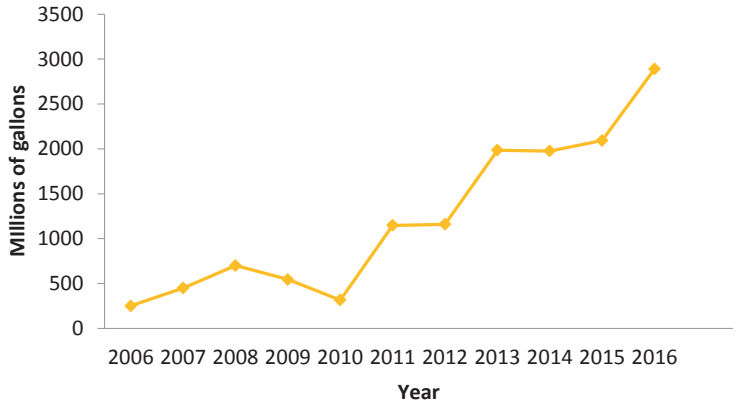

Figure 10. Biodiesel production in the US [50]

1.3.6 Glycerol conversion to methane (green gas)

Glycerol reforming to methane has been studied in detail in the last decade. It involves the treatment of glycerol in combination with a suitable catalyst at elevated temperatures and pressures, often in sub- and supercritical water. Several reactions appear to be involved, including dehydration and dehydrogenation reactions (Figure 11). [51]

Typically, the reactions produce limited amounts of methane. Methane formation can be enhanced by using suitable catalysts, particularly those which are active for the hydrogenation of CO and CO_2 (eq 1–2):

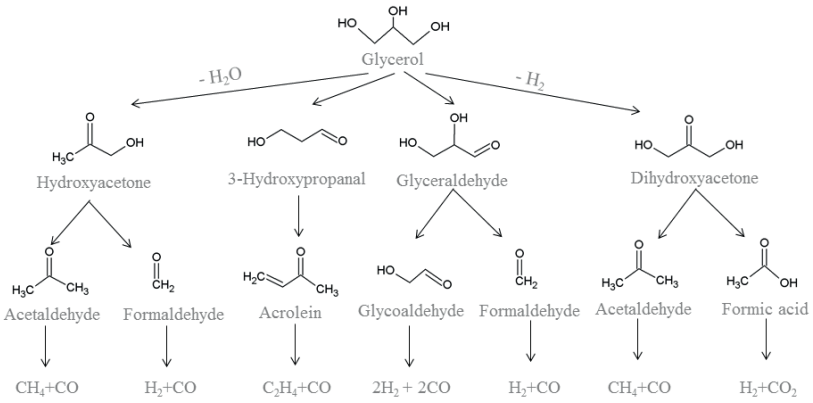

Figure 11. Mechanism of glycerol gasification by dehydrogenation and dehydration reactions [51]

$CO + 3H_2 \leftrightarrow CH_4 + H_2O$ $\Delta H^\circ = -206.18\,kJ/mol$ (1)

$CO_2 + 4H_2 \leftrightarrow CH_4 + 2H_2O$ $\Delta H^\circ = -165.01\,kJ/mol$ (2)

A number of secondary gas phase reactions need to be considered as they may alter the composition of the produced gas. These include the water gas shift reaction and methane reforming (equation 3–4):[52]

$CO + H_2O \leftrightarrow CO_2 + H_2$ $\Delta H^\circ = -41.17\,kJ/mol$ (3)

$CH_4 + H_2O \leftrightarrow CO + 3\,H_2$ $\Delta H^\circ = +206.18\,kJ/mol$ (4)

An additional reaction to be considered is the Boudouard reaction (eq 5):

$2CO \leftrightarrow CO_2 + C(s)$ $\Delta H^\circ = -172.43\,kJ/mol$ (5)

All reactions are equilibrium limited and thus the composition of the gas phase after reaction will be determined by the temperature and pressure. Low temperatures are favoured to enhance methane formation and to reduce coke formation.

Typically glycerol reforming in water is performed at relatively high temperatures (230–800 °C) and pressures (240–350 bar), though some research has been performed at lower pressures (20–32 bar), see Table 5 for details. Typically supported methanation catalysts were used, such as Ru, Ni and Pt on various supports (TiO_2, Al_2O_3, C, ZrO_2 and SiO_2) both in batch and continuous set-ups. In some cases, only the supports (C and TiO_2) were tested. Catalytic reactor wall effects (e.g. Inconel and Hasteloy) were explored by Kersten and Rossum.[53,54]

When using batch systems, the reported CH_4 yields are relatively low (only 7–20 %), see first entries of Table 5. In a continuous set-up (see Table 5), a methane yield of 58 % was obtained at 400 °C and a pressure of 300 bar for residence times between 7–20 s using a Ru/C catalyst and relatively high substrate concentrations (20 wt % glycerol).[55]

1.4 Thesis outline

In this thesis, experimental studies are reported with a focus on the conversion of two important bio-based platform alcohols, *viz.* HMF and glycerol, to interesting derivatives with high application potential. For HMF, the emphasis was on the selective reduction to FDM

Table 5. Overview of studies on glycerol reforming in SCWG using heterogenous catalysts

Catalyst	Glycerol (wt %)	Temp. (°C)	P (bar)	Mode	Reaction/ residence time (s)	Results (mol %)	Ref.
Ru/TiO_2	10	600	n.d.	Batch	n.d.	Conversion: n.d. Gas composition: H_2:22; CH_4:12	53
Ru/TiO_2	17–19	550–700	250	Batch	60	Conversion: 45–90 Gas composition: H_2:8–15; CO_2:8–16; CO:30–65; CH_4:7–20	54
Ru/C	20	400	300	Continuous	7–20	Conversion: n.d.. Gas composition: H_2:0–2; CO:0; CO_2:40–42; CH_4:56–58	55
Ru/ZrO_2	5	510–550	350	Continuous	8.5	Conversion: 100 Gas composition: H_2:4–55, CO:≤21; CO_2:≤40; CH_4:≤	56
$Ru/\gamma\text{-}Al_2O_3$	2.5–40	700–800	241	Continuous	1–4	Conversion: 93–98 Gas composition: H_2:42–70 CO:0–4 CO_2:25–35 CH_4:4–20	57
Ni/Al_2O_3	10	230	32	Continuous	2400–14400	Conversion: n.d. Gas composition: H_2:41–95; CO_2:6–24; CO:≤0.05; CH_4:≤16	58
Ni/TiO_2 Ni/ZrO_2	10	500–650	n.d.	Continuous	18000–72000	Conversion: <10–72 Gas composition: H_2: <5–65	59
Ni/TiO_2 Ni/SiO_2 Ni/ZrO_2	n.d.	650		Continuous	18000–72000	Conversion: 71–100 Gas composition: CO:7–44; CO_2:53–94; CH_4:≤3	60
$Ni/CaO\text{-}6Al_2O_3$	3–10	675–725	240–270	Continuous	30–35	Conversion: 95–100 Gas composition: H_2:44–67; CO:1–21; CO_2:16–34	61
TiO_2, WO_3/TiO_2	0.46	400	330	Continuous	n.d.	Conversion: >99 Gas composition: n.d. (focus on liquid products)	62

[a]n.d. = not determined or not reported

and DMF and the synthesis of BTO. For glycerol, the product aimed for was green gas (Figure 12). The overall objectives were to improve the product yields by selection and screening of suitable catalysts and to optimize process conditions. In addition, the conversions were preferably carried out using environmentally benign solvents like water and ethanol.

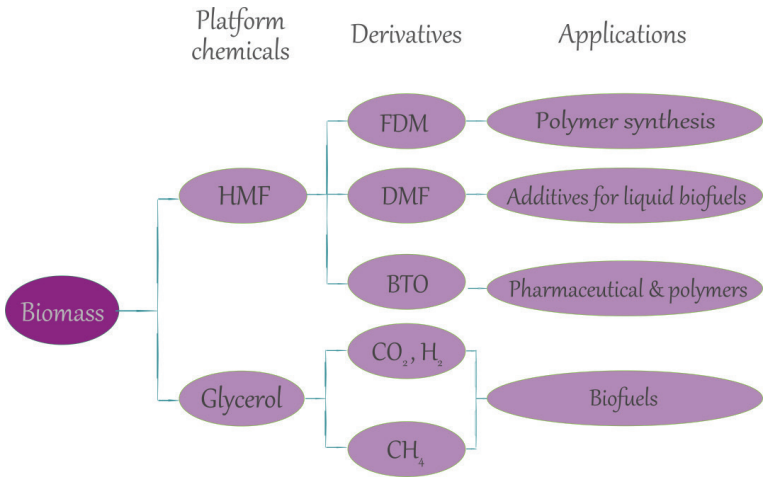

Figure 12. Overview of thesis content

In **Chapter 2**, the synthesis, characterization and screening of noble-metal-free catalysts and novel copper-doped porous metal oxides (PMOs) with a very low Ru loading for the synthesis of FDM from HMF are reported in a batch reactor set-up. Process conditions (temperature, pressure, solvents) were optimized to maximize HMF conversion and FDM yield. Intermediate products were identified and a reaction network is proposed. The stability of the catalysts was investigated by performing a number of recycling experiments.

In **Chapter 3,** the use of nanopowder copper-based catalysts is reported for the hydrogenation of HMF to DMF in batch reactor set-up. Operation conditions were optimized and various alcohol-based solvents were tested to optimize the HMF conversion and the DMF yield. Recycling studies were performed to determine the stability of the nanopowder catalysts. Besides the use of HMF as the starting material, studies were performed to synthesize FDM directly from fructose in a one pot reaction.

In **Chapter 4**, experimental studies are described on the synthesis of BTO from HMF using Lewis and Brønsted acid catalysts in a batch set-up. Particular attention was given to byproduct formation and particularly the formation of higher molecular weight products. For the best catalyst, a range of process conditions was tested to improve the BTO yield. Finally, the use of BTO as a precursor for cyclohexanone/cyclohexanol, an important feedstock for caprolactam synthesis, was investigated using a hydrogenation approach.

In **Chapter 5**, systematic experimental studies on the reforming of glycerol in supercritical water to methane was investigated in a batch set-up using supported monometallic Ni and Ru catalysts and bimetallic Ni-Ru catalysts. The catalysts were characterized in detail and process conditions were optimized to maximize CH_4 yield. Catalyst stability was assessed for the best catalyst and changes in morphology and structure of the catalyst during the reaction were investigated.

References

[1] F. Birol, Key world energy statistics 2016, International Energy Agency (IEA), Paris, 2016.

[2] REN21 Steering Committee, Renewables 2016 global status report, Renewable Energy Policy Network REN21 Secretariat for the 21st Century, Paris, 2016.

[3] P. Basu, Biomass gasification and pyrolysis practical design and theory, Elsevier, U. S., 2009.

[4] H. Balat and E. Kırtay, Hydrogen from biomass-present scenario and future prospects, Int. J. Hydrogen Energy 35 (2010) 7416–7426.

[5] M. Naqvia, J. Yana, E. Dahlquistb, S. R. Naqvi, Waste biomass gasification based off-grid electricity generation: A case study in Pakistan, Energy Procedia 103 (2016) 103, 406–412.

[6] M. W. Vis, P. Reumerman, S. Gärtner, Cascading in the wood sector 1741, BTG Biomass Technology Group B.V., http://www.btgworld.com/nl/nieuws/cascading-wood-sectorfinal-report-btg.pdf, Accessed online: May 24th 2017.

[7] T. Werpy and G. Petersen, Top value added chemicals from biomass volume I: Results of screening for potential candidates from sugars and synthesis gas. U. S. Department of Energy (DOE) by the Pacific Northwest National Laboratory (PNNL) and National Renewable Energy Laboratory (NREL) a DOE National Laboratory, Oak Ridge, TN, 2004.

[8] J. J. Bozell, Technology development for the production of bio-based products from biorefinery carbohydrates-The US Department Energy's 'Top 10' revisited, Green Chemistry 12 (2010) 539–554.

[9] M. J. Biddy, C. Scarlata and C. Kinchin, Chemicals from biomass: A market assessment of bioproducts with near-term potential, National Renewable Energy Laboratory (NREL), US, 2016.

[10] F. H. Isikgor and C. R. Becer, Lignocellulosic biomass: a sustainable platform for the production of bio-based chemicals and polymers, **Polym. Chem.** 6 (2015) 4497–4559.

[11] X. Tong, Y. Ma, Yong and Li, Biomass into chemicals: Conversion of sugars to furan derivatives by catalytic processes, Applied Catalysis A: General 385 (2010) 1–13.

[12] R. J. van Putten, J. C. van der Waal, E. de Jong, C. B. Rasrendra, H. J. Heeres and J. G. de Vries, Hydroxymethylfurfural, a versatile platform chemical made from renewable resources, *Chem. Rev.* 113 (2013) 1499–1597.

[13] T. Buntara, S. Noel, P. H. Phua, I. M. Cabrera, J. G. de Vries, H. J. Heeres, Caprolactam from renewable resources: Catalytic conversion of 5-hydroxymethylfurfural into caprolactone, Angewandte 50 (2011) 7083–7087.

[14] T. Thananatthanachon and T. B. Rauchfuss, efficient route to hydroxymethylfurans from sugars via transfer hydrogenation, ChemSusChem 3 (2010) 1139 – 1141.

[15] Avantium, Products & apllications, https://www.avantium.com/yxy/products-applications/, Accessed online: July 20th, 2017.

[16] A. A. Rosatella, S. P. Simeonov, R. F. M. Frade and C. A. M. Afonso, 5-Hydroxymethylfurfural (HMF) as a building block platform: Biological properties, synthesis and synthetic applications, Green Chem 13 (2011) 754–793.

[17] M. Chatterjee, T. Ishizaka and H. Kawanami, Selective hydrogenation of 5-hydroxymethylfurfural to 2,5-bis-(hydroxymethyl)furan using Pt/MCM-41 in an aqueous medium: a simple approach, Green Chem. 16 (2014) 4734–4739.

[18] M. A. Lilga, R. T. Hallen, T. A. Werpy, J. F. White, J. E. Holladay, J. G. Frye JR., A. H. Zacher (Battelle Memorial Institute), Hydroxymethylfurfural reduction methods and methods of producing furandimethanol, US Patent 2007287845 (2007).

[19] R. Alamillo, M. Tucker, M. Chia, Y. P. Torres and J. Dumesic, The selective hydrogenation of biomass-derived 5-hydroxymethylfurfural using heterogeneous catalysts, Green Chem. 14 (2012) 1413–1419.

[20] J. Ohyama, A. Esaki, Y. Yamamoto, S. Arai and A. Satsuma, Selective hydrogenation of 2-hydroxymethyl-5-furfural to 2,5 bis(hydroxymethyl) furan over gold sub-nano clusters, RSC Adv. 3 (2013) 1033–1036.

[21] M. Tamura, K. Tokonami, Y. Nakagawa and K. Tomishige, Rapid synthesis of unsaturated alcohols under mild conditions by highly selective hydrogenation, Chem. Commun. 49 (2013) 7034—7036.

[22] Y. R. Leshkov, C. J. Barrett, Z. Y. Liu, J. A. Dumesic, Production of dimethylfuran for liquid fuels from biomass-derived carbohydrates, Nature 447 (2007) 982– 986.

[23] M. Chidambaram and A. T. Bell, A two-step approach for the catalytic conversion of glucose to 2,5-dimethylfuran in ionic liquids, Green Chem. 12 (2010) 1253–1262.

[24] G. H. Wang, J. Hilgert, F. H. Richter, F. Wang, H. J. Bongard, B. Spliethoff, C. Weidenthaler and F. Schüth, Platinum–cobalt bimetallic nanoparticles in hollow carbon nanospheres for hydrogenolysis of 5-hydroxymethylfurfural, Nature Materials 13 (2014) 293–300.

[25] J. Jae, W. Zheng, R. F. Lobo and D. G. Vlachos, Production of dimethylfuran from hydroxymethylfurfural through catalytic transfer hydrogenation with Ru supported on carbon, ChemSusChem 6 (2013) 1158 – 1162.

[26] J. Zhang, L. Lin and S. Liu, Efficient production of furan derivatives from a sugar mixture by catalytic process, Energy Fuels 26 (2012) 4560–4567.

[27] Y. Zu, P. Yang, J. Wang, X. Liu, J. Ren, G. Lu, Y. Wang, Efficient production of the liquid fuel 2,5-dimethylfuran from 5-hydroxymethylfurfural over Ru/Co_3O_4 catalyst, Applied Catalysis B: Environmental 146 (2014) 244–248.

[28] J. Tuteja, H. Choudhary, S. Nishimura and K. Ebitani, Direct synthesis of 1,6-hexanediol from HMF over a heterogeneous Pd/ZrP catalyst using formic acid as hydrogen source, ChemSusChem 7 (2014) 96–100.

[29] J. Mitra, X. Zhou and T. Rauchfuss, Pd/C-catalyzed reactions of HMF: Decarbonylation, hydrogenation, and hydrogenolysis, Green Chem. 17 (2015), 307–313.

[30] J. B. Binder, R. T. Raines, Simple chemical transformation of lignocellulosic biomass into furans for fuels and chemicals, J. Am. Chem. Soc. 131 (2009) 1979–1985.

[31] T. S. Hansen, K. Barta, P. T. Anastas, P. C. Ford and A. Riisager, One-pot reduction of 5-hydroxymethylfurfural via hydrogen transfer from supercritical methanol, Green Chem. 14 (2012) 2457–2461.

[32] Y. B. Huang, M. Y. Chen, L. Yan, Q. X. Guo and Y. Fu, Ni–tungsten carbide catalysts for the production of 2,5-dimethylfuran from biomass-derived molecules, ChemSusChem 7 (2014) 1068–1070.

[33] X. Kong, Y. Zhu, H. Zheng, F. Dong, Y. Zhu and Y. W. Li, Switchable synthesis of 2,5-dimethylfuran and 2,5-dihydroxymethyltetrahydrofuran from 5-hydroxymethylfurfural over Raney Ni catalyst, RSC Adv. 4 (2014) 60467–60472.

[34] D. Scholz, C. Aellig and I. Hermans, Catalytic transfer hydrogenation/hydrogenolysis for reductive upgrading of furfural and 5-(hydroxymethyl) furfural, ChemSusChem 7 (2014) 268–275.

[35] A. Suzuki, A. Fujii, H. Jokura, I. Tokimitsu, T. Hase and I. Saito, Hydroxyhydroquinone interferes with the chlorogenic acid-induced restoration of endothelial function in spontaneously hypertensive rats, American Journal of Hypertension 21 (2008) 24–27.

[36] G. C. A. Luijkx, F. van Rantwijk, H. van Bekkum, Formation of 1,2,4-benzenetriol by hydrothermal treatment of carbohydrates, Recueil des Travaux des Pays-Mas 110 (1991) 343–344.

[37] G. C. A. Luijkx, F. van Rantwijk, H. van Bekkum, Hydrothermal formation of 1,2,4-benzenetriol from 5-hydroxymethyl-2-furaldehyde and D-fructose, Carbohydrate Research 242 (1993) 131–139.

[38] S. Rieble, D. K. Joshi, M. H. Gold, Purification and characterization of a 1, 2, 4-trihydroxybenzene 1, 2-dioxygenase from the basidiomycete *Phanerochaete chrysosporium*, Journal of Bacteriology *176* (1994) 4838–4844.

[39] Z. Srokol, A. G. Bouche, A. van Estrik, R. C. J. Strik, T. Maschmeyer and J. A. Peters, Hydrothermal upgrading of biomass to biofuel: Studies on some monosaccharide model compounds, J. Carbohydrate Research 339 (2004) 1717–1726.

[40] T. M. Aida, Y. Sato, M. Watanabe, K. Tajima, T. Nonaka, H. Hattori and K. Arai, Dehydration of D-glucose in high temperature water at pressures up to 80 Mpa, J. of Supercritical Fluids 440 (2007) 381–388.

[41] A. Chuntanapum, T. L. K Yong, S. Miyake and Y. Matsumura, Behaviour of 5-HMF in subcritical and supercritical water, Ind. Eng. Chem. Res. 47 (2008) 2956–2962.

[42] L. U Huisheng, L. Xiangke, Z. Minhua, Decomposition of cellulose to produce 5-hydroxymethyl-furaldehyde in subcritical water, Transaction of Tianjin University 14 (2008) 198–201.

[43] A. Chuntanapum and Y. Matsumura, Formation of tarry material from 5-HMF in subcritical and supercritical water, Ind. Eng. Chem. Res. 48 (2009) 9837–9846.

[44] A. Chuntanapum and Y. Matsumura, Char formation mechanism in supercritical water gasification process: A study of model compound, Ind. Eng. Chem. Res. 49 (2010) 4055–4062.

[45] Material Safety Data Sheet 1,2,4-Benzenetriol, 99%, https://fscimage.fishersci.com/msds/56075.htm, Accessed online January 3, 2017.

[46] T. Z. D. de Mes, A. J. M. Stams, J. H. Reith, G. Zeeman, Methane production by anaerobic digestion of wastewater and solid wastes, bio-methane & bio-hydrogen: Status and perspectives of biological methane and hydrogen production, Petten: Dutch Biological Hydrogen Foundation–Petten (2003) 58–102.

[47] Epicerol, http://www.solvay.com/en/markets-and-products/featured-products/epicerol.html, Accessed online at July 20th, 2017.

[48] M. Pagliaro, R. Ciriminna, H. Kimura, M. Rossi, C. Della Pina, From glycerol to value-added products, Angewadnte Chemie International 46 (2007) 4434–4440.

[49] Team of ENI (Ente Nazionale Idrocarburi), World oil & gas review 2012, https://www.eni.com/docs/en_IT/enicom/publicationsarchive/publications/wogr/2012/wogr-2012_completo.pdf, Accessed online at May 24th, 2017.

[50] Biodiesel, http://biodiesel.org/production/production-statistics, Accessed online: July 20th, 2017.

[51] M. J. Antal Jr., W. S. L. Mok, J. C. Roy, A. T. Raissi, Pyrolytic sources of hydrocarbons from biomass, Journal of Analytical and Applied Pyrolysis 8 (1985) 291–303.

[52] F. J. G. Ortiz; A. Serrera; S. Galera; P. Ollero, Experimental study of the supercritical water reforming of glycerol without the addition of a catalyst, Energy 56 (2013) 193–206.

[53] G. V. Rossum, B. Potic, S. R. A. Kersten, W. P. M. Van Swaaij, Catalytic gasification of dry and wet biomass, Catalysis Today 145 (2009) 10–18.

[54] S. R. A. Kersten, B. Potic, W. Prins, W. P. M. Van Swaaij, Gasification of model compounds and wood in hot compressed water, Industrial and Engineering Chemistry Research 45 (2006) 4169–4177.

[55] M. Schubert, Catalytic hydrothermal gasification of biomass–salt recovery and continuous gasification of glycerol solutions, PhD Thesis, ETH, Zürich (2010).

[56] A. May, J. Salvadó, C. Torras, D. Montané, Catalytic gasification of glycerol in supercritical water, Chemical Engineering Journal 160 (2010) 751–759.

[57] A. J. Byrd, K. K. Pant, R. B. Gupta, Hydrogen production from glycerol by reforming in supercritical water over Ru/Al_2O_3 catalyst, Fuel 87 (2008) 2956–2960.

[58] G. D. Wen, Y. P. Xu, H. J. Ma, Z. S. Xu, Z. J. Tian, Production of hydrogen by aqueous-phase reforming of glycerol, International Journal Hydro Energy 33 (2008) 6657–6666.

[59] V. Nichele, M. Signoretto, F. Menegazzo, A. Gallo, V. Dal Santo, G. Cruciani, G. Cerrato, Glycerol steam reforming for hydrogen production: Design of Ni supported catalyst, Applied Catalysis B: Environmental 111–112 (2012) 225–232.

[60] I. Rosetti, A. Gallo, V. Dal Santo, C. L. Bianchi, V. Nichele, M. Signoretto, E. Finocchio, G. Ramis, A. Di Michele, Ni catalysts supported over TiO_2, SiO_2 and ZrO_2 for the steam reforming of glycerol, ChemCatChem 5 (2013) 294–306.

[61] J. G. van Bennekom, R. H. Venderbosch, D. Assink, K. P. J. Lemmens, H. J. Heeres, Bench scale demonstration of the supermethanol concept: the synthesis of methanol from glycerol derived syngas, Chemical Engineering Journal 207 (2012) 245–253.

[62] M. Akizuki and Y. Oshima, Kinetics of glycerol dehydration with WO_3/TiO_2 in supercritical water, Industrial and Engineering Chemistry Research 51 (2012) 12253–12257.

Chapter 2

Tunable and selective conversion of 5-HMF to 2,5-furandimethanol and 2,5-dimethylfuran over copper-doped porous metal oxides

Abstract

Tunable and selective hydrogenation of the platform chemical 5-hydroxymethylfurfural into valuable C6 building blocks and liquid fuel additives is achieved with copper-doped porous metal oxides in ethanol. A new catalyst composition with improved hydrogenation/hydrogenolysis activity is obtained by introducing small amounts of Ru dopant into the previously reported Cu0.59Mg2.34Al1.00 structure. At a mild reaction temperature (100 °C), 2,5-furandimethanol is obtained with excellent selectivity up to >99 %. Higher reaction temperatures (220 °C) favor selective deoxygenation to 2,5-dimethylfuran and minor product 2,5-dimethyltetrahydrofuran with a combined yield as high as 81 %. Notably, these high product yields are maintained at a substrate concentration up to 10 wt % and a low catalyst loading. The influence of different alcohol solvents on product selectivity is explored. Furthermore, reaction intermediates formed at different reaction temperatures are identified. The composition of these product mixtures provides mechanistic insight into the nature of the reduction pathways that influence product selectivity. The catalysts are characterized by elemental analysis, TEM, and BET techniques before and after the reaction. Catalyst recycling experiments are conducted in batch and in a continuous-flow setup.

Keywords: hydrogenation, 5-hydroxymethylfurfural, HMF, building blocks, 2,5-furandimethanol, FDM, 2,5-dimethylfuran, DMF, catalyst, copper-doped, porous metal oxide, biomass, biofuels

A. J. Kumalaputri, G. Bottari, P. M. Erne, H. J. Heeres and K. Barta, Tunable and Selective Conversion of 5-HMF to 2,5-Furandimethanol and 2,5-Dimethylfuran over Copper-Doped Porous Metal Oxides, ChemSusChem 7 (2014) 2266–2275.

2.1 Introduction

Inedible, carbon-neutral lignocellulosic biomass represents the most promising renewable starting material for the synthesis of high-value-added products. 5-Hydroxymethylfurfural (HMF) was identified by the U.S. Department of Energy (DOE)[1] as one of the top ten bio-based platform chemicals with significant market potential.[2] This molecule, which is derived from the C6 sugar fraction of lignocellulosic biomass, mainly by a biphasic solvent approach,[3] may undergo several chemical transformations to give valuable chemicals and fuels.[4] For example, it can be oxidized into 2,5-diformylfuran (DFF)[5] and furan 2,5-dicarboxylic acid (FDCA)[6] to provide building blocks for the polymer industry. It can also be reduced to 2,5-furandimethanol (FDM) or biofuel additive 2,5-dimethylfuran (DMF).[7]

FDM has been identified as a useful building block in the synthesis of macromolecules.[8] Stoichiometric reduction of HMF with a twofold excess of sodium borohydride leads to FDM in 97% yield.[9] Catalytic approaches are more attractive and several examples have already been reported. Alamillo et al. described 81% selectivity to FDM by using a Ru/CeOx catalyst, with 2,5-tetrahydrofurandimethanol (THFDM) as the reduction coproduct.[10] Nakagawa et al. used a Ni–Pd bimetallic catalyst supported on silica for the hydrogenation of HMF with the prevailing formation of mixtures of FDM/THFDM and THFDM in a yield of up to 96% under optimized conditions.[11] Recently, the same research group reported the use of a highly selective $IrReOx/SiO_2$ catalyst in the hydrogenation of HMF to form FDM (99% yield) under mild reaction conditions.[12] Gold nanoclusters supported on alumina showed good activity in the hydrogenation of HMF to FDM (up to 96% yield).[13] Homogeneous catalysts, such as [Ir(Cp*)(TsDPEN)] (Cp*=C_5Me_5; TsDPEN=H2NCHPhCHPhNTs; Ts=tosyl) proved to be very active and selective in the transfer hydrogenation of HMF with formic acid, giving 99% yield of FDM.[14] Furthermore, THFDM and the corresponding alcohol derivatives [e.g., 1,2,6-hexanetriol (1,2,6-HT) or 1,2-hexanediol (1,2-HD)] represent important precursors for the synthesis of polymers.[15] Reductive deoxygenation of HMF leads to DMF. Dumesic et al. reported a high yield in the production of DMF (up to 79%) directly from fructose in a biphasic process by using a Ru–Cu-based catalyst.[16] Bell and Chidambaram used glucose as a feedstock in ionic liquids or acetonitrile.[17] Hydrogenation of HMF to form DMF was achieved with a Pd/C catalyst. Catalytic transfer hydrogenation by means of a Ru/C catalyst and isopropanol as the hydrogen donor also

led to a DMF selectivity of up to 81%.[18] Recently, Wang et al. showed that Ru/Co_3O_4 catalysts led to very selective formation of DMF (94.1% from HMF and 75.1% from fructose, with full substrate conversion).[19] In a recent paper, Chatterjee et al. reported the use of a Pd/C catalyst in supercritical carbon dioxide/water with very high DMF selectivities.[20] Also, Pd/Fe_2O_3 was used in a continuous flow setup and proved to be effective in the conversion of HMF to DMF (up to 72% yield).[21] Elaborately designed bimetallic PtCo nanoparticles encapsulated in carbon nanospheres afforded 98% yield of DMF from HMF; the best result related to DMF production reported so far.[22]

In general, the clean and selective conversion of HMF is particularly challenging due to the inherent reactivity of this molecule, especially at higher reaction temperatures. Riisager et al. previously showed that HMF could be reduced in supercritical methanol by using copper-doped porous metal oxides (PMOs), in the temperature range of 240–300 °C.[23] The hydrogen equivalents needed for the diverse reductions originated from the solvent itself, upon reforming, and no higher boiling side products were detected. Although a good combined yield of DMF+DMTHF was obtained, product selectivity suffered from side processes due to reactive intermediates formed through the concomitant methanol reforming process.

Herein, we report on a tunable and highly selective system for the conversion of HMF to either FDM or DMF by using both previously reported noble-metal-free and novel copper-doped PMOs, comprising a very low Ru loading, in contrast to many commercial catalysts with a high noble-metal content. Biocompatible ethanol is used as a solvent, and milder reaction temperatures (100–220 °C) and 50 bar (1 bar=1.10^5 Pa) of H_2 pressure are applied. Similarly to the already reported protocol in supercritical methanol, there is no evidence for humin formation, even at HMF concentrations as high as 10%. Identification of the reaction intermediates formed during reduction processes and their evolution in time is discussed at various reaction temperatures.

2.2 Results and discussion

2.2.1 Catalyst preparation and characterization

Two different PMO catalysts were prepared by calcination of hydrotalcite (HTC) precursors. These HTCs were synthesized by coprecipitation of Na_2CO_3 and NaOH with aqueous solutions of aluminum,

magnesium, and additional copper salts. In one case, the molar ratio of M^{3+}/M^{2+} was kept at 1:3, while 20 mol% of the Mg^{2+} ions were replaced with Cu^{2+}. This composition was previously described and the corresponding PMO was successfully used to convert various biomass resources.[24] In another case, a new composition was prepared by the same method, additionally replacing 2% of Al^{3+} with Ru^{3+} ions. Although Ru-Mg-Al[25] and Ru-Cu-Al[26] compositions are known, to the best of our knowledge, the corresponding Ru-Cu-Mg-Al HTC and PMO has not yet been synthesized or characterized.

The synthesized HTCs were analyzed by powder XRD and displayed distinct features consistent with a double-layered structure (XRD traces are shown Figure S1 in Supporting Information).[27] The XRD patterns were recorded in the 2θ range of 10–70°, with sharp diffraction peaks for lower 2θ values (10–37°), and broad peaks at higher 2θ values (37–70°); the doublet at 60–62° is a typical indication of a crystalline double-layered structure.[27] No diffraction peaks related to Cu or Ru oxide crystallites could be detected; this observation is in agreement with a homodisperse distribution of both metals in the HTC structure. After calcination at 460 °C for 24 h, PMOs of different compositions were obtained. BET surface area values are comparable for both PMOs. There was very good agreement between the theoretical and empirical composition, as determined by elemental analysis of the PMOs, which indicated that all metals were incorporated into the HTC structure. Catalyst codes, the corresponding compositions, and BET surface area values are summarized in Table 1. Additional pore volume and average pore size values for both catalysts are listed in Table S8 in the Supporting Information.

Table 1. Compositions and BET areas of the PMO catalysts used in this study

Catalyst code [a]	Composition theoritical	Composition empirical	BET area [m^2g^{-1}]
Cu20-PMO	$Cu_{0.60}Mg_{2.40}Al_{1.00}$	$Cu_{0.59}Mg_{2.34}Al_{1.00}$	196
Cu20-Ru2-PMO	$Cu_{0.60}Mg_{2.40}Al_{0.98}Ru_{0.02}$	$Cu_{0.61}Mg_{2.33}Al_{0.98}Ru_{0.02}$	208

[a] The code indicates the Cu or Ru mol percentage, respectively, with respect to the M^{2+} or M^{3+} total content. [b] The numbers refer to molar ratios of individual metals, as determined by inductively coupled plasma (ICP) analysis. All metals are normalized to Al.

2.2.2 Tunable and selective conversion of HMF to FDM or DMF

First, we were interested in finding the optimal conditions for selective carbonyl reduction of HMF to give FDM (Scheme 1). Catalytic runs were performed by using HMF (0.5 g) and Cu20-PMO (0.1 g) in ethanol under 50 bar of H_2 in the temperature range of 80–140 °C for 3 h. The selectivity values for the main components are shown in Table 2 (and see Table S1 in the Supporting Information for all components).

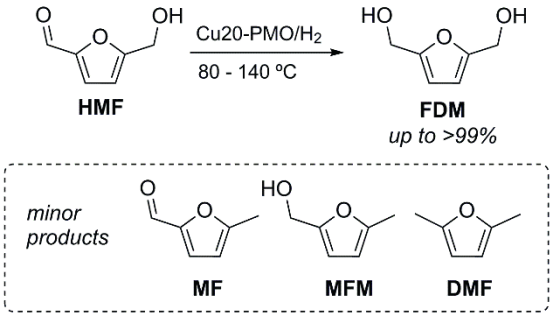

Scheme 1. Selective conversion of HMF into FDM at mild reaction temperatures

Already at 80 °C, 95 % of the starting material was converted into FDM with 91 % selectivity (Table 2, entry 1). Excellent results were achieved at 100 °C, with full conversion of the starting material and exceptionally high FDM selectivity (>99 %; Table 2, entry 2; see also Figure S2 in the Supporting Information for the corresponding GC trace).

At 120 and 140 °C, FDM selectivity decreased due to the formation of 5-methylfurfural (MF) and 5-methyl-2-furanmethanol (MFM) intermediates (Table 2, entries 3 and 4, respectively). These intermediates were also seen in the run performed for a longer time (6 h) at 100 °C, albeit to a much lesser extent (91 % FDM; Table 2, entry 5). Cu20-Ru2-PMO was also tested at 100 °C for 3 h, and gave rise to 98 % FDM selectivity (Table 2, entry 6); a value very similar to the one obtained with Cu20-PMO. In a separate experiment pure FDM (0.489 g) was isolated in a yield of 97 % under the optimized reaction conditions (100 °C, 50 bar H_2, 3 h). For the corresponding NMR spectra, see Figures S3 and S4 in the Supporting Information.

Next, we turned our attention to the more challenging reductive deoxygenation of HMF to demonstrate the utility of inexpensive non-noble-metal-based Cu20-PMO catalyst, as well as Cu20-Ru2-PMO

Table 2. Selectivity values (determined by GC-FID) in the hydrogenation of HMF at mild temperatures for the optimized production of FDM [a]

Entry [a]	Catalyst	T (°C)	FDM	THFDM	DMF+ DMTHF	MF	MFM	THMFM	1,2-HD	1,2,6-HT	Others
1 [b]	Cu20	80	91	0	0	4	0.2	0	0	0	0.8
2	Cu20	100	>99	0	0.1	0.1	0.1	0	0	0	0.3
3	Cu20	120	89	0	0.7	5	1	0	0	0	3
4	Cu20	140	79	0.3	4	4	5	0.4	2	2	3
5 [c]	Cu20	100	91	0.3	0.1	6	1	0	0.2	0.2	0.8
6	Cu20-Ru2	100	98	0	0.2	0.8	0.2	0	0	0	0.3

[a] Reaction conditions: 0.5 g HMF, 0.1 g catalyst, 0.250 mL toluene (internal standard), 20 mL ethanol, 3 h reaction time, 50 bars H_2 (HMF conversion was >99 % in all entries). [b] HMF conversion was 95 %. [c] Reaction time was 6 h.

catalyst, containing only small amount of Ru, in the production of DMF, according to Scheme 2.

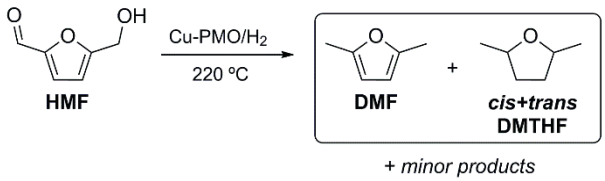

Scheme 2. Production of DMF and DMTHF at 220 °C

Catalytic runs were first conducted in the temperature range 140–220 °C at 6 h with Cu20-PMO. The results are summarized in Figure 1 (see Table S2 in the Supporting Information for more details).

In all cases, full HMF conversion was seen. In the lower temperature range (100–140 °C), FDM was the main reaction product. At 180 °C, more desired product was formed, but intermediates FDM and MFM were still present in considerable quantities. The best product selectivity was achieved at 220 °C; and therefore we chose this temperature for further studies. At all reaction temperatures, a mixture of DMF and 2,5-dimethyltetrahydrofuran (DMTHF) was obtained, of which DMF was the prevailing product. The yields of DMF and DMTHF were determined by using calibration curves and toluene as an internal standard. The selectivity and yield values are in very good agreement, which indicates that no higher boiling point side products were formed and all components of the reaction mixtures were detected by GC analysis.

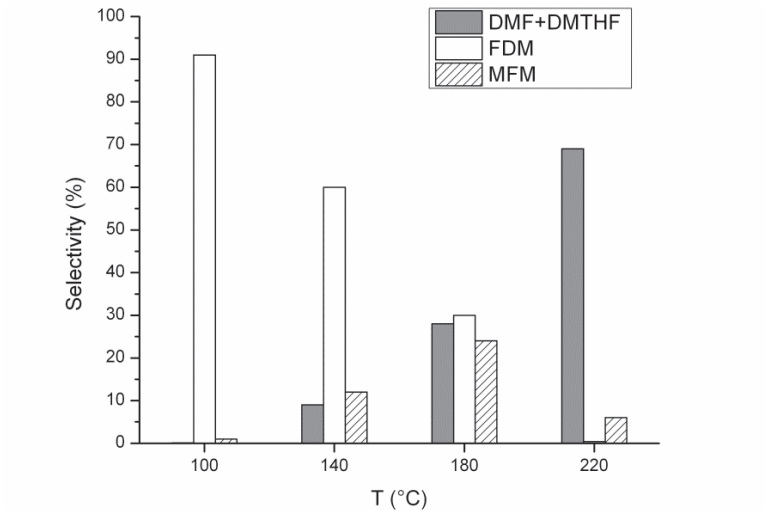

Figure 1. Plot of DMF selectivity as a function of reaction temperature with the Cu20-PMO catalyst (6 h runs)

After only 1 h, a 49 % yield of DMF+DMTHF was obtained with Cu20-PMO (Table 3, entry 1; see also Table S7 in the Supporting Information for more details). The product yield gradually improved from 54 % at 3 h to 66 % at 6 h (Table 3, entries 2 and 3). This already surpasses our previous results with the same catalysts in supercritical methanol.[23] Prolonging the reaction time to 12 and 18 h did not lead to any relevant changes (Table 3, entries 4 and 5).

With these promising results in hand, we performed the same series of reactions with the new Cu20-Ru2-PMO catalyst. Ru is highly active for C-O bond hydrogenolysis;[6,18] thus we expected a possible cooperative effect between Cu and small amounts of Ru in the new catalyst composition. We would like to point out that a low catalyst loading was maintained and the weight percentage of Ru in our new Cu20-Ru2-PMO was 0.6 %. The Ru loading with respect to the substrate is 0.12 %. The results from these runs are shown in Table 4 (see also Table S6 in the Supporting Information).

A comparison of product yields obtained with Cu20-PMO and Cu20-Ru2-PMO is shown in Figure 2. Indeed, the novel catalyst composition is very efficient in HMF reduction/deoxygenation. A product yield of DMF+DMTHF as high as 55 % at 1 h, 66 % at 3 h, and 70 % at 6 h was reached with the Cu20-Ru2-PMO catalyst (Table 4, entries 1, 2, and 3, respectively). The DMF+DMTHF yield further increased to

Table 3. Dependence of DMF+DMTHF selectivity and yield on the reaction time with the Cu20-PMO catalyst at 220 °C.

Entry [a]	t [h]	DMF+DMTHF		DMF/DMTHF ratio
		Selectivity (%) [b]	Yield (%) [c]	
1	1	52	49	3.3
2	3	54	54	5.8
3	6	69	66	3.6
4	12	67	65	3.2
5	18	69	65	3.1

[a] Reaction conditions: HMF (0.5 g), catalyst (0.1 g), toluene (0.250 mL; internal standard), ethanol (20 mL), 220 °C, 50 bar H_2. Full conversion in all cases. [b] Determined by GC-FID. [c] Determined by calibration curves and internal standard.

Table 4. Dependence of DMF+DMTHF selectivity and yield on the reaction time with the Cu20-Ru2-PMO catalyst at 200 °C

Entry [a]	t [h]	DMF+DMTHF		DMF/DMTHF ratio
		Selectivity (%) [b]	Yield (%) [c]	
1	1	55	55	5.9
2	3	68	66	4.2
3	6	71	70	3.4
4	12	79	79	3.4
5	18	77	75	3.3

[a] Reaction conditions: HMF (0.5 g), catalyst (0.1 g), toluene (0.250 mL; internal standard), ethanol (20 mL), 220 °C, 50 bar H_2. Full HMF conversion in all cases. [b] Determined by GC-FID. [c] Determined by calibration curves and internal standard.

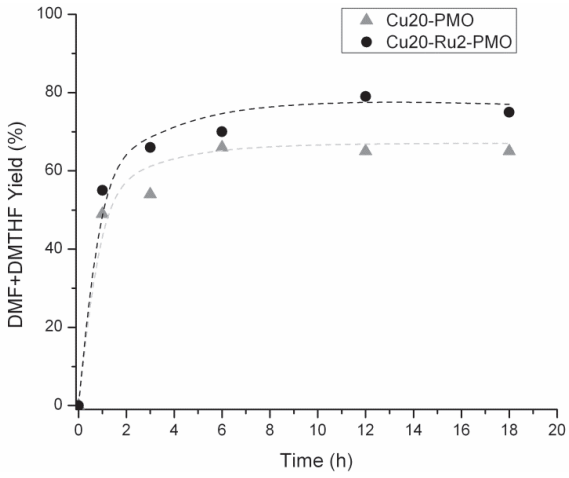

Figure 2. Plot of DMF+DMTHF yield with Cu20-PMO and Cu20-Ru2-PMO at different reaction times (dashed lines are added for visual interpretation of data)

79 % at 12 h; a notable improvement compared with the 66 % yield obtained with Cu20-PMO.

In general, the product mixtures were very clean, and almost all intermediates that might have led to DMF were consumed after 6 h (Table S6, Supporting Information). After 18 h, the product yield only slightly decreased to 75 %. The yield of DMF+DMTHF could be further improved to 80 % after only 6 h by increasing the Cu20-Ru2-PMO loading to 0.250 g (Table 5, entry 5). Slight irregularities in yields were seen at 3 h with Cu20-PMO and at 6 h with Cu20-Ru2-PMO, even after repeating these experiments several times. We tentatively attribute this to adsorption phenomena, although further detailed studies are required.

In all cases, the formation of DMF was accompanied by the corresponding over-reduction product, DMTHF. The DMF/DMTHF ratio remained relatively constant at all reaction times when Cu20-PMO was used; however, a slight discrepancy could be seen at 3 h. This is the same data point that corroborates the decrease in the overall DMF+DMTHF yield. The DMF/DMTHF ratio gradually, but only slightly, decreased from 5.9 at 1 h to 3.3 at 18 h with Cu20-Ru2-PMO. This indicates that DMF is not the main source of DMTHF in our system (see also the section on reaction pathways and intermediates). The individual selectivity values of DMF and DMTHF for runs with Cu20-Ru2-PMO are shown in Figure 3 (for the corresponding values obtained with the Cu20-PMO catalyst, see Figure S5 in the Supporting Information).

Because the nature of the solvent may have a crucial influence on the studied reaction,[18] we evaluated different alcohols, including methanol, isopropanol, and MIBC, as reaction solvents with Cu20-Ru2-PMO and Cu20-PMO (Table 5; for detailed information, see Table S3 in the Supporting Information).

Interestingly, significant solvent effects were seen with Cu20-PMO, for which the product yield improved from 66 % in ethanol to 77 % in isopropanol (Table 5, entries 1 and 2, respectively). Because, during these runs, 0.250 g of PMO was used, this result also shows that the catalyst loading did not greatly affect the overall product yield, although the DMF/DMTHF ratio slightly changed (Table 3, entry 3 versus Table 5, entry 1).

Higher HMF concentrations were adopted to prove the validity of our catalytic system in conditions usually affording HMF self-condensation products. Increasing the HMF concentration to 8 wt % (Table 5, entry 3) still led to a good product yield of 60 %. This reaction time was not enough to fully convert all reaction intermediates (Table S3, entry 3 in the Supporting Information). Next, we adopted a 10 wt % HMF

Table 5. Selectivity values (determined by GC-FID) with Cu20-PMO and Cu20-Ru2-PMO catalysts in different solvents and catalyst loading at 220 °C [a]

			DMF+DMTHF								
Entry	Catalyst	Solvent	Selectivity (%) [b]	Yield (%) [c]	DMF/ DMTHF ratio	THFDM	MFM	THMFM	1,2-HD	2-hexanol	Others
1	Cu20	EtOH	72 (61+11)	66	5.5	2	2	2	3	<1	18 (12) [e]
2	Cu20	iPrOH	81 (64+17)	77	3.8	3	-	3	5	3	5
3 [f]	Cu20	iPrOH	69 (59+10)	60	5.9	2	10	3	3	1	12
4 [g]	Cu20	iPrOH	80 (70+10)	75	7.0	1	2	1	4	1	11
5	Cu20-Ru2	EtOH	84 (65+19)	80	3.4	1	<1	3	3	<1	8
6	Cu20-Ru2	iPrOH	81 (63+18)	79	3.5	1	-	3	7	5	3
7[b]	Cu20-Ru2	iPrOH	84 (65+19)	78	3.4	1	-	3	6	3	3
8[c]	Cu20-Ru2	iPrOH	84 (65+19)	81	3.4	2	1	7	2	2	2
9 [d]	Cu20-Ru2	MeOH	18 (17+1)	17	17.0	1	2	1	3	-	75
10	Cu20-Ru2	MIBC	70 (54+16)	n.d.	3.3	2	-	3	8	10	7

[a] Reaction conditions: 0.5 g HMF, 0.250 g catalyst, 0.250 mL toluene (internal standard), 20 mL solvent, 220 °C, 6 h (unless otherwise stated), 50 bars H_2 (HMF conversion was >99 % in all entries). [b] Reaction time was 4 h. [c] Reaction time was 1 h. [d] Reaction was carried out with 0.100 g of catalyst. Methyl ether species account for 56 % in the column 'others'. [e] Number in brackets refers to selectivity values for all other minor components excluding two main components at 7.58 and 7.86 min. [f] The HMF concentration was increased to 8 wt %, maintaining the same solvent volume (1.258 g HMF/20 mL *i*PrOH). [g] The HMF zconcentration was increased to 10 wt %, maintaining the same solvent volume (1.572 g HMF/20 mL *i*PrOH) and reaction time was 18 h.

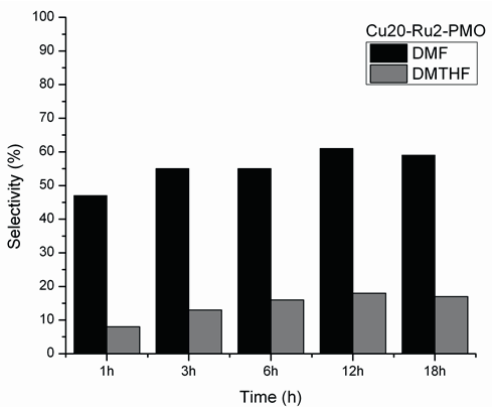

Figure 3. Individual DMF and DMTHF selectivities plotted separately versus reaction time (220 °C, 50 bar H_2, EtOH)

concentration while prolonging the reaction time up to 18 h. A colorless solution, accounting for an excellent 75 % yield of DMF+DMTHF and good DMF/DMTHF ratio (Table 5, entry 4), was obtained. For both of these runs, a catalyst loading of 0.250 g was maintained. To the best

of our knowledge, only Dumesic et al. successfully reported DMF production from 10 wt % HMF, albeit in the vapor phase.[16] It is noteworthy that no char formation was detected, as evidenced by the clear and colorless solution obtained upon dissolving the catalyst residue in HNO_3 (Figure S14 in the Supporting Information). This was additionally confirmed by thermogravimetric analysis (TGA) of the solids (Figure S15 in the Supporting Information).

Next, we screened the Cu20-Ru2-PMO composition in different solvents at higher catalyst loading. In contrast to Cu20-PMO, no further improvement took place when using Cu20-Ru2-PMO in isopropanol, for which an almost identical, high yield of 79 % was obtained compared with 80 % in ethanol (Table 5, entry 6 versus entry 5). Because no furan ring-containing reaction intermediates, by only ring-opening products, were present as minor side products in these runs, we first shortened the reaction time to 4 h and subsequently to 1 h to enhance the product yields; however, this did not lead to significant changes (Table 5, entries 7 and 8). Nonetheless, under these conditions, the reaction afforded the desired product in excellent yield (81 %) and selectivity (84 %) after only 1 h (the corresponding GC trace is shown in Figure S6 in the Supporting Information).

As expected, the reaction carried out in methanol gave rise to significant amounts of ethers and only 17 % yield of DMF+DMTHF (Table 5, entry 9). Among these ethers, several, namely, 2-(methoxymethyl)-5-methylfuran; 2,5 bis(methoxymethyl)furan; and [5-(methoxymethyl) furan-2-yl]methanol (A, B, and C, respectively, shown in Scheme S1 in the Supporting Information), were identified by mass and their characteristic fragmentation pattern. Together they accounted for 56 % GC selectivity.

The reaction performed in MIBC (Table 5, entry 10) showed lower DMF+DMTHF selectivity (the yield could not be determined due to the overlap of the internal standard with the solvent peak), but the higher boiling point difference between the solvent (131.6 °C) and DMF (92–94 °C) allowed an attempt to separate the product by distillation. For this experiment, HMF (1.0 g) and Cu20-Ru2-PMO (0.4 g) were used, and indeed DMF (0.195 g) could be isolated in 85 % GC purity (for ^{1}H and ^{13}C NMR spectra, see Figures S7 and S8 in the Supporting Information). This procedure demonstrates that MIBC could be, after optimization, the solvent of choice for easy separation of pure DMF from the reaction mixture.

Furthermore, the catalyst stability at 220 °C was tested. As a representative example, the Cu20-Ru2-PMO catalyst was recovered after the

4 h run in iPrOH (Table 5, entry 7). Elemental analysis showed very good agreement between the fresh catalyst and spent catalyst residue. In addition, trace-metal analysis of the product solution confirmed no metal leaching (see Table S4 in the Supporting Information for more details).

2.2.3 Reaction pathways and intermediates

The reaction of HMF with H_2 may generate a mixture of several partially reduced products, such as FDM, MF, and MFM, and products of ring hydrogenation, such as THFDM and 5-methyl-2-tetrahydrofuranmethanol (THMFM). Ring-opening products 2-hexanol, 1,2-HD, and 1,2,6-HT are also expected under the reaction conditions used. We have identified the vast majority of these reaction intermediates by GC-MS analysis and authentic standards. The main products and pathways are summarized in Scheme 3 (see also Scheme S2 in the Supporting Information).

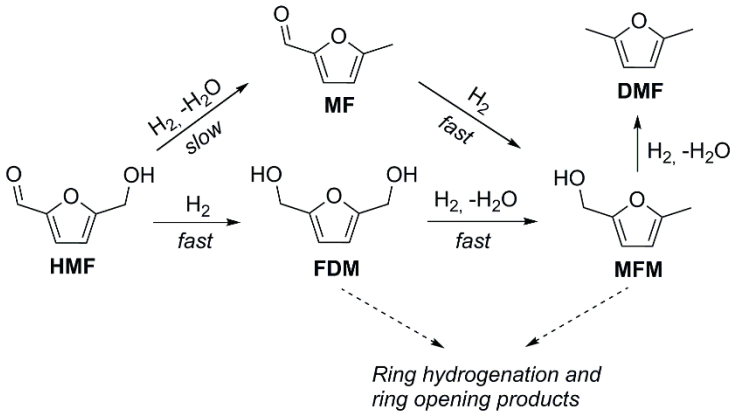

Scheme 3. Reaction pathways for HMF conversion with copper-doped PMO catalysts

We first studied the composition of reaction mixtures as a function of time by using Cu20-PMO at 140 °C to gain an insight into the evolution of earlier, partially reduced reaction intermediates (Figure 4, see also Table S5 in the Supporting Information).

At 140 °C, most of HMF is converted after 1 h and the main process is carbonyl reduction to form FDM. FDM represents the main

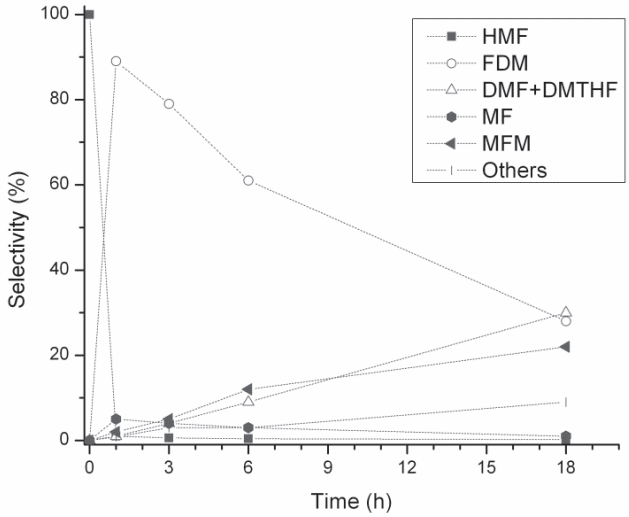

Figure 4. Composition of the reaction mixture at 140 °C with the Cu20-PMO catalyst

component of all reaction mixtures up to 12 h, whereupon its amount gradually decreases, giving rise to the second main intermediate, MFM. This intermediate, upon hydrogenolysis, is converted into the desired product, DMF. The amount of MF stays consistently low at all reaction times, which indicates that carbonyl hydrogenation is more rapid than the loss of the alcohol functionality in HMF. These data also indicate that the loss of one -OH from FDM is more rapid than the loss of the second -OH from MFM, which is a more persistent intermediate.

The relative amount of all other reaction intermediates (products of ring opening or furan ring hydrogenation) stays below 5 %. However, their presence indicates that these competing pathways cannot be completely prevented and represents the main bottleneck towards exclusive product formation.

Further studies were conducted by using both Cu20-PMO (see Figures S11 and S12 and Table S7 in the Supporting Information) and Cu20-Ru2-PMO catalysts (Figure 5 and Figure S9 and S10 and Table S6 in the Supporting Information) at 220 °C; the temperature most ideal for DMF formation.

At 220 °C with Cu20-Ru2-PMO, the amount of partially reduced reaction intermediates is much lower than that of the runs at 140 °C, and already after 1 h a significant amount of product DMF+DMTHF is formed. One of the reaction intermediates is MFM, which accounts for 14 %

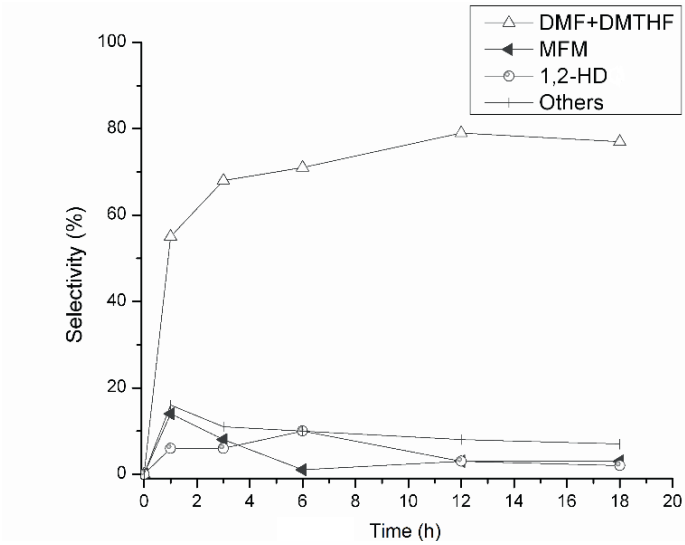

Figure 5. Composition of the mixture at 220 °C with the Cu20-Ru2-PMO catalyst

selectivity, whereas FDM is only present in negligible quantities due to its higher reactivity under these conditions. Ring-opening product 1,2-HD is also present, already after 1 h, in 6 % selectivity. In addition, two components belonging to retention times of 7.57 and 7.85 min can be detected, which together account for 5%. Their abundance shows a decreasing trend over time (2 % after 6 h and <1% after 18 h; see Table S6 in the Supporting Information). From all relatively abundant intermediates, these are the only ones we have not yet convincingly identified. However, they could be attributed to products formed from MFM because they are also present in significant quantities (≈ 10 %) when MFM is used as substrate (see Table 6, entry 2). All other reaction intermediates (included in 'other compounds') were present in less than 1 % selectivity. At 3 and 6 h reaction time, remaining MFM is gradually consumed, giving rise to 68 and 71 % DMF+DMTHF selectivity, respectively. We attribute the further increase in product selectivity (79 %) seen at 12 h to desorption of excess material from the catalyst surface (notably, the 6 h data point gave slightly decreased product yields). Indeed, after 6 h, all intermediates that might lead to the product are already consumed. The slight decrease in product selectivity (from 79 to 77 %) at 18 h could be due to further, slow conversion of DMF (see also Table 6, entry 6). In conclusion, the main pathway identified in this study is the conversion of MFM to the DMF+DMTHF product within 6 h at 220 °C.

Table 6. Conversion of key reaction intermediates with Cu20-PMO at 220 °C

			Intermediates formed (%)								
Entry [a]	Substrate	Conversion (%)[b]	DMF+ DMTHF [b]	THFDM [b]	MFM [b]	MF [b]	THMFM [b]	1,2-HD [b]	1,2,6-HT [b]	EMMF [b]	Others [b]
1	FDM	>99	50 (40+10)	4	13	-	5	14	5	<1	10 (8)
2	MFM	61	38 (33+5)	-	39	<1	1	2	-	1	18 (7)
3 [c]	MFM	96	79 (60+19)	-	4	-	2	<1	-	3	12 (7)
4	MF	>99	33 (31+2)	-	44	<1	1	3	-	1	17 (7)
5	DMF	2	99 (98+1)	-	-	-	-	-	-	-	1
6 [d]	DMF	3	99 (97+2)	-	-	-	-	-	-	-	1
7	THFDM	-	-	-	-	-	-	-	-	-	-

[a] Reaction conditions: substrate (4 mmol), catalyst (0.100 g), toluene (0.250 mL; internal standard), ethanol (20 mL), 220 °C, 3 h, 50 bar H_2. [b] Determined by GC-FID. [c] The experiment was run for 12 h. [d] Cu20-Ru2-PMO was used as catalyst. [e] Numbers in parentheses indicate selectivity for other compounds, excluding the two main components at 7.58 and 7.86 min.

Table 7. Selectivity and yield values (determined by GC-FID) with Cu20-Ru2-PMO catalyst at 220 °C [a]

t	DMF+DMTHF		FDM	THFDM	MFM	THMFM	1,2-HD	1,2,6-HT	EMMF	Others[b]
[h]	Selectivity (%) [b]	Yield (%) [c]								
1	55 (47+8)	55	1	2	14	3	6	1	2	16 (11)
3	68 (55+13)	66	<1	2	8	3	6	<1	1	11 (9)
6	71 (55+16)	70	0	2	1	4	10	1	1	10 (10)
12	79 (61+18)	79	0	2	3	4	3	<1	1	8 (7)
18	77 (59+18)	75	0	2	3	5	2	<1	3	7 (7)

[a] Reaction conditions: 0.5 g HMF, 0.1 g Cu20-Ru2-PMO, 0.250 mL toluene (internal standard), 20 mL ethanol, 220 °C, 50 bars H_2 (HMF conversion was >99 % in all entries). [b] Numbers in brackets refer to selectivity values for all other minor components excluding two main components at 7.58 and 7.86 min.

Already in the first hour, a significant amount of desired product is formed and its amount remains relatively constant over time.

Similarly, other fully hydrogenated intermediates, such as THFDM, THMFM, and ring-opening product alcohols, formed already after 1 h and are constant over time, with variation in the relative amounts below 5 % (for a full description of the reaction intermediates and graphs, see Table 7, Figures 6 and 7, and Scheme 4).

Very similar product profiles were obtained with Cu20-PMO, albeit with an overall lower DMF+DMTHF selectivity. The product selectivity reaches its maximum (69%) at 6 h, with no significant further changes with time (for a full description of the reaction intermediates and graphs, see Table S6 and Figures S10 and S11 in the Supporting Information).

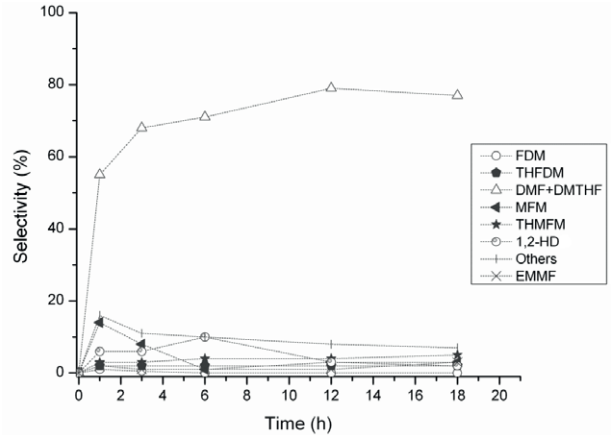

Figure 6. Plot of selectivities of the identified and not identified products *versus* reaction time from the hydrogenation of HMF at 220 °C with Cu20-Ru2-PMO

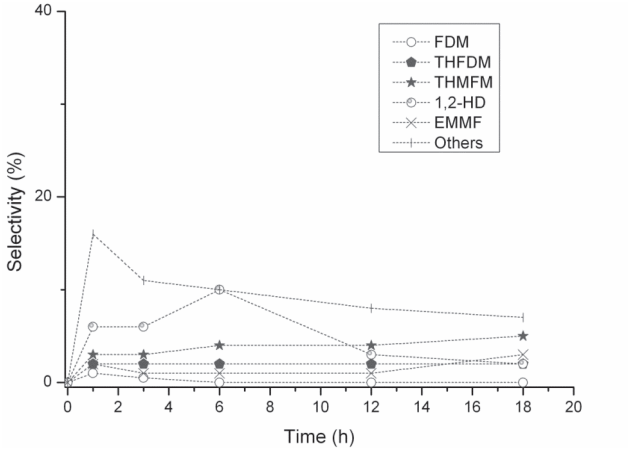

Figure 7. Plot of selectivities to minor products *versus* reaction time from the hydrogenation of HMF at 220 °C with Cu20-Ru2-PMO

Preliminary kinetic modeling [28] (of runs in ethanol) suggests that the main role of Cu20-Ru2-PMO lies in increasing the rate of reduction of the main reaction intermediate, MFM, to DMF. Because reaction intermediate MFM is a source of ring-opening products and engages in side reactions with ethanol, more rapid reduction of MFM to DMF with Cu20-Ru2-PMO explains the cleaner reaction mixtures and higher product yields.

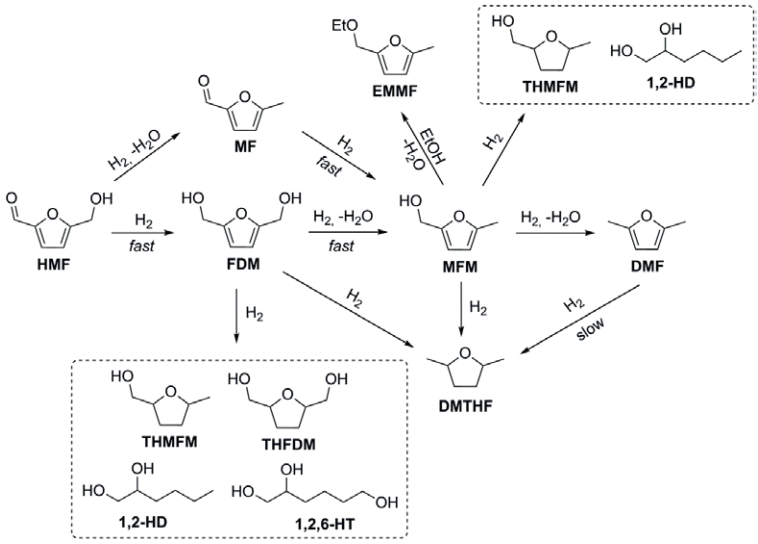

Scheme 4. Reaction pathways in the hydrogenation of HMF using copper doped porous metal oxide catalysts in ethanol

To gain further insight into the formation pathways of the ring-opening and furan ring hydrogenation products, we conducted reactions at 3 h with the partially reduced reaction intermediates, FDM, MFM, MF, and THFDM, and product DMF. The results are summarized in Table 7 and Scheme 5.

Surprisingly, some of these intermediates resulted in the formation of considerably more ring-opening products than HMF itself. For example, after 3 h, all FDM was consumed and yielded 50 % DMF+DMTHF and 13 % MFM, whereas the amount of various ring-opening alcohol products combined was as high as 23 % (Table 6, entry 1). This result indicates that FDM is the main source of these side products in this system.

Reactions with MFM revealed that this substrate was converted at a slower rate (61 % conversion), resulting in a lower quantity of DMF+DMTHF, but also less ring-opening products after 3 h compared with FDM. The selectivity to the unidentified products is 18 %. Among these, 11 % can be attributed to the same two major components at 7.58 and 7.86 min as those previously seen during HMF conversion with Cu20-Ru2-PMO.

Interestingly, at a prolonged reaction time (12 h, Table 6, entry 3), most MFM was consumed and delivered higher product selectivity at 12 h than HMF itself (Table 6, entry 6 versus Table 3, entry 4). The

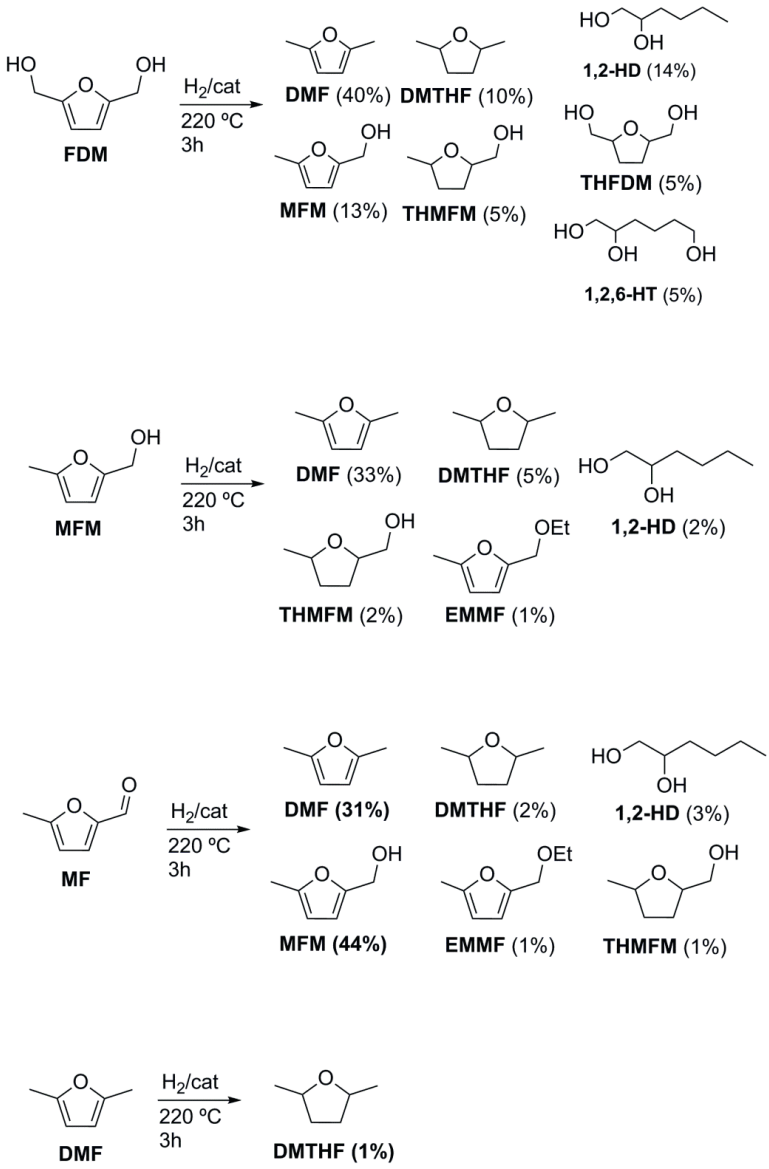

Scheme 5. Conversion of main intermediates with Cu20-PMO catalyst (220 °C, 50 bar H_2, 3 h, EtOH)

ethyl ether of MFM, 3 % of 2-(ethoxymethyl)-5-methylfuran (EMMF), was also detected. This compound can be also seen in the HMF reactions at longer reaction times with Cu20-PMO.

MF was highly reactive and was fully converted to its reduction product MFM. This reaction gave very similar results to the reaction in which MFM was used as a substrate. This shows that C=O reduction is much faster than the hydrogenolysis of MFM to DMF and is in agreement with data obtained at 140 °C.

Lastly, the reactivity of product DMF was investigated both with Cu20-PMO and Cu20-Ru2-PMO; the former resulted in only 2 % and the latter in 3 % conversion after 3 h. The corresponding over-reduction product, DMTHF, was detected in small quantities, which was in agreement with the slight change in the ratio between these two components towards longer reaction times. However, DMF is considerably more stable under these reaction conditions than the partially reduced intermediates FDM or MFM. Furthermore, no conversion of THFDM was seen after 3 h, which was in agreement with previous data.

Overall, the above-described results indicate that ring-opening products and DMTHF are likely to originate from partially reduced, furanic intermediates and are not from the product DMF or ring hydrogenation products THFDM and THMFM. Ring opening of HMF and other highly functionalized furan derivatives was also observed by Dumesic et al.[10]

It appears that substrates with relatively high amounts of polar -OH groups, such as FDM, have more affinity to the catalyst surface.

2.2.4 Recyclability tests

Catalyst recycling experiments were performed at 100 °C with Cu20-PMO (0.1 g) and HMF (0.5 g) for 3 h of reaction time. The catalyst was recovered at the end of each run, washed with ethanol and THF, and reused after drying overnight at 100 °C. The catalyst activity was maintained for 3 cycles, then the FDM selectivity gradually decreased to 61, 53, 38, and 19% in the 4th to 7th cycles, respectively (Figure 8).

After the 7th cycle, the HMF conversion was only 20 %. After this run, 72 mg of catalyst was recovered and subsequently calcined at 460 °C for 24 h. After calcination, the catalyst residue (63 mg) was used in a further experiment at 100 °C for 3 h, resulting in 93 % HMF conversion and 92 % FDM selectivity. Thus, upon recalcination, the catalyst regained its activity.

We next set up a gram-scale continuous-flow experiment for the production of FDM by using similar experimental conditions to those used in the corresponding batch reactions. The catalyst remained

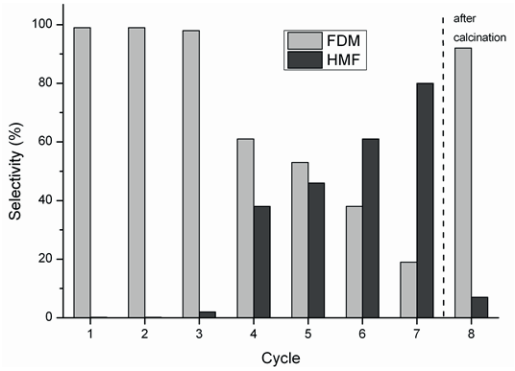

Figure 8. Catalyst recycling experiments (HMF 0.5 g), Cu20-PMO (0.1 g), 50 bar H_2, 100 °C, 3 h

active for 10 h without remarkable loss of performance and FDM formed with very high selectivity (Figure 9).

2.2.5 TEM measurements

We carried out TEM measurements for both PMO catalysts before and after reaction. Images before the reaction for Cu20-PMO (Figure 10, right) and Cu20-Ru2-PMO (Figure 10, left) showed irregular flakes, which is a morphology observed in related systems, such as Cu/Cr HTC-like materials [9] and $Cu/MgAl_2O_4$.[4a] No nanoparticles that could be CuO or RuO_2 were detected by TEM analysis, even at higher magnification. We believe that highly dispersed Cu and Ru species are present in the PMO structures, as evidenced by the lack of peaks related to these metals in the XRD pattern. Additionally, parent Cu/Mg catalysts with a copper content comparable to that of our systems (16 wt %) showed that very small aggregates (<3 nm) could be formed;[30] the method of preparation in our study (coprecipitation to form of regular HTC structure additionally involving aluminum) was very likely to improve copper dispersion to prevent the formation of visible crystallites of CuO. Ternary CuMgAl mixed oxides with a lower copper content did not show any crystalline aggregation either.[31]

Upon imaging the Cu20-Ru2-PMO (Figure 11, left) and Cu20-PMO (Figure 11, right) catalysts after 6 h of reaction time in EtOH, both samples showed, in addition to the irregular sheets, dark spherical particles with diameters of 10(± 1) and 12(± 2) nm, respectively. These

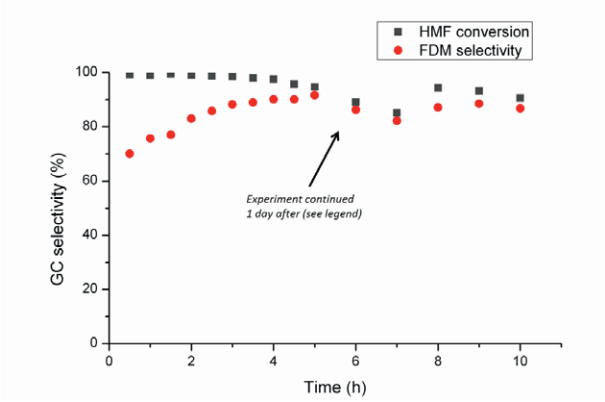

Figure 9. Continuous flow experiment for the production of FDM

The deviation at 6 h is due to the interruption of the experiment, which was continued the day after for additional 4 h. Experimental conditions: 0.3 g Cu20-PMO, 1.5 g HMF in 0.4 L EtOH, 1.5 mL/min solvent flow, 50 bar, 30 mL/min H_2 flow, 100 °C. Additional 1.0 g HMF in 0.2 L EtOH were used after 1 day.

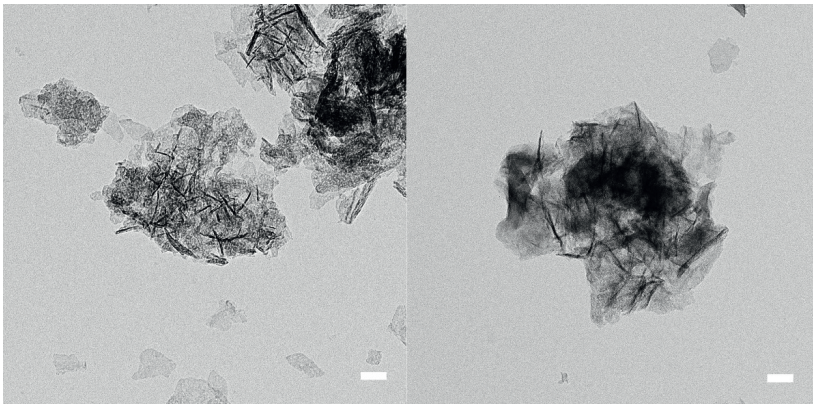

Figure 10. TEM images of fresh Cu20-Ru2-PMO (left) and Cu20-PMO catalysts (right). Scale bar, 50 nm.

could be attributed to clusters of Cu metal, formed by the reduction of CuO originally present in the fresh catalyst. Similar behavior was previously observed by Ford et al., who used the Cu20-PMO catalyst in supercritical methanol.[32] Further literature precedent attributes the formation of particles to sintering of copper under reducing conditions.[33,4a] The influence of this phenomenon on catalyst activity and stability should be further investigated with different catalysts

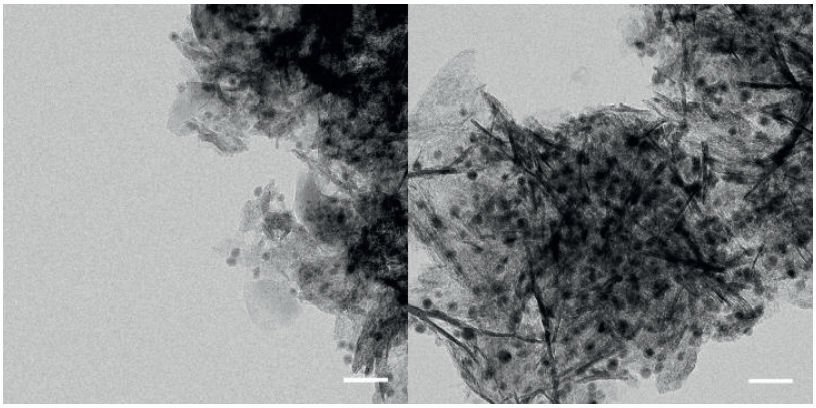

Figure 11. TEM images of Cu20-Ru2-PMO (left) and Cu20-PMO catalysts (right) after 6 h of reaction time (Table 4, entry 3, and Table 3, entry 3, respectively). Scale bar, 50 nm.

supports. No apparent difference in morphology between the catalyst containing or lacking Ru (Figure 11) could be detected; this was likely to be due to an insufficient amount of Ru dopant.

2.3 Conclusions

We developed a tunable and highly selective method for the conversion of HMF to either FDM or DMF (Scheme 6) by using known and new HTC-based catalysts.

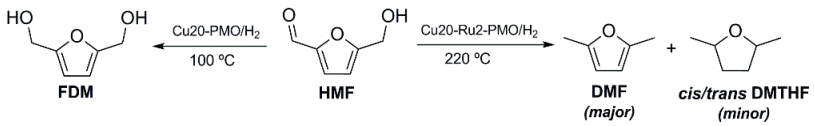

Scheme 6. Tunable conversion of HMF to FDM and DMF+DMTHF

These catalysts consisted of inexpensive, earth-abundant starting materials and no or a small amount of Ru as the hydrogenation metal, and were an economically competitive alternative to commercial noble-metal-based catalysts frequently used in these reactions. Reactions carried out at 100 °C with Cu20-PMO only led to carbonyl reduction with high selectivity (>99 %) and the isolation of FDM in 97 % yield.

The catalyst could be recycled and was stable under continuous-flow conditions. Higher temperatures (220 °C) favored deoxygenation to DMF and DMTHF; the former was the prevalent product. In isopropanol, a DMF+DMTHF yield of 81 % was obtained only after 1 h. In addition, we were able to isolate DMF from a reaction mixture by using MIBC under optimized reaction conditions. No catalyst leaching was observed under these conditions. Finally, our methodology proved to be efficient in the clean conversion of HMF to DMF, even at very high substrate concentrations (up to 10 wt %) and low catalyst loadings; this represents a distinct advantage of the copper-doped PMOs in the clean conversion of HMF.

Current efforts are focused on the development of new catalyst compositions, with the aim of minimizing the ring-opening processes, and one-pot procedures to allow the production of DMF directly from fructose or glucose.

2.4 Experimental section

2.4.1 Catalyst preparation

The HTC catalyst precursors were prepared by a coprecipitation method, according to reported procedures [23,32]. The new Cu20-Ru2-HTC composition was prepared according to the following procedure: A solution containing $AlCl_3 \cdot 6H_2O$ (11.83 g, 0.049 mol), $Cu(NO_3)2 \cdot 2.5H_2O$ (6.98 g, 0.03 mol), $MgCl_2 \cdot 6H_2O$ (24.40 g, 0.12 mol), and $RuCl_3 \cdot H_2O$ (0.22 g, 0.001 mol) in deionized water (0.2 L) was added to a solution containing Na_2CO_3 (5.30 g, 0.05 mol) in water (0.3 L) at 60 °C under vigorous stirring. The pH was maintained between 9 and 10 by addition of small portions of a 1 M solution of NaOH. The mixture was vigorously stirred at 60 °C for 72 h. After cooling to room temperature, the dark-green solid was filtered and resuspended in a 2 M solution of Na_2CO_3 (0.3 L) and stirred overnight at 40 °C. The catalyst precursor was filtered and washed with deionized water until it was chloride-free. After drying the solid under vacuum for 6 h at 100 °C, Cu20-Ru2-HTC (15.8 g) was obtained. Cu20-Ru2-HTC (8.75 g) of this material was calcined at 460 °C for 24 h in air to give Cu20-Ru2-PMO (4.98 g).

2.4.2 Catalyst test

A stainless-steel autoclave (100 mL) equipped with a mechanical stirrer was charged with catalyst (0.100 g), HMF (0.500 g), and toluene (0.250 mL; internal standard) in the appropriate solvent (20 mL). The reactor was sealed and pressurized with H_2 (50 bar), heated to the desired temperature, and stirred at 800 rpm. After the reaction, the autoclave was cooled to room temperature, the content was transferred to a centrifuge tube, centrifuged, and the reaction mixture was separated from the solids by decantation. Samples of the filtered solutions were injected into a Hewlett Packard 5890 GC-MS-FID with a Restek RTX-1701 capillary column. Selectivity was defined as the ratio of the peak area of a given compound to the total area of all the compounds produced in the reaction. Yield values were calculated based on the use of internal standard and calibration curves.

For the experiment aimed to DMF distillation, HMF (1.0 g, 0.008 mol), Cu20-Ru2-PMO (0.4 g), and MIBC (20 mL) were placed in a Parr reactor, pressurized with 50 bar H_2, and heated at 220 °C for 4 h. After cooling, the crude mixture was quantitatively transferred to a centrifuge tube. The residual solid was washed with additional MIBC (5 mL) and the solutions were combined. Distillation of DMF was performed by using a 50 mL round-bottomed flask equipped with a cooler and Vigreaux condenser. Two colorless fractions were collected at 100 °C (0.072 g and 0.123 mg, respectively). After confirming that the composition of both fractions was identical, these were combined. GC measurements were in accordance with the retention time determined for DMF with known standards; ^{1}H and ^{13}C NMR spectroscopic analysis in $CDCl_3$ (see Figures S7 and S8 in the Supporting Information) was consistent with known spectral data for DMF.

2.4.3 Catalyst recycling tests

For reusability tests, catalytic runs were performed as described above. The catalyst was separated from the reaction solution by centrifugation and subsequent decantation, additionally washed with ethanol (1–10 mL), then with THF (1–10 mL), and dried overnight at 100 °C prior to the next run. After the 7th cycle, catalyst residue (72 mg) was recovered. This was additionally calcined at 460 °C for 24 h, resulting in a solid (62 mg). This solid was reused in the 8th run.

2.4.4 Continuous-flow experiment for FDM production

The experiment was performed first for 6 h in a 30 cm reactor tube charged with Cu20-PMO catalyst (0.3 g) and fed with a solution of HMF (1.5 g in EtOH (0.4 L)) at a rate of 1.5 mL.min^{-1} at 50 bar pressure, 30 mL.min^{-1} H_2 flow, and 100 °C, as in the corresponding batch conditions. The next day, additional solution of HMF (1.0 g in EtOH (0.2 L)) was added to the reactor and the experiment was performed for an additional 4 h under the same experimental conditions as those previously described with no relevant changes to the catalytic performance.

Acknowledgements

We thank the Indonesian Directorate General of Higher Education (DIKTI) for financial sponsorship. We gratefully acknowledge Chris Bernt of the Center for Sustainable Use of Renewable Feedstocks (NSF CHE-1240194) and the University of California, Santa Barbara (UCSB), for the precious support in the kinetic modeling. We also thank Arjan Kloekhorst, Erwin Wilbers, Marcel de Vries, Anne Appeldoorn, Jan Henk Marsman, Leon Rohrbach, and Maarten Vervoort for their technical support.

References

[1] a) Top value-added chemicals from biomass, Vol. I—Results of screening for potential candidates from sugars and synthesis gas (Eds.: T. Werpy, G. Petersen), U.S. Department of Energy (DOE) by the National Renewable Energy Laboratory a DOE national Laboratory, Oak Ridge, TN 2004 http://www.eere.energy.gov/biomass/pdfs/35523.pdf, 2004; b) J. J. Bozell, G. R. Petersen, Catalytic conversion of biomass to biofuels, Green Chem. 12 (2010) 539–554.

[2] (a) R. J. Van Putten, J. C. Van der Waal, E. De Jong, C. B. Rasrendra, H. J. Heeres, J. G. De Vries, Hydroxymethylfurfural, A versatile platform chemical made from renewable resources, Chem. Rev. 113 (2013) 1499–1597; b) A. A. Rosatella, S. P. Simeonov, R. F. M. Fradea, C. A. M. Afonso, Hydroxymethylfurfural (HMF) as a building block platform: Biological properties, synthesis and synthetic applications, Green Chem. 13 (2011) 754–793.

[3] a) B. Saha, M. M. Abu-Omar, Advances in 5-hydroxymethylfurfural production from biomass in biphasic solvents, Green Chem. 16 (2014) 24–38;
b) V. V. Ordomsky, J. van der Schaaf, J. C. Schouten, T. A. Nijhuis, Glucose dehydration to 5-hydroxymethylfurfural in a biphasic system, ChemSusChem 6 (2013) 1697–1707;
c) V. V. Ordomsky, J. van der Schaaf, J. C. Schouten, T. A. Nijhuis, Fructose dehydration to 5-hydroxymethylfurfural over solid acid catalysts in a biphasic system, ChemSusChem 5 (2012) 1812–1819; d) T. Okano, K. Qiao, Q. Bao, D. Tomida, H. Hagiwara, C. Yokoyama, Dehydration of fructose to 5-hydroxymethylfurfural (HMF) in an aqueous acetonitrile biphasic system in the presence of acidic ionic liquids, Appl. Catal. A 451 (2013) 1–5.

[4] a) K. Pupovac, R. Palkovits, Cu/$MgAl_2O_4$ as bifunctional catalyst for aldol condensation of 5-hydroxymethylfurfural and selective transfer hydrogenation, ChemSusChem 6 (2013) 2103–2110;
b) D. M. Alonso, S. G. Wettstein, J. A. Dumesic, Bimetallic catalysts for upgrading of biomass to fuels and chemicals, Chem. Soc. Rev. 41 (2012) 8075–8098;
c) BASF Se (Ludwigshafen, Germany), Separating off 5 hydroxymethylfurfural (HMF) from reaction solutions by steam distillation, US Patent US20130345450, 2013; Dalian Institute of Chemical Physics, Chinese Academy of Sciences (Dalian, Liaoning Province, P.R. China), Method of catalytic conversion of carbohydrates into 5-hydroxymethylfurfural, US Patent US20130281719, 2013; E. I. Du Pont De Nemours and Co. (Wilmington, DE, USA), Production of hydroxymethylfurfural from levoglucosenone, US Patent US20130172580, 2013.

[5] a) N. T. Le, P. Lakshmanan, K. Cho, Y. Han, H. Kim, Selective oxidation of 5-hydroxymethyl-2-furfural into 2, 5-diformylfuran over VO^{2}+ and Cu^{2+} ions immobilized on sulfonated carbon catalyst, Appl. Catal. A 464–465 (2013) 305–312;
b) T. S. Hansen, I. Sadaba, E. J. Garcia-Suarez, A. Riisager, Cu catalyzed oxidation of 5- hydroxymethylfurfural to 2,5-diformylfuran and 2,5-furandicarboxylic acid under benign reaction conditions, Appl. Catal. A 456 (2013) 44–50;
c) A. Takagaki, M. Takahashi, S. Nishimura, K. Ebitani, One-pot synthesis of 2,5-diformylfuran from carbohydrate derivatives by sulfonated resin and hydrotalcite-supported Ru catalysts, ACS Catal. 1 (2011) 1562–1565.

[6] a) H. Ait Rass, N. Essayem, M. Besson, Selective aqueous phase oxidation of 5-hydroxymethylfurfural to 2,5-furandicarboxylic acid over

Pt/C catalysts: Influence of the base and effect of bismuth promotion, Green Chem. 15 (2013) 2240–2251;
b) A. Villa, M. Schiavoni, S. Campisi, G. M. Veith, L. Prati, Pd-modified Au on carbon as an effective and durable catalyst for the direct oxidation of HMF to 2,5-furandicarboxylic acid, ChemSusChem 6 (2013) 609–612;
c) S. E. Davis, B. N. Zope, R. J. Davis, On the mechanism of selective oxidation of 5-hydroxymethylfurfural to 2, 5-furandicarboxylic acid over supported Pt and Au catalysts, Green Chem. 14 (2012) 143–147;
d) O. Casanova, S. Iborra, A. Corma, Biomass into chemicals: Aerobic oxidation of 5-hydroxymethyl-2-furfural into 2,5-furandicarboxylic acid with gold nanoparticle catalysts, ChemSusChem 2 (2009) 1138–1144;
e) T. B. Rauchfuss, T. Todsapon (University of Illinois, USA), Efficient method for preparing 2,5-dimethylfuran, US Patent US8324409, 2011;
f) C. R. Adams (Shell Oil Co.), Dimethyl furan production from mesityl oxide, US Patent US3228966, 1963.

[7] Y. Nakagawa, M. Tamura, K. Tomishige, Catalytic reduction of biomass-derived furanic compounds with hydrogen, ACS Catal. 3 (2013) 2655–2668.

[8] a) N. R. Janga, H. R. Kimb, C. T. Houc, B. Soo Kim, Novel bio-based photo-crosslinked polymer networks prepared from vegetable oil and 2,5-furan diacrylate, Polym. Adv. Technol. 24 (2013) 814– 818;
b) S. Goswami, S. Dey, S. Jana, Design and synthesis of a unique ditopic macrocyclic fluorescent receptor containing furan ring as a spacer for the recognition of dicarboxylic acids, Tetrahedron 64 (2008) 6358–6363.

[9] L. Cottier, G. Descotes, Y. Soro, Heteromacrocycles from ring-closing metathesis of unsaturated furanic ethers, Synth. Commun. 33 (2003) 4285–4295.

[10] R. Alamillo, M. Tucker, M. Chia, Y. Pagán-Torres, J. Dumesic, The selective hydrogenation of biomass-derived 5-hydroxymethylfurfural using heterogeneous catalysts, Green Chem. 14 (2012) 1413 –1419.

[11] Y. Nakagawa, K. Tomishige, Total hydrogenation of furan derivatives over silica-supported Ni–Pd alloy catalyst, Catal. Commun. 12 (2010) 154–156.

[12] M. Tamura, K. Tokonami, Y. Nakagawa, K. Tomishige, Synthesis of unsaturated alcohol in mild conditions by highly selective hydrogenation, Chem. Commun. 49 (2013) 7034 –7036.

[13] J. Ohyama, A. Esaki, Y. Yamamoto, S. Arai, A. Satsuma, Selective hydrogenation of 2-hydroxymethyl-5-furfural to 2,5-bis(hydroxymethyl)furan over gold sub-nano clusters, RSC Adv. 3 (2013) 1033–1036.

[14] T. Thananatthanachon, T. Rauchfuss, Efficient route to hydroxymethylfurans from sugars via transfer hydrogenation, ChemSusChem 3 (2010) 1139–1141.

[15] a) T. Buntara, I. Melian-Cabrera, Q. Tan, J. L. G. Fierro, M. Neurock, J. G. de Vries, H. J. Heeres, Catalyst studies on the ring opening of tetrahydrofuran–dimethanol to 1,2,6-hexanetriol, Catal. Today 210 (2013) 106–116;

b) T. Buntara, S. Noel, P. Huat Phua, I. Melián-Cabrera, J. G. de Vries, H. J. Heeres, From 5-hydroxymethylfurfural (HMF) to polymer precursors: Catalyst screening studies on the conversion of 1,2,6-hexanetriol to 1,6-hexanediol, Top. Catal. 55 (2012) 612–619;

c) T. Buntara, S. Noel, P. Huat Phua, I. Melian-Cabrera, J. G. de Vries, H. J. Heeres, Caprolactam from renewable resources: catalytic conversion of 5-hydroxymethylfufural into caprolactone, Angew. Chem. Int. Ed. 50 (2011) 7083–7087; Angew. Chem. 123 (2011) 7221–7225.

[16] Y. Román-Leshkov, C. J. Barrett, Z. Y. Liu, J. A. Dumesic, Production of dimethylfuran for liquid fuels from biomass-derived carbohydrates, Nature 447 (2007) 982– 986;

[17] M. Chidambaram, A. T. Bell, A two-step approach for the catalytic conversion of glucose to 2,5 dimethylfuran in ionic liquids, Green Chem. 12 (2010) 1253–1262.

[18] J. Jae, W. Zheng, R. F. Lobo, D. G. Vlachos, Production of dimethylfuran from hydroxymethylfurfural through catalytic transfer hydrogenation with Ru supported on carbon, ChemSusChem 6 (2013) 1158–1162.

[19] Y. Zu, P. Yang, J. Wang, X. Liu, J. Ren, G. Lu, Y. Wang, Efficient production of the liquid fuel 2,5-dimethylfuran from 5-hydroxymethylfurfural over Ru/Co_3O_4 catalyst, Appl. Catal. B 146 (2014) 244–248.

[20] M. Chatterjee, T. Ishizaka, H. Kawanami, Hydrogenation of 5-hydroxymethylfurfural in supercritical carbon dioxide–water: A tunable approach to dimethylfuran selectivity, Green Chem. 16 (2014) 1543–1551.

[21] D. Scholz, C. Aellig, I. Hermans, Catalytic transfer hydrogenation/hydrogenolysis for reductive upgrading of furfural and 5-(hydroxymethyl)furfural, ChemSusChem 7 (2014) 268–275.

[22] G. H. Wang, J. Hilgert, F. H. Richter, F. Wang, H. J. Bongard, B. Spliethoff, C. Weidenthaler, F. Schüth, Platinum-cobalt bimetallic nanoparticles in hollow carbon nanospheres for hydrogenolysis of 5-hydroxymethylfurfural, Nat. Mater. 13 (2014) 293–300.

[23] T. S. Hansen, K. Barta, P. T. Anastas, P. C. Ford, A. Riisager, One-pot reduction of 5-hydroxymethylfurfural via hydrogen transfer from supercritical methanol, Green Chem. 14 (2012) 2457 –2461.

[24] a) T. D. Matson, K. Barta, A. V. Iretskii, P. C. Ford, One-pot catalytic conversion of cellulose and of woody biomass solids to liquid fuels, J. Am. Chem. Soc. 133 (2011) 14090–14097;
b) K. Barta, T. D. Matson, M. L. Fettig, S. L. Scott, A. V. Iretskii, P. C. Ford, Catalytic disassembly of an organosolv lignin via hydrogen transfer from supercritical methanol, Green Chem. 12 (2010) 1640– 1647;
c) K. Barta, G. Warner, E. S. Beach, P. T. Anastas, Depolymerization of organosolv lignin to aromatic compounds over Cu-doped porous metal oxides, Green Chem. 16 (2014) 191–196.

[25] a) K. Motokura, D. Nishimura, K. Mori, T. Mizugaki, K. Ebitani, K. Kaneda, A Ru-grafted hydrotalcite as a multifunctional catalyst for direct α-alkylation of nitriles with primary alcohols, J. Am. Chem. Soc. 126 (2004) 5662– 5663;
b) S. K. Sharma, P. A. Parikh, R. V. Jasra, Ru containing hydrotalcite as a solid base catalyst for C=C double bond isomerization in perfumery chemicals, J. mol. Catal. A 317 (2010) 27–33;
c) S. K. Sharma, K. B. Sidhpuria, R. V. Jasra, Ru containing hydrotalcite as a heterogeneous catalyst for hydrogenation of benzene to cyclohexane, J. mol. Catal. A 335 (2011) 65–70.

[26] H. B. Friedrich, F. Khan, N. Singh, M. van Staden, The Ru-Cu-Al-hydrotalcite-catalysed oxidation of alcohols to aldehydes or ketones, Synlett (2001) 0869–0871.

[27] F. Cavani, F. Trifir, A. Vaccari, Hydrotalcite-type anionic clays: Preparation, properties and applications, Catal. Today 11 (1991) 173–301.

[28] Q. Jiao, H. Liu, Y. Zhao, Z. Zhang, Preparation and application of Cu/Cr hydrotalcite-like compound, J. Mater. Sci. 44 (2009) 4422–4428.

[29] B. M. Nagaraja, V. Siva Kumar, V. Shashikala, A. H. Padmasri, S. Sreevardhan Reddy, B. D. Raju, K. S. Rama Rao, Effect of method of preparation of copper-magnesium oxide catalyst on the dehydrogenation of cyclohexanol, J. mol. Catal. A 223 (2004) 339–345.

[30] M. Dixit, M. Mishra, P. A. Joshi, D. O. Shah, Physico-chemical and catalytic properties of Mg–Al hydrotalcite and Mg–Al mixed oxide supported copper catalysts, J. Ind. Eng. Chem. 19 (2013) 458– 468.

[31] G. S. Macala, T. D. Matson, C. L. Johnson, R. S. Lewis, A. V. Iretskii, P. C. Ford, Hydrogen transfer from supercritical methanol over a solid base catalyst: A model for lignin depolymerisation, ChemSusChem 2 (2009) 215–217.

[32] a) P. L Gai, E. D Boyes, electron microscopy in heterogeneous catalysis, CRC Press, Boca Raton, 2003, p. 180;
b) A. MartÍnez-Arias, A. B. HungrÍa, G. Munuera, D. Gamarra, Preferential oxidation of CO in rich H_2 over CuO/CeO_2: Details of selectivity and deactivation under the reactant stream, Appl. Catal. B 65 (2006) 207–216.

Supporting Information

All chemicals and solvents were used as received. 5-methyl-2-furanmethanol (MFM) 97 % was purchased from Acros Organics. 2,5-dimethylfuran (DMF, 99 %), 5-methylfurfural (MF, 99 %), 5-(hydroxymethyl)furfural (HMF, ≥99 %), 2,5-dimethyltetrahydrofuran (DMTHF 96 %, mixture of *cis* and *trans*), sodium carbonate (≥99.5 %), aluminum chloride hexahydrate (99 %), magnesium chloride hexahydrate (≥99%), copper(II) nitrate hemi(pentahydrate) (≥98 %), Ni(II) chloride hexahydrate (≥98 %) and Ru chloride hydrate were purchased from Sigma Aldrich. 2,5-furandimethanol (FDM, 98 %) was purchased from Toronto Research Chemicals. Tetrahydrofuran-2,5-diyl-dimethanol (THFDM) was supplied by GLSyntech.

GC-MS-FID analyses were performed with a Hewlett Packard 5890 series II plus with a Quadrupole Hewlett Packard 5972 MSD and a FID. The GC is equipped with a 60 × 0.25 mm i.d. and 0.25 μm film Restek RTX-1701 capillary column and a 1:1 split ratio to the MSD and FID was set. Temperature of injector and detector were set at 250 °C and 285 °C, respectively. The program temperature starts from 40 °C

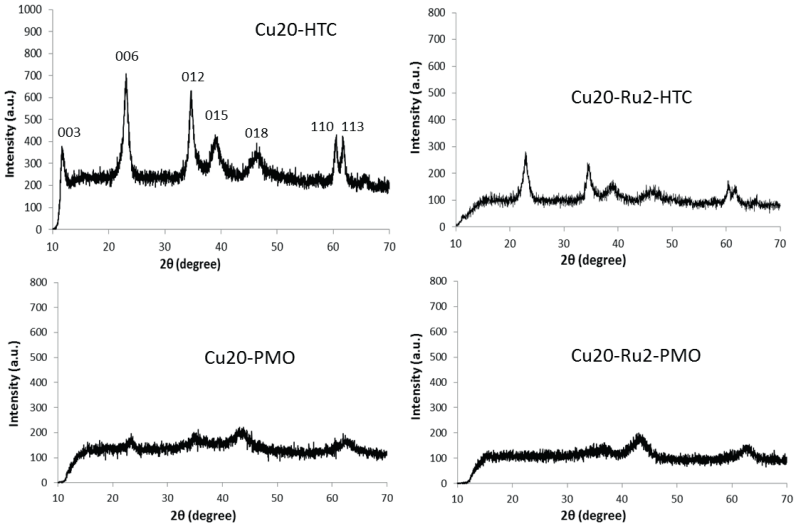

Figure S1. XRD patterns of the hydrotalcite (HTC) precursors and the corresponding porous metal oxides (PMO), Cu20-PMO and Cu20-Ru2-PMO, after calcination. Crystallographic planes are indicated for Cu20-HTC and are agreement with the literature. Amorphous PMOs only show residual XRD signals corresponding to MgO diffraction.

(10 min) and is then increased up to 250 °C with a heating rate of 10 °C/min.

Hydrotalcite samples were calcined in a Linn High Therm oven with controller G 800 P at 460 °C for 24 h. ^{1}H and ^{13}C NMR spectra were recorded on a Varian AMX400 spectrometer. Powder Xray analysis was performed on a Bruker XRD diffractometer using Cu Kα radiation and the spectra were recorded in the 2θ angle range of 10 °–70 °.

The TEM images were recorded on a FEI T20 electron microscope with a slow scan CCD camera at 200 keV. The solid samples were suspended in ethanol and deposited on a plain carbon coated copper grids. The surface area was calculated using the standard BET method (S_{BET}).[1] Microanalyses were performed on a Perkin Elmer instrument (Optima 7000DV). Kinetic modeling of the HMF conversion to the main intermediates and DMF was performed with DynaFit 4.[2]

Table S1. Selectivity values (determined by GC-FID) in the hydrogenation of HMF at mild temperatures for the optimized production of FDM [a]

Entry	Catalyst (-PMO)	T (°C)	FDM	THFDM	DMF+ DMTHF	MF	MFM	THMFM	1,2-HD	1,2,6-HT	Others
1 [b]	Cu20	80	90	0	0	4	0.2	0	0	0	0.8
2	Cu20	100	99.2	0	0.1	0.1	0.1	0	0	0	0.3
3	Cu20	120	89	0	0.7	5	1	0	0	0	3
4	Cu20	140	79	0.3	4	4	5	0.4	2	2	3
5 [c]	Cu20	100	91	0.3	0.1	6	0.6	0	0.2	0.2	0.8
6	Cu20-Ru2	100	98	0	0.2	0.8	0.2	0	0	0	0.3

[a] Reaction conditions: 0.5 g HMF, 0.1 g catalyst, 0.250 mL toluene (internal standard), 20 mL ethanol, 3 h reaction time, 50 bars H_2 (HMF conversion was >99 % in all entries). [b] HMF conversion was 95 %. [c] Reaction time was 6 h.

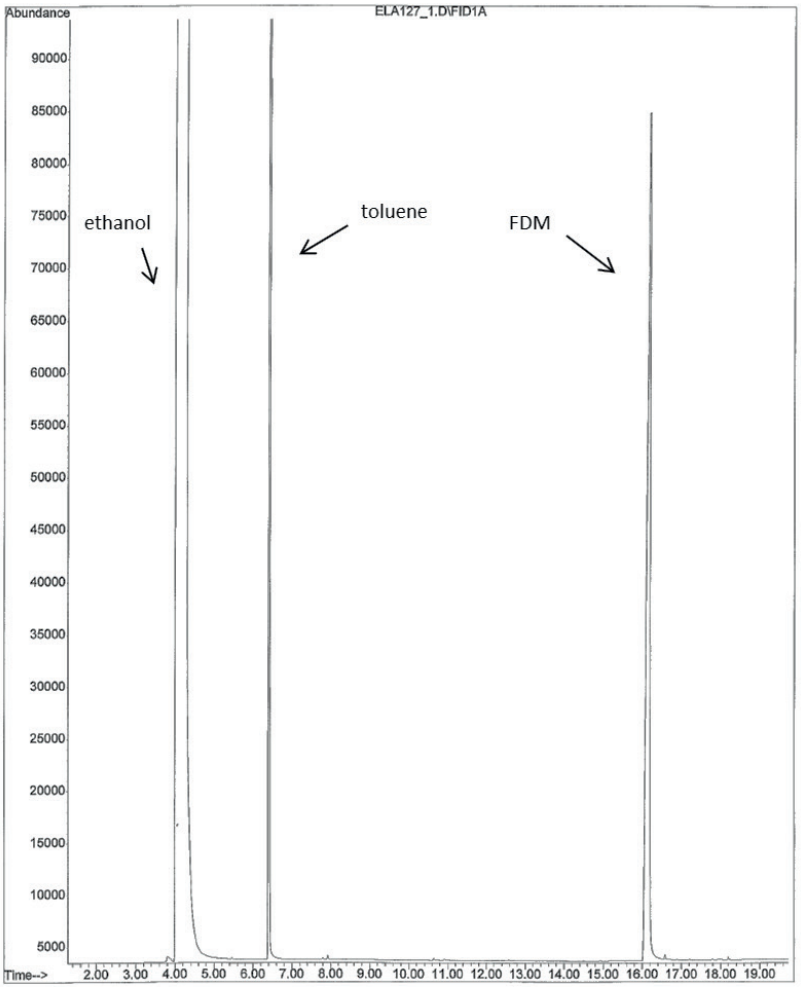

Figure S2. GC trace of FDM production under optimized conditions (>99 %, Table S1, entry 2)

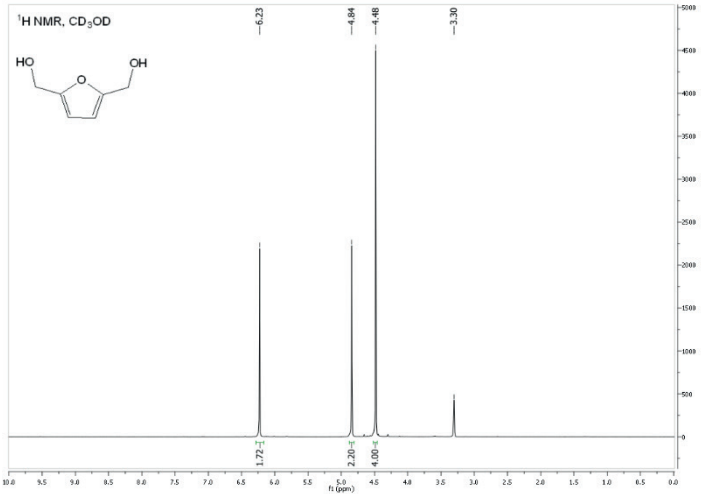

Figure S3. ^{1}H NMR spectrum of FDM (CD_3OD, 400 MHz)

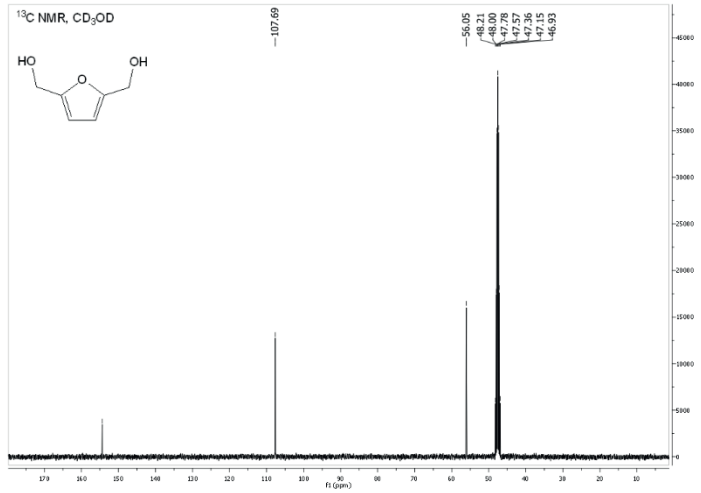

Figure S4. ^{13}C NMR spectrum of FDM (CD_sOD, 100 MHz)

Table S2. Selectivity values (determined by GC-FID) in the temperature screening for the optimization of DMF production with Cu20-PMO catalyst [a]

T (°C)	FDM	THFDM	DMF+ DMTHF	MF	MFM	THMFM	1,2-HD	1,2,6-HT	Others
100	91	0.1	0.1	6	1	0	0	0	1
140	60	1	9 (8+1)	3	12	1	5	5	4
180	30	3	28 (19+9)	<1	24	4	7	1	3
220	<1	3	69 (54+15)	0	6	4	7	<1	11

[a] Reaction conditions: 0.5 g HMF, 0.1 g Cu20-PMO, 0.250 mL toluene (internal standard), 20 mL ethanol, 6 h, 50 bars H_2 (HMF conversion was >99 % in all entries).

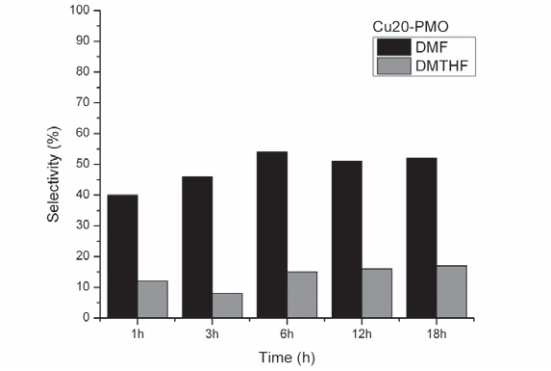

Figure S5. Individual DMF and DMTHF selectivities from the hydrogenation of HMF at 220 °C with Cu20-PMO at different reaction times

Table S3. Selectivity values (determined by GC-FID) with Cu20-PMO and Cu20-Ru2-PMO catalysts in different solvents and catalyst loading at 220 °C[a]

Entry	Catalyst (PMO)	Solvent	DMF+DMTHF (%)		THFDM	MFM	THMFM	1,2-HD	2-hexanol	Others
			Selectivity	Yield						
1	Cu20	EtOH	72(61+11)	66	2	2	2	3	<1	18 (12)[e]
2	Cu20	*i*PrOH	81(64+17)	77	3	-	3	5	3	5
3[f]	Cu20	*i*PrOH	69(59+10)	60	2	10	3	3	1	12
4[g]	Cu20	*i*PrOH	80(70+10)	75	1	2	1	4	1	11
5	Cu20-Ru2	EtOH	84(65+19)	80	1	<1	3	3	<1	8
6	Cu20-Ru2	*i*PrOH	81(63+18)	79	1	-	3	7	5	3
7[b]	Cu20-Ru2	*i*PrOH	84(65+19)	78	1	-	3	6	3	3
8[c]	Cu20-Ru2	*i*PrOH	84(65+19)	81	2	1	7	2	2	2
9[d]	Cu20-Ru2	MeOH	18(17+1)	17	1	2	1	3	-	75
10	Cu20-Ru2	MIBC	70(54+16)	n.d.	2	-	3	8	10	7

[a] Reaction conditions: 0.5 g HMF, 0.250 g catalyst, 0.250 mL toluene (internal standard), 20 mL solvent, 220 °C, 6 h (unless otherwise stated), 50 bars H_2 (HMF conversion was >99 % in all entries). [b] Reaction time was 4 h. [c] Reaction time was 1 h. [d] Reaction was carried out with 0.100 g of catalyst. Methyl ether species account for 56 % in the column 'others'. [e] Number in brackets refers to selectivity values for all other minor components excluding two main components at 7.58 and 7.86 min. [f] The HMF concentration was increased to 8 wt %, maintaining the same solvent volume (1.258 g HMF/20 mL *i*PrOH). [g] The HMF concentration was increased to 10 % wt, maintaining the same solvent volume (1.572 g HMF/20 mL *i*PrOH) and reaction time was 18 h.

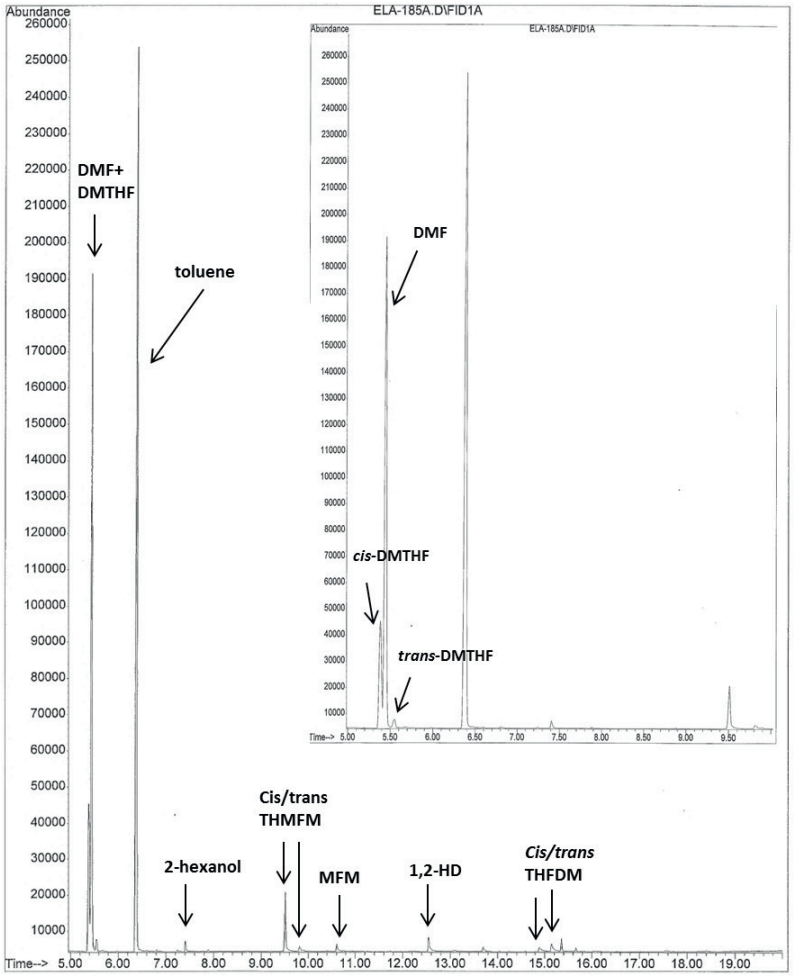

Figure S6. GC trace with labeled main components in the reaction for the optimized production of DMF (Table S3, entry 6)

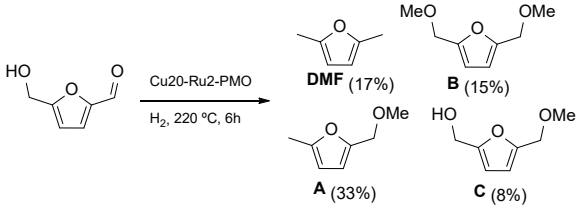

Scheme S1. Hydrogenation of HMF in methanol (only main products are shown for sake of clarity)

Reaction conditions: 0.5 g HMF, 0.1 g Cu20-Ru2-PMO, 220 °C, 50 bar H_2, 6 h.

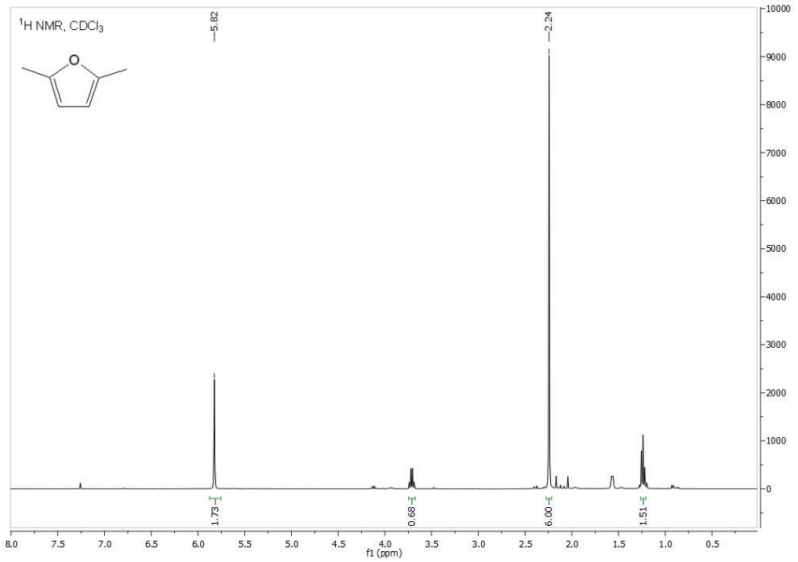

Figure S7. ^{1}H NMR spectrum of DMF isolated by distillation ($CDCl_3$, 400 MHz)

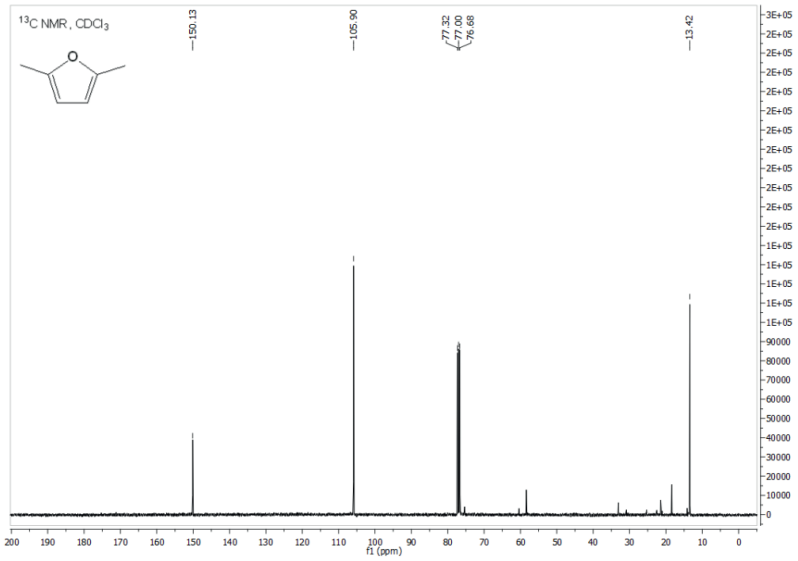

Figure S8. ^{13}C NMR spectrum of DMF isolated by distillation ($CDCl_3$, 100 MHz)

Table S4. Elemental analysis of Cu20-Ru2-PMO (after the reaction) and leaching analysis of the solution [a]

Catalyst	Before the reaction	After the reaction	Leaching analysis (mg/L)
Cu20-Ru2-PMO	Cu/Mg/Al/Ru= 0.61/2.33/0.98/0.02	Cu/Mg/Al/Ru= 0.60/2.32/0.98/0.02	Cu <1, Al <1, Mg <1, K <1 Na 1, Ru <1

[a] Experimental conditions: 0.500 g HMF, 0.250 g catalyst, 0.250 mL toluene (internal standard), 220 °C, 4h, 20 mL *i*PrOH, 50 bars H_2.

Table S5. Selectivity and yield values (determined by GC-FID) with Cu20-PMO at 140 °C

t (h)	FDM	DMF+DMTHF	MF	MFM	THMFM	1,2-HD	1,2,6-HT	Others
1	89	1	5	2	0.1	0.6	0.3	<1
3	79	4 (3+1)	4	5	0.3	3	2	2.4
6	60	9 (8+1)	3	12	1	5	5	4
18	28	30 (25+4)	1	22	2	4	2	9

[a] Reaction conditions: 0.5 g HMF, 0.1 g Cu20-PMO, 0.250 mL toluene (internal standard), 20 mL ethanol, 220 °C, 50 bars H_2 (HMF conversion was >99 % in all entries).

Table S6. Selectivity and yield values (determined by GC-FID) with Cu20-PMO catalyst at 220 °C[a]

	DMF+DMTHF									
t [h]	Selectivity (%) [b]	Yield (%) [c]	FDM	THFDM	MFM	THMFM	1,2-HD	1,2,6-HT	EMMF	Others[b]
1	52 (40+12)	49	7	3	17	4	7	2	<1	8 (6)
3	54 (46+8)	54	1	3	18	2	7	1	<1	14 (7)
6	69 (54+15)	66	<1	3	6	4	7	<1	<1	11 (8)
12	67 (51+16)	65	0	3	3	5	9	1	1	12 (11)
18	69 (52+17)	65	0	2	1	5	5	<1	3	14 (12

[a] Reaction conditions: 0.5 g HMF, 0.1 g Cu20-PMO, 0.250 mL toluene (internal standard), 20 mL ethanol, 220 °C, 50 bars H_2 (HMF conversion was >99% for all entries). [b] Numbers in brackets refer to selectivity values for all other minor components excluding two main components at 7.58 and 7.86 min.

Table S7. Characterization of pore size and volume of Cu20-PMO and Cu20-Ru2-PMO catalysts

Catalyst	Composition	Pore volume (cm^3/g)	Average pore size (Å)
Cu20-PMO	$Cu_{0.59}Mg_{2.34}Al_{1.00}$	0.96	197
Cu20-Ru2-PMO	$Cu_{0.61}Mg_{2.33}Al_{0.98}Ru_{0.02}$	0.88	169

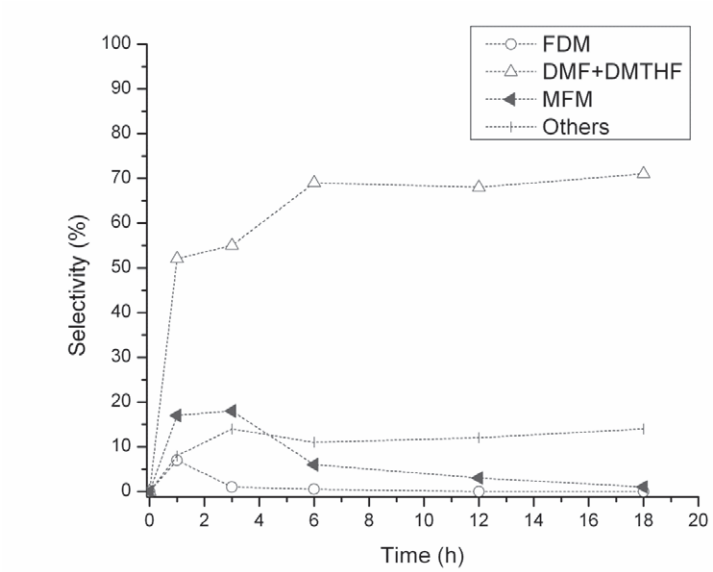

Figure S9. Plot of selectivities to major products, including unidentified compounds, *versus* reaction time from the hydrogenation of HMF at 220 °C with Cu20-PMO

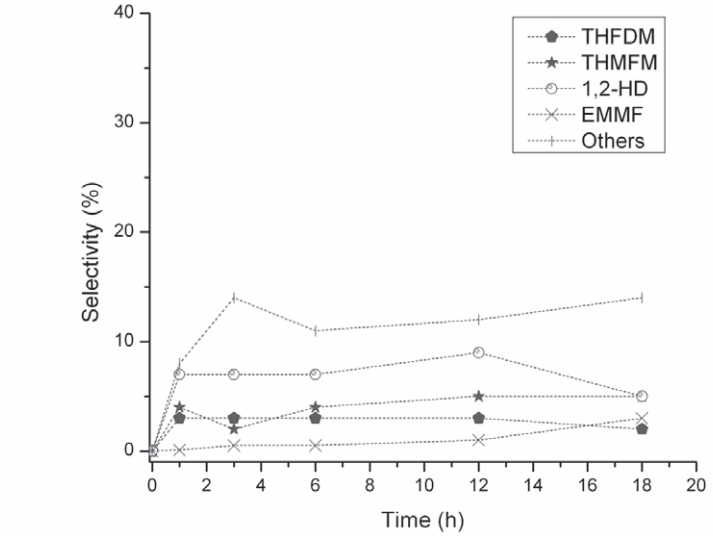

Figure S10. Plot of selectivities to minor products *versus* reaction time from the hydrogenation of HMF at 220 °C with Cu20-PMO

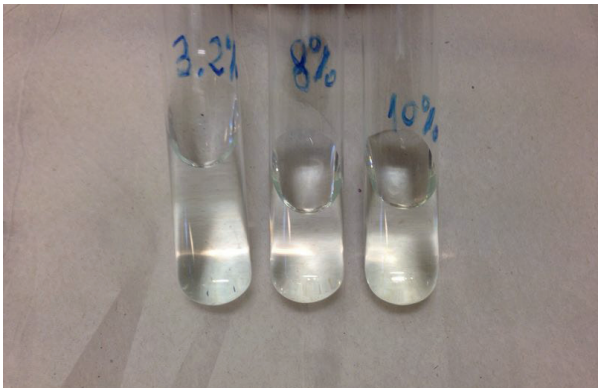

Figure S11. Clear and colorless solutions obtained after dissolving the solid catalyst residue (obtained at different HMF starting concentration, 3.2 %, 8 % and 10 %) in HNO_3

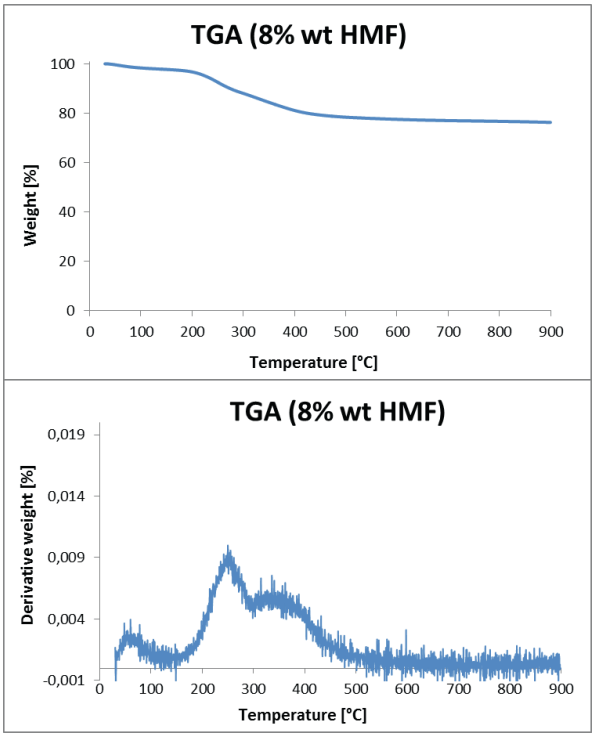

Figure S12. TGA traces of the solid residue obtained after reaction with 8 % starting HMF concentration

Reaction conditions: 1.26 g HMF, 0.25 g Cu20-PMO, 20 mL isopropanol, 6 h, 50 bar H_2.

References

[1] S. Brunauer, P. H. Emmett, E. Teller, Adsorption of gases in multimolecular layers, J. Am. Chem. Soc. 60 (1938), 309–319.

[2] P. Kuzmicˇ, Program DYNAFIT for the analysis of enzyme kinetic data: Application to HIV proteinase, Anal. Biochem. 237 (1996) 260–273.

Chapter 3

Copper–zinc alloy nanopowder: a robust precious-metal-free catalyst for the conversion of 5-hydroxymethylfurfural

Abstract

Noble-metal-free copper–zinc nanoalloy (<150 nm) is found to be uniquely suited for the highly selective catalytic conversion of 5-hydroxymethylfurfural (HMF) to potential biofuels or chemical building blocks. Clean mixtures of 2,5-dimethylfuran (DMF) and 2,5-dimethyltetrahydrofuran (DMTHF) with combined product yields up to 97 % were obtained at 200–220 °C using 20–30 bar H_2. It is also possible to convert 10 wt % HMF solutions in CPME, with an excellent DMF yield of 90 %. Milder temperatures favor selective (95 %) formation of 2,5-furandimethanol (FDM). The one-pot conversion of fructose to valuable furan-ethers was also explored. Recycling experiments for DMF production show remarkable catalyst stability. Transmission electron microscopy (TEM) characterization provides more insight into morphological changes of this intriguing class of materials during catalysis.

Keywords: hydrogenation, 5-hydroxymethylfurfural, HMF, building blocks, 2,5-furandimethanol, FDM, 2,5-dimethyltetrahydrofuran (DMTHF), catalyst, copper-zinc.

G. Bottari, A. J. Kumalaputri, K. K. Krawczyk, B. L. Feringa, H. J. Heeres and K. Barta, Copper-zinc alloy nanopowder: a robust precious-metal-free catalyst for the conversion of 5-hydroxymethylfurfural, ChemSusChem 2015, 8, 1323–1327

3.1 Introduction

The development of new, robust, and efficient catalysts, primarily ones that consist of earth-abundant metals, is of crucial importance and will enable the sustainable chemical conversion of nonedible lignocellulosic biomass resources[1] or platform molecules derived from such resources.[2] One of the most versatile platform chemicals is 5-hydroxymethylfurfural (HMF),[2,3] which can be readily obtained from sugars.[3b] Various conversion routes have been investigated[4] and among these, reductive methods are of special importance.[4a] A variety of new methodologies have been developed for selective carbonyl reduction to give 2,5-furan dimethanol (FDM) at milder temperatures.[5] More extensive deoxygenation of HMF to potential biofuels or the fuel additive 2,5-dimethylfuran (DMF) has been first proposed by Dumesic.[6a] A number of very efficient catalysts, mainly based on Ru[6] or other noble metals, have been developed since,[2,7] including very efficient examples that use milder temperatures.[8] In contrast, only a few non-precious-metal-based catalysts have been reported. Recently Fu et al. described a Ni-W carbide catalyst that gave up to 96 % DMF yield.[9] Zhu et al. reported on Raney Ni catalysts with good DMF yields (88.5 %) at 180 °C.[10] Despite these promising results, the development of inexpensive, precious metal-free, and highly effective catalysts for this transformation is still highly desired.

Herein, we report on the use of a robust, sustainable, and commercially available new catalyst class that allows for modular and highly selective conversion of HMF to either FDM (up to 95 %) or DMF (up to 90 %). Under optimized conditions remarkably clean mixtures of the two biofuels DMF and DMTHF (97 % yield) can be obtained.

Previously we reported on the use of copper-doped porous metal oxides[11] in the conversion of HMF and other biomass resources.[12] Although a promising combined DMF and DMTHF[11b] yield of about 80 % was obtained, ring-opening processes could not be completely prevented owing to the strong interaction of the relatively basic support with HMF and derived intermediates FDM and MFM (shown in Scheme 1).

Thus, we set out to investigate other suitable classes of copper-containing catalysts, preferably ones that do not readily undergo deactivation (e.g., by sintering) at elevated temperatures,[13] and possess a relatively large surface area. We turned our attention to commercially available copper nanopowders, which are relatively unexplored in catalysis.

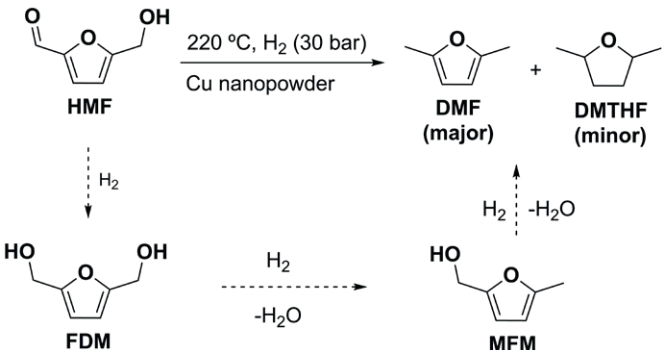

Scheme 1. Hydrogenation/hydrogenolysis of HMF to DMF and DMTHF mixture (dashed arrows show the simplified pathway involving intermediatte FDM and MFM)

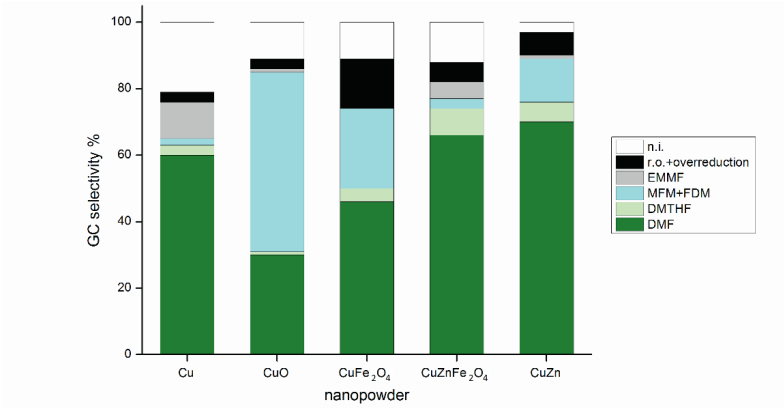

Figure 1. Comparison of the product distribution (GC selectivities) obtained in the HMF hydrodeoxygenation over different copper nanopowders.

Conditions: 0.500 g HMF, 0.100 g copper nanopowder, EtOH (20 mL), 220 °C, 30 bar H_2, 6 h (n.i: not identified; r.o.: ring-opening products). The corresponding numerical values are displayed in Table S2.

3.2 Results and discussion

We first screened commercial copper-containing nanopowders of different composition (characterized by elemental analysis and XRD, see Table S1 and Figure S1) in the conversion of HMF to DMF (Scheme 1). All reactions were carried out in ethanol at 220 °C using 30 bar H_2 pressure for 6 h (Figure 1; Supporting Information, Table S2).

Complete or nearly complete (95 % with $CuZnFe_2O_4$) conversion of HMF was achieved with all tested nanopowders, but variations in the composition of the obtained product mixtures were significant. Copper nanopowder showed a good (55 %) DMF+DMTHF yield, with a DMF/DMTHF ratio of 20:1. Ether 2-(ethoxymethyl)-5-methylfuran (EMMF) was found as a main reaction product, and a small amount of ring-opening and hydrogenation products were also seen.

In this run many smaller peaks were also detected, which accounted for about 20 % of unidentified products, likely caused by the relatively high loading of copper (20 wt %). As a comparison with CuO, a low DMF yield was found, and the biggest fraction of the product mixture (50 %) consisted of FDM and MFM, indicating an overall slower reaction. Similarly, mixed copper-iron oxide nanopowder led to only 45 % product. $CuZnFe_2O_4$ of similar composition performed better (73 % product yield), however 12 % of the products still remained unidentified. Best among the tested catalyst was the CuZn nanoalloy, which afforded 75 % DMF+DMTHF yield with a DMF/DMTHF ratio of 14:1, while the two main 'precursors' to DMF (FDM and MFM) still represented 13 % of the product mixture after 6 h reaction time. Overall, the cleanest product mixtures were obtained with this catalyst since only 3 % of the products were unidentified.

Thus CuZn nanopowder was selected for further studies (Supporting Information, Table S3). First, the reaction time was prolonged to 18 h to ensure a full conversion of intermediates (FDM and MFM). Indeed, the product yield improved from 75 % to 83 %. Adjusting the H_2 pressure allowed for a further small increase to a very good, 88 % product yield. The solvent engaged to a small extent in side reactions, as evidenced by the formation of 5 % EMMF (Table S3 in Supporting Information, Scheme 1). To minimize these side processes and improve product yields even further, bulkier alcohol solvents were screened, as was earlier reported with copper porous metal oxides.[11b] Indeed, with *i*PrOH and methyl isobutyl carbinol (MIBC) excellent product yields were obtained (91 % and 93 % respectively). No corresponding etherification products were observed with bulkier alcohols. The quantity of unidentified compounds was below 3 %. Interestingly, the DMF/DMTHF ratio reduced from 14:1 in EtOH to 4:1 in MIBC (Figure 2).

Ethereal solvents such as 2-MeTHF (2-methyltetrahydrofuran) and CPME (cyclopentyl methyl ether) were also tested. 2-MeTHF, which is directly accessible from renewable resources,[14] performed comparably high to MIBC and *i*PrOH. To our delight CPME, a favorable solvent

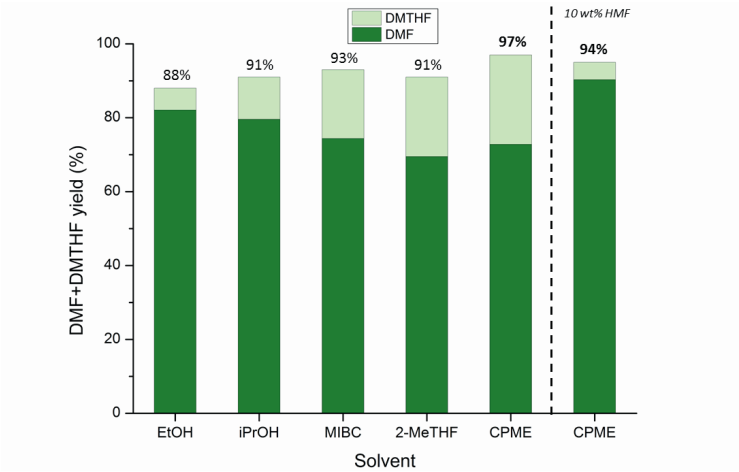

Figure 2. Effect of different solvents for DMF+DMTHF production

(0.500 g HMF, 0.100 g CuZn, 220 °C, 18 h, 20 bar H_2). On the right, the 10 wt % HMF experiment was conducted in CPME (1.72 g HMF, 0.2 g CuZn, 200 °C, 6 h, 20 bar H_2).

with low toxicity and negligible peroxide formation[15] afforded the highest DMF+DMTHF yield (97 %; see Supporting Information Figure S8 for the corresponding GC trace). This practically means that upon HMF conversion under these conditions, analytically pure fuel mixtures were obtained.

In both these solvents, the DMF/DMTHF ratio was lower than in ethanol. Figure 3 shows an overview of the increase of the overall DMF+DMTHF yield from ethanol to CPME; however, at the expense of the DMF/DMTHF ratio.

The reaction conditions were further optimized in CPME. The reaction time could be reduced to 3 h at 200 °C with no apparent change in product yield, but increase in DMF content (Table 1, entries 1–3). To our delight, even concentrated HMF solutions (1 wt %) were cleanly converted into a mixture of DMF and DTMHF (94 % yield; entry 4 and Figure 2) in CPME, while DMF yield was 90 %. Similarly a 10 wt % HMF solution was converted in MIBC at 220 °C and longer reaction time, albeit with slightly lower DMF+DMTHF yield (88 %). Interestingly, a 5 wt % catalyst loading (3 wt % Cu), typical for noble metal catalysts was adopted in CPME solvent with full substrate conversion, 89 % combined fuel yield, and excellent DMF/DMTHF ratio of 35:1. This holds much promise for future upscaling, and continuous operation of this system.

Table 1. DMF+DMTHF production in CPME solvent

Entry [a]	t (h)	T (°C)	DMF+DMTHF yield (%) [b]	DMF/DMTHF ratio [b]
1	6	220	97	3:1
2	6	200	97	5:1
3	3	200	96	5:1
4 [c]	6	200	94	18:1
5 [d]	18	220	89	35:1

[a] Reaction conditions: 0.500 g HMF, 0.100 g CuZn, 20 mL CPME, 0.250 mL decane, 20 bar H_2. Full HMF conversion. [b] Determined by GCFID. [c] 10 wt % HMF concentration (1.72 g HMF in 20 mL CPME) and 0.2 g catalyst were used (7 % Cu/HMF ratio). [d] 2.00 g HMF in 30 mL CPME, 40 bar H_2, and 0.1 g catalyst were used (3 % Cu/HMF ratio).

In addition, 5-(ethoxymethyl)furfural (EMF) was used as starting material instead of HMF in CPME (220 °C, 18 h, 20 bar H_2). This ether also underwent hydrogenolysis, resulting in good DMF+DMTHF yield (78 %). The corresponding EMMF, a potential fuel additive was detected as second major product (10 %). This is promising regarding possible DMF production directly from hexoses, through HMF ethers.[16]

The catalyst residues from the 10 wt % runs in CPME and MIBC were recovered and analyzed by transmission electron microscopy (TEM), and compared with the fresh catalyst (Figure S4). The spent catalyst recovered from the run in CPME (Table 1, entry 4) mainly showed agglomerated particles with a core-shell structure. However, after reaction in MIBC (Table 3, entry 7), spike-shaped objects were visible on the catalyst surface in addition to coagulated rounded particles, also present in the fresh catalyst. For further direct morphological comparison, the reaction was also carried out in CPME using the same experimental conditions as in MIBC (10 wt % HMF, 220 °C, 18 h). No spiked objects were detected and cleaner product mixtures and higher DMF+DMTHF yields were observed in CPME. This shows that changes in catalyst morphology are dependent on the nature of the solvent and might influence catalytic activity.

The local composition of the spiked nanostructures was determined by energy dispersive X-ray (EDX) analysis, which revealed that these mostly comprise zinc (>90 %) as highlighted by elemental analysis and lattice constant value (Figure 3 and Supporting Information S5).

In the bulk, core-shell structures in which the zinc is covering highly copper-dense particles were observed. These morphological changes in the alloy structure are probably due to copper migration, which becomes relevant above 200 °C.[17] Despite these variances, only

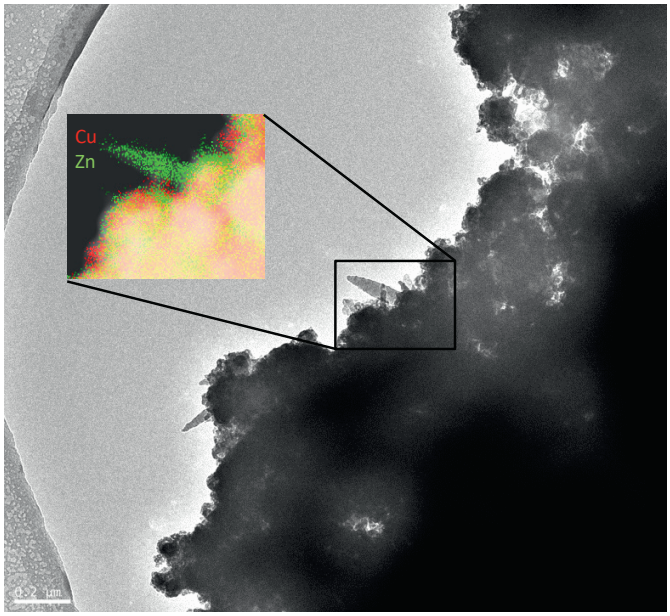

Figure 3. TEM image of spent catalyst after the run at 10 wt % HMF concentration in MIBC (Table S3, entry 7)

In the insert, a magnification of a spikedlike object and the corresponding elemental mapping by EDX are provided

a slight difference between the bulk composition of the spent catalyst (MIBC) and the fresh catalyst could be determined by ICP analysis (Supporting Information Table S7), showing practically no metal loss into the solution. In addition, combustion analysis detected an elevated carbon content (0.6 %; Supporting Information Table S7) in the spent catalyst (MIBC), and accordingly thermogravimetric analysis (Supporting Information, Figure S2) showed a slight (<2 %) decrease in weight between 100 °C and 400 °C, which can be attributed to adsorbed organics.

Recycling experiments were successfully performed in both these solvents, with better performance in CPME. Experiments in MIBC were carried out with 0.5 g HMF and 0.2 g CuZn at 220 °C for 15 h (Supporting Information Figure S7 and Table S9). Interestingly, with decreasing activity, the DMF/DMTHF ratio increased up to 30:1, the 2nd cycle representing an almost perfect DMF selectivity. After the 2nd cycle, the product yield gradually decreased from ca. 90 % (1–2nd cycle) to 17 % (4th cycle). Notably, calcination of the spent catalyst after

the 4th run at 500 °C for 6 h recovered the catalytic activity and even the DMF/DMTHF ratio in the 5th run was precisely identical to the initial value. Accordingly, TEM analysis of the catalyst recovered after the 4th run showed core-shell structures (Supporting Information, Figure S6), not present in the original solid; this morphological change together with the presence of organics adsorbed on the catalyst surface might be the cause of deactivation. After calcination, the morphology of the catalyst (Figure S6) displays a substantial regeneration of the original alloy structure. The transition from a core-shell structure into a homogeneous alloy has already been reported.[18]

The catalyst has proven even more stable in CPME (Figure S7 and Table S10). Recycling tests in CPME were performed at 220 °C using 0.5 g HMF and 0.2 g CuZn nanoalloy. No relevant loss in catalytic activity was observed in the first 5 cycles (ca. 90 %), then the DMF+DMTHF yield decreased to 66 % after the 6th cycle, and 3 % product yield was observed in the 7th cycle, corresponding to a total of 3.5 g HMF converted. At this point, calcination was performed and the initial activity regained. From the above experiments it can be concluded that CuZn is a robust and highly active catalyst for the conversion of HMF to DMF, suitable for continuous-flow setup.

The specific roles of the copper and zinc metals in catalysis, or their oxides, which might also be present in smaller amounts, has yet to be elucidated. Recent photoelectron spectroscopy studies reported the formation of zinc oxide islands on particle surface in CuZn nanoalloys.[19] The presence of the ZnO phase was confirmed during XRD analysis of the CuZn nanopowder (Figure S1). The beneficial effect on DMF production of acidic Zn^{2+} sites contained in Pd/Zn/C catalysts was recently proposed by Abu Omar et al.[20] It seems plausible that active Cu^0 species are responsible for hydrogenation/hydrogenolysis with the assistance of Lewis-acidic ZnO sites. Similar synergistic effects were observed in a recent catalytic application.[21] Cooperative effect in bimetallic noble metal catalysts designed for HMF to DMF conversion has been recently reported.[22]

Particle size is a crucial parameter, and determining ideal size ranges is essential for catalytic application of 'brasses'.[5d,23,27] We have briefly addressed this point by comparing the catalytic activity of commercially available CuZn alloys of various sizes. Indeed, CuZn alloys with 25–250 μm and <25 μm particle size showed low activity at 220 °C for 6 h in EtOH, thus it appears that the <150 nm size is crucial. For future studies, several procedures for the synthesis of different nanosized CuZn structures with a bottom-up approach are available.[23]

Another important aspect, using the commercially obtained CuZn nanopowder, is the reproducibility of results regarding batch to batch variations. No significant variation (within 6 %) in DMF selectivities was observed when using four different batches from two different suppliers (Supporting Information Table S8).

Next, the copper zinc nanopowder was tested in the hydrogenation of HMF at mild temperature to provide useful diol building blocks (Scheme 2).

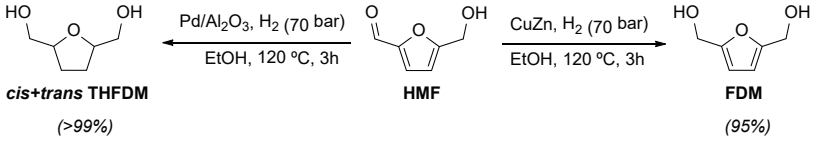

Scheme 2. Selective formation of useful diol building blocks from HMF

It is known that α,ω-diols, for example, 1,6-hexanediol are important polymer precursors.[24] A screening of various commercial catalysts was carried out in ethanol at 120 °C for 3 h (for detail see Supporting Information Table S5-S6). All catalysts prefentially afforded either THFDM (2,5-tetrahydrofurandimethanol), depending on compositions. The best FDM selectivity (95 %; Supporting Information, Figure S9 for GC trace) was achieved with the CuZn nanoalloy while >99 % THFDM, was obtained over Pd/Al_2O_3 as a mixture of cis and trans isomer in 9:1 ratio (Supporting Information, Table S5, entry 7; Figures S10–S12).

Given the excellent performance of the CuZn nanoalloy in FDM formation, we next attempted the more challenging one pot dehydration/hydrogenation reaction starting directly from fructose. An elegant approach for obtaining HMF and its ethers from fructose in isopropanol solvent has recently been reported.[25] First, fructose dehydration was conducted at 120 °C in iPrOH using different acid resins. HMF (4) and the corresponding isopropyl ether (5) were the main products, their ratio being dependent on the type of acidic catalyst used (Scheme 3; Supporting Information, Table S11).

Amberlyst 15 and Nafion SAC-13 preferentially afforded HMF while with Dowex 50WX8 resin ether, 5 was found as main product. Attempts to hydrogenate the crude mixtures with CuZn nanopowder after removal of the acidic resin by simple filtration were moderately successful. 1, 2, and 3 were obtained in modest yields (20 % in both

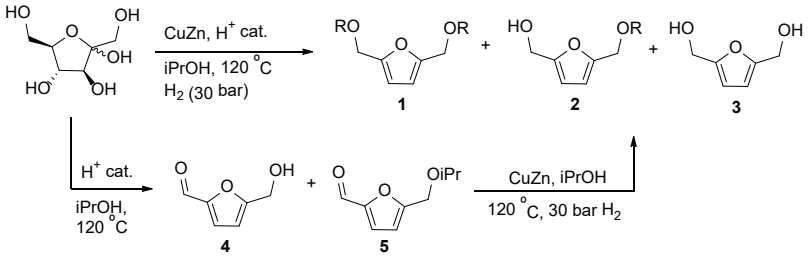

Scheme 3. One-pot and two-step strategies for the valorization of fructose in iPrOH

cases, Table S12) when a mixture of 4 and 5 obtained by dehydration with Nafion SAC-13 and Amberlyst 15 were hydrogenated using 120 °C and 30 bar H_2. Interestingly, the corresponding one-pot process starting directly from fructose with CuZn catalyst and Nafion SAC-13 or Amberlyst 15 (Supporting Information, Table S13) was more successful. In this case, fructose conversion was 96 % using Nafion SAC-13 and 1 and 2 were found as only products in 1 % and 33 % yields, respectively. With Amberlyst 15, a good combined 50 % yield of 1 and 2 was observed at full fructose conversion, in addition 7 % FDM was detected. These results compare well with the yields found in the literature using noble metal catalysts. [26]

3.3 Experimental section

General procedure for hydrogenation reactions: in a typical experiment, a glass insert containing 5-(hydroxymethyl)furfural (0.500 g), the catalyst (0.100 g) and toluene or decane (0.250 mL, internal standard) in the appropriate solvent (20 mL) was placed in a 100 mL stainless-steel Parr reactor. After purging 3 times with H_2, the reactor was pressurized at the desired pressure, heated, and stirred with a mechanical stirrer (600 rpm). After reaction, the reactor was cooled down to room temperature and the mixture was filtered and injected into a GC-MS-FID to determine conversion, product selectivity, and yield (by internal standard method). For characterization of the spent catalyst, the reaction mixture was centrifuged and the solid was washed two additional times with acetone and dried at 110 °C for 6 h. Recycling experiments are described in detail in the Supporting Information.

3.4 Conclusions

In conclusion, a noble-metal-free copper–zinc nanoalloy is applied for the first time in the highly selective hydrodeoxygenation of HMF to biofuels (up to 97% DMF+DMTHF yield) and diol building blocks (up to 95% FDM). Alloys play a crucial role in heterogeneous catalysis, however, 'nanobrasses' are not yet explored in catalysis.[5d,27] Recent reports identify CuZn alloys as promising systems for methanol[23a] and dimethylether synthesis.[21] Based on these studies and the results reported in this paper, we foresee a more general use of 'nanobrasses' in the conversion of renewable resources in the future.

Acknowledgements

The authors acknowledge support from the European Commission's Framework Programme 7, through the Marie Curie IEF scheme. We are also grateful to Dr. Marc Stuart for the TEM and EDX measurements.

References

[1] a) M. Sankar, N. Dimitratos, P. J. Miedziak, P. P. Wells, C. J. Kiely, G. J. Hutchings, Designing bimetallic catalysts for a green and sustainable future, Chem. Soc. Rev. 41 (2012) 8099–8139;
b) C. O. Tuck, E. Pérez, I. T. Horváth, R. A. Sheldon, M. Poliakoff, Valorization of biomass: Deriving more value from waste, Science 337 (2012) 695–699;
c) Catalysis for Renewables (Eds.: G. Centi, R. A. van Santen), Wiley-VCH, Weinheim, 2007.

[2] a) C. Chatterjee, F. Pong, A. Sen, Chemical conversion pathways for carbohydrates, Green Chem. 17 (2015) 40–71;
b) J. J. Bozell, G. R. Petersen, Technology development for the production of bio-based products from biorefinery carbohydrates—the US Department of Energy's 'Top 10' revisited, Green Chem. 12 (2010) 539–554;
c) M. Besson, P. Gallezot, C. Pinel, Conversion of biomass into chemicals over metal catalysts, Chem. Rev. 114 (2014) 1827–1870.

[3] a) R. J. Van Putten, J. C. Van der Waal, E. De Jong, C. B. Rasrendra, H. J. Heeres, J. G. de Vries, Hydroxymethylfurfural, A versatile platform chemical made from renewable resources, Chem. Rev. 113 (2013) 1499–1597;
b) B. Saha, M. M. Abu-Omar, Advances in 5-hydroxymethylfurfural production from biomass in biphasic solvents, Green Chem. 16 (2014) 24–38.

[4] a) Y. Nakagawa, M. Tamura, K. Tomishige, Catalytic reduction of biomass-derived furanic compounds with hydrogen, ACS Catal. 3 (2013) 2655–2668;
b) O. O. James, S. Maity, L. Ajao Usman, K. O. Ajanaku, O. O. Ajani, T. O. Siyanbola, S. Sahuc, R. Chaubey, Towards the conversion of carbohydrate biomass feedstocks to biofuels via hydroxylmethylfurfural, Energy Environ. Sci. 3 (2010) 1833–1850
c) F. M. A. Geilen, T. Vom Stein, B. Engendahl, S. Winterle, M. A. Liauw, J. Klankermayer, W. Leitner, Highly selective decarbonylation of 5-(hydroxymethyl)furfural in the presence of compressed carbon dioxide, Angew. Chem. Int. Ed. 50 (2011) 6831–6834; Angew. Chem. 123 (2011) 6963–6966;
d) A. D. Sutton, F. D. Waldie, R. Wu, M. Schlaf, L. A. Silks, J. C. Gordon, Nat. Chem. 5 (2013) 428–432;
e) I. Sádaba, Y. Y. Gonznnev, S. Kegnaes, S. Sankar, R. Putluru, R. W. Berg, A. Riisager, Catalytic performance of zeolite-supported vanadia in the aerobic oxidation of 5-hydroxymethylfurfural to 2,5-diformylfuran, ChemCatChem 5 (2013) 284–293.

[5] a) M. Chatterjee, T. Ishizaka, H. Kawanami, Selective hydrogenation of 5-hydroxymethylfurfural to 2,5-bis-(hydroxymethyl)furan using Pt/MCM-41 in an aqueous medium: a simple approach, Green Chem. 16 (2014) 4734–4739;
b) M. Tamura, K. Tokonami, Y. Nakagawa, K. Tomishige, Rapid synthesis of unsaturated alcohols under mild conditions by highly selective hydrogenation, Chem. Commun. 49 (2013) 7034–7036;
c) J. Ohyama, A. Esaki, Y. Yamamoto, S. Arai, A. Satsuma, Selective hydrogenation of 2-hydroxymethyl-5-furfural to 2,5-bis(hydroxymethyl) furan over gold sub nano clusters, RSC Adv. 3 (2013) 1033–1036;
d) R. Alamillo, M. Tucker, M. Chia, Y. Pagán-Torres, J. Dumesic, The selective hydrogenation of biomass-derived 5-hydroxymethylfurfural using heterogeneous catalysts, Green Chem. 14 (2012) 1413–1419;
e) T. Thananatthanachon, T. Rauchfuss, Efficient route to hydroxymethylfurans from sugars via transfer hydrogenation, ChemSusChem 3 (2010) 1139–1141.

[6] a) Y. Román-Leshkov, C. J. Barrett, Z. Y. Liu, J. A. Dumesic, Production of dimethylfuran for liquid fuels from biomass-derived carbohydrates, Nature 447 (2007) 982–986;
b) L. Hu, X. Tang, J. Xu, Z. Wu, L. Lin, S. Liu, Selective transformation of 5-hydroxymethylfurfural into the liquid fuel 2,5-dimethylfuran over carbon-supported Ru, Ind. Eng. Chem. Res. 53 (2014) 3056–3064;

c) J. Jae, W. Zheng, A. M. Karim, W. Guo, R. F. Lobo, D. G. Vlachos, The role of Ru and RuO_2 in the catalytic transfer hydrogenation of 5-hydroxymethylfurfural for the production of 2,5-dimethylfuran, ChemCatChem 6 (2014) 848–856;

d) Y. Zu, P. Yang, J. Wang, X. Liu, J. Ren, G. Lu, Y. Wang, Efficient production of the liquid fuel 2,5-dimethylfuran from 5-hydroxymethylfurfural over Ru/Co_3O_4 catalyst, Appl. Catal. B 146 (2014) 244–248;

e) J. Jae, W. Zheng, R. F. Lobo, D. G. Vlachos, Production of dimethylfuran from hydroxymethylfurfural through catalytic transfer hydrogenation with Ru supported on carbon, ChemSusChem 6 (2013) 1158–1162; J. B. Binder, R. T. Raines, Simple chemical transformation of lignocellulosic biomass into furans for fuels and chemicals, J. Am. Chem. Soc. 131 (2009) 1979–1985.

[7] a) S. Nishimura, N. Ikeda, K. Ebitani, Selective hydrogenation of biomass-derived 5-hydroxymethylfurfural (HMF) to 2,5-dimethylfuran (DMF) under atmospheric hydrogen pressure over carbon supported PdAu bimetallic catalyst, Catal. Today 232 (2014) 89–98;

b) D. Scholz, C. Aellig, I. Hermans, Catalytic transfer hydrogenation/hydrogenolysis for reductive upgrading of furfural and 5-(hydroxymethyl)furfural, ChemSusChem 7 (2014) 268–275.

[8] a) J. Mitra, X. Zhou, T. Rauchfuss, Pd/C-catalyzed reactions of HMF: decarbonylation, hydrogenation, and hydrogenolysis, Green Chem. 17 (2015) 307–313;

b) M. Chatterjee, T. Ishizaka, H. Kawanami, Hydrogenation of 5-hydroxymethylfurfural in supercritical carbon dioxide–water: a tunable approach to dimethylfuran selectivity, Green Chem. 16 (2014) 1543–1551.

[9] Y. B. Huang, M. Y. Chen, L. Yan, Q. X. Guo, Y. Fu, Ni-tungsten carbide catalysts for the production of 2,5-dimethylfuran from biomass-derived molecules, ChemSusChem 7 (2014) 1068–1070.

[10] X. Kong, Y. Zhu, H. Zheng, F. Dong, Y. Zhu, Y. W. Li, Switchable synthesis of 2,5-dimethylfuran and 2,5-dihydroxymethyltetrahydrofuran from 5-hydroxymethylfurfural over Raney Ni catalyst, RSC Adv. 4 (2014) 60467–60472.

[11] a) T. S. Hansen, K. Barta, P. T. Anastas, P. C. Ford, A. Riisager, One-pot reduction of 5-hydroxymethylfurfural via hydrogen transfer from supercritical methanol, Green Chem. 14 (2012) 2457–2461;

b) A. J. Kumalaputri, G. Bottari, P. M. Erne, H. J. Heeres, K. Barta, Tunable and selective conversion of 5-HMF to 2,5-furandimethanol and 2,5-dimethylfuran over copper-doped porous metal oxides, ChemSusChem 7(2014) 2266–2275.

[12] K. Barta, P. C. Ford, Catalytic conversion of nonfood woody biomass solids to organic liquids, Acc. Chem. Res. 47 (2014) 1503–1512.

[13] B. J. O'vNeill, et al., Stabilization of copper catalysts for liquid-phase reactions by atomic layer deposition, Angew. Chem. Int. Ed. 52 (2013) 13808–13812; Angew. Chem. 125 (2013) 14053–14057.

[14] a) H. Mehdi, V. Fábos, R. Tuba, A. Bodor, L. T. Mika, I. T. Horváth, Integration of homogeneous and heterogeneous catalytic processes for a multi-step conversion of biomass: from sucrose to levulinic acid, γ-valerolactone, 1, 4-pentanediol, 2-methyl-tetrahydrofuran, and alkanes, Top. Catal. 48 (2008) 49–54;
b) F. M. A. Geilen, B. Engendahl, A. Harwardt, W. Marquardt, J. Klankermayer, W. Leitner, Selective and flexible transformation of biomass-derived platform chemicals by a multifunctional catalytic system, Angew. Chem. Int. Ed. 49 (2010) 5510–5514; Angew. Chem. 122 (2010) 5642–5646;
c) V. Pace, P. Hoyos, L. Castoldi, P. Domínguez de María, A. R. Alcántara, 2-Methyltetrahydrofuran (2-methf): A biomass-derived solvent with broad application in organic chemistry, ChemSusChem 5 (2012) 1369–1379.

[15] a) K. Watanabe, N. Yamagiwa, Y. Torisawa, Cyclopentyl methyl ether as a new and alternative process solvent, Org. Process Res. Dev. 11 (2007) 251–258;
b) K. Watanabe, The toxicological assessment of cyclopentyl methyl ether (CPME) as a green solvent, molecules 18 (2013) 3183–3194.

[16] a) C. M. Lew, N. Rajabbeigi, M. Tsapatsis, One-pot synthesis of 5-(ethoxymethyl)furfural from glucose using Sn-BEA and amberlyst catalysts, Ind. Eng. Chem. Res. 51 (2012) 5364–5366;
b) L. Bing, Z. Zhang, K. Deng, Efficient one-pot synthesis of 5-(ethoxymethyl)furfural from fructose catalyzed by a novel solid catalyst, Ind. Eng. Chem. Res. 51 (2012) 15331–15336;
c) Z. Zhang, Y. Wang, Z. Fang, B. Liu, Synthesis of 5-Ethoxymethylfurfural from fructose and inulin catalyzed by a magnetically recoverable acid catalyst, ChemPlusChem 79 (2014) 233–240;
d) B. Liu, Z. Zhang, One-pot conversion of carbohydrates into 5-ethoxymethylfurfural and ethyl D-glucopyranosidein ethanol catalyzed by a silica supported sulfonic acid catalyst, RSC Adv. 3 (2013) 12313–12319.

[17] M. V. Twigg, M. S. Spencer, Deactivation of supported copper metal catalysts for hydrogenation reactions, Appl. Catal. A 212 (2001) 161–174.

[18] a) A. R. Wilson, K. Sun, M. Chi, R. M. White, J. M. LeBeau, H. H. Lamb, B. J. Wiley, From Core–Shell to Alloys: The preparation and characterization of solution-synthesized AuPd nanoparticle catalysts, J. Phys. Chem. C 117 (2013) 17557–17566;

b) L. Arroyo-Ramírez, C. Chena, M. Cargnello, C. B. Murray, P. Fornasiero, R. J. Gorte, Supported platinum–zinc oxide core–shell nanoparticle catalysts for methanol steam reforming, J. Mater. Chem. A 2 (2014) 19509–19514.

[19] K. Ozawa, Y. Mimori, H. Kato, S. Imanishi, K. Edamoto, K. Mase, Photoelectron spectroscopy study of interaction of oxygen with the (111) surface of a Cu–Zn alloy, Surf. Sci. 623 (2014) 1–5.

[20] B. Saha, C. M. Bohn, M. M. Abu-Omar, Zinc-assisted hydrodeoxygenation of biomass-derived 5-hydroxymethylfurfural to 2,5-dimethylfuran, ChemSusChem 7 (2014) 3095–3101.

[21] J. Sun, G. Yang, Q. Ma, I. Ooki, A. Taguchi, T. Abe, Q. Xie, Y. Yoneyama, N. Tsubaki, Fabrication of active Cu–Zn nanoalloys on H-ZSM5 zeolite for enhanced dimethyl ether synthesis *via* syngas, J. Mater. Chem. A 2 (2014) 8637–8643.

[22] G. H. Wang, J. Hilgert, F. H. Richter, F. Wang, H. J. Bongard, B. Spliethoff, C. Weidenthaler, F. Schüth, Platinum-cobalt bimetallic nanoparticles in hollow carbon nanospheres for hydrogenolysis of 5-hydroxymethylfurfural, Nat. Mater. 13 (2014) 293–300.

[23] a) K. Schütte, H. Meyer, C. Gemel, J. Barthel, R. A. Fischer, C. Janiak, Synthesis of Cu, Zn and Cu/Zn brass alloy nanoparticles from metal amidinate precursors in ionic liquids or propylene carbonate with relevance to methanol synthesis, Nanoscale 6 (2014) 3116–3126;
b) M. Cokoja, H. Parala, M. K. Schroeter, A. Birkner, M. W. Van den Berg, K. V. Klementiev, W. Gruenert, R. A. Fischer, Nano-brass colloids: synthesis by co-hydrogenolysis of [CpCu(PMe_3)] with [$ZnCp^*_2$] and investigation of the oxidation behaviour of α/β-CuZn nanoparticles, J. Mater. Chem. 16 (2006) 2420–2428.

[24] a) J. Tuteja, H. Choudhary, S. Nishimura, K. Ebitani, Direct synthesis of 1,6-hexanediol from HMF over a heterogeneous Pd/ZrP catalyst using formic acid as hydrogen source, ChemSusChem 7 (2014) 96–100;
b) T. Buntara, S. Noel, P. Huat Phua, I. Melián-Cabrera, J. G. de Vries, H. J. Heeres, From 5-hydroxymethylfurfural (HMF) to polymer precursors: catalyst screening studies on the conversion of 1,2,6-hexanetriol to 1,6-hexanediol, Top. Catal. 55 (2012) 612–619;
c) T. Buntara, S. Noel, P. Huat Phua, I. Melián-Cabrera, J. G. de Vries, H. J. Heeres, Caprolactam from renewable resources: catalytic conversion of 5-hydroxymethylfurfural into caprolactone, Angew. Chem. Int. Ed. 50 (2011) 7083–7087; Angew. Chem. 123 (2011) 7221–7225.

[25] L. Lai, Y. Zhang, The production of 5-hydroxymethylfurfural from fructose in isopropyl alcohol: a green and efficient system, ChemSusChem 4 (2011) 1745–1748.

[26] M. Balakrishnan, E. R. Sacia, A. T. Bell, Etherification and reductive etherification of 5-(hydroxymethyl) furfural: 5-(alkoxymethyl) furfurals and 2, 5-bis (alkoxymethyl) furans as potential bio-diesel candidates, Green Chem. 14 (2012) 1626–1634.

[27] a) S. Zafeiratos, S. Piccinin, D. Teschner, Alloys in catalysis: phase separation and surface segregation phenomena in response to the reactive environment, Catal. Sci. Technol. 2 (2012) 1787–1801;
b) R. Ferrando, J. Jellinek, R. L. Johnston, Nanoalloys: from theory to applications of alloy clusters and nanoparticles, Chem. Rev. 108 (2008) 845–910.

Supporting Information

Materials and methods

All solvents and reagents were used as received without further purification. 2,5-dimethylfuran (DMF, 99 %), 5-(hydroxymethyl)furfural (HMF, ≥99 %), 2,5-dimethyltetrahydrofuran (DMTHF, 96 %, mixture of *cis* and *trans*), Cu, Cuo, CuZn, $CuZnFe_2O_4$ and $CuFe_2O_4$ nanopowders, CuZn powder (60 mesh), Nafion® SAC-13, Amberlyst® 15 and Dowex® 50WX8 were purchased from Sigma Aldrich. 5-hydroxymethylfurfural (98 %) was purchased from Alfa Aesar. 5-Methyl-2-furanmethanol (MFM, 97%) and D-(-)-fructose were purchased from Acros Organics. 2,5-furandimethanol (FDM, 98 %) was purchased from Toronto Research Chemicals. Tetrahydrofuran-2,5-diyl-dimethanol (THFDM) was supplied by GLSyntech.

GC-MS-FID analyses were performed with a Hewlett Packard 5890 series II plus with a Quadrupole Hewlett Packard 5972 MSD and a FID. The GC is equipped with a 60 × 0.25 mm i.d. and 0.25 μm film Restek RTX-1701 capillary column and a 1:1 split ratio to the MSD and FID was set. Temperature of injector and detector were set at 250 °C and 285 °C, respectively. The program temperature starts from 40 °C (10 min) and is then increased up to 250 °C with a heating rate of 10 °C/min.

HPLC analyses were conducted on a Agilent Technologies equipment consisting of a HP 1050 isocratic pump and a Waters 410 differential refractometer. The HPLC is equipped with a Bio-Rad organic acid column Aminex HPX-87H and analyses were operated at 60 °C with 5 mM aqueous solution of sulfuric acid as eluent at a flow rate of 0.55 mL/min.

^{1}H and ^{13}C NMR spectra were recorded on a Varian AMX400 spectrometer. The TEM images were recorded on a FEI T20 electron microscope with a slow scan CCD camera at 200 keV. The solid samples were suspended in ethanol and deposited on a plain carbon coated copper grids. For EDX analysis, molybdenum windows with a holey carbon film were used.

Microanalyses for metal content were performed on a ICP Perkin Elmer instrument (Optima 7000DV) while combustion analysis was carried out on a EA3000 Elemental Analyser. Thermogravimetric analysis was performed on a TGA 7 instrument from Perkin-Elmer; the samples were heated in a nitrogen atmosphere with a heating rate 10 °C/min and a temperature range between 25–900 °C.

Recycling experiments

Copper zinc alloy nanopowder (0.200 g), 5-(hydroxymethyl)furfural (0.500 g), decane (0.250 mL, internal standard) and the appropriate solvent (MIBC or CPME, 20 mL) were placed in a 100 mL stainless steel Parr reactor using a glass insert. The reactor was purged three times with H_2 and pressurized at 20 bar. The temperature was set at 220 °C and the reaction mixture was stirred with a mechanical stirrer for the desired reaction time. After cooling down and releasing the pressure, the mixture was centrifuged and the recovered solid was washed twice (1× reaction solvent, 1× acetone, 10 mL each) while the supernatant was directly analyzed by GC-MS-FID for determining the product yield (based on calibration curves and internal standard). The solid was dried at 100 °C for 3 h and used for the next run. The recalcination of the spent catalysts after the 5^{th} (in case of MIBC) and 7^{th} (in case of CPME) was performed in a Linn High Therm oven with controller G 800 P at 500 °C for 6 h.

Fructose dehydration and sequential hydrogenation

In a 25 mL glass vial, fructose (0.450 g), the appropriate acidic resin (0.090 g), iPrOH (5 mL) and dioxane (0.020 mL, internal standard) were placed. The vial was sealed and heated in an oil bath to 120 °C for 6 h. The mixture was filtered through a PTFE filter and analyzed by HPLC and ^{1}H NMR to determine fructose conversion and product selectivity. After dilution to 15 mL with additional iPrOH, the resulting

solution was placed in a glass insert in a 100 mL stainless steel Parr reactor equipped with mechanical stirrer. CuZn nanoalloy (0.100 g) and decane (0.100 mL) were added, the autoclave was pressurized with H_2 (30 bar) and heated to 120 °C. After 6 h, the reactor was cooled down and the mixture was filtered and analyzed by GC-FID. Product 1, 2, and 3 yields were determined using calibration curves and internal standard.

Tandem fructose dehydration/reductive etherification

A glass insert was loaded with fructose (0.450 g), CuZn nanopowder (0.100 g), acidic resin (5 wt % Amberlyst® 15 or 20 wt % Nafion® SAC-13) and iPrOH (10 mL) and placed in a 100 mL Parr reactor equipped with mechanical stirrer. The reactor was pressurized with H_2 (after purging for 3 times), heated to 120 °C and stirred at 600 rpm for 12 h. After cooling down, the residue was filtered and the solution was analyzed by HPLC and GC-FID. Product 1, 2 and 3 yields were determined based on calibration curves and internal standard.

Table S1. Particle size (the analytical technique used is reported in brackets) and elemental composition (determined by ICP analysis) of commercial copper nanopowders (Sigma Aldrich)

Nanopowder	Particle size	Cu (wt %)	Zn (wt %)	Fe (wt %)
Cu	40–60 nm (SAXS)	98.9	-	-
CuO	<50 nm (TEM)	88.2	-	-
$CuFe_2O_4$	<100 nm (BET)	27.3	-	46.3
$CuZnFe_2O_4$	<100 nm (BET)	20.1	21.1	26.8
CuZn	<150 nm (SEM)	59.9	33.0	-

Products obtained during catalytic conversion of HMF over various Cu nanopowders in different solvents

Table S2. Products and product selectivity values (in percentages, determined by GC-FID) obtained during the conversion of HMF using different copper nanopowders in ethanol solvent [a]

Catalyst	DMF+DMTHF [b]	MFM	EMMF	THMFM	FDM	THFDM	1,2- HD	2,5- HD	n. i.
Cu	60+3 (55)	2	11	1	-	-	2	-	21
CuO	30+1 (30)	20	1	<1	34	1	1	1	11
$CuFe_2O_4$	46+4 (45)	17	-	2	7	3	4	6	11
$CuZnFe_2O_4$[c]	66+8 (73)	<1	5	6	2	-	-	-	12
CuZn	70+6 (75)	12	1	1	1	1	2	3	3

[a] Reaction conditions: 0.500 g HMF, 0.100 g catalyst, 20 mL EtOH, 0.250 mL toluene (internal standard), 220 °C, 30 bar H_2, 6 h. Full HMF conversion. [b] Yields (calculated based on calibration curves and an internal standard) are reported in brackets. [c] 95 % HMF conversion.

Table S3. Products and product selectivity values (determined by GC-FID) obtained during the conversion of HMF using CuZn nanopowder in different solvents [a]

Entry	Solvent	DMF+ DMTHF [b] (%)	MFM (%)	EMMF (%)	THMFM (%)	FDM (%)	THFDM (%)	1,2- HD (%)	2,5- HD (%)	n. i. (%)
1[c]	EtOH	80+5 (84)	4	2	1	-	1	1	1	5
2	EtOH	83+6 (88)	<1	5	1	-	1	1	1	2
3	iPrOH	80+11 (91)	2	-	1	<1	<1	1	2	2
4	MIBC	73+20 (93)	-	-	2	-	-	2	2	2
5	MeTHF	71+22 (91)	-	-	2	-	-	1.5	1.5	2
6	CPME	71+26 (97)	-	-	2	-	-	1	-	<1
7 [d]	MIBC	74+17 (88)	-	-	2	-	-	2	3	2

[a] Reaction conditions: 0.500 g HMF, 0.100 g catalyst, 20 mL solvent, 0.250 mL internal standard (decane or toluene), H_2 (20 bar), 220 °C, 18 h. Full HMF conversion. [b] Yields (calculated based on calibration curves and an internal standard) are reported in brackets. [c] 30 bar H_2 were applied. [d] A 10 wt % HMF concentration (1.67 g HMF in 20 mL MIBC) and 0.3 g catalyst were used.

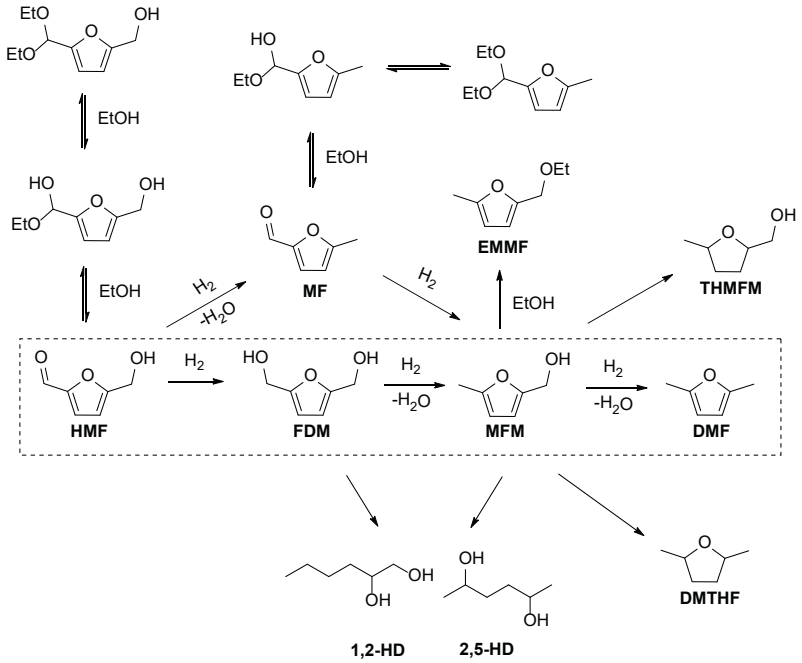

Scheme S1. Proposed reaction network of HMF hydrodeoxygenation over copper nanopowders in ethanol solvent
Structures of intermediates abbreviated in Tables S2-S3

Table S4. Products and product selectivity values (in percentage, determined by GC-FID) obtained during the conversion of HMF using CuZn nanopowder in CPME solvent[a]

Entry	DMF+DMTHF [b]	MFM	THMFM	1,2-HD	2,5-HD	n. i.
1	80+16 (96)	-	1	2	<1	<1
2	80+16 (96)	<1	1	2	<1	<1
3	90+5 (95)	<1	1	-	<1	3
4 [c]	90+5 (94)	<1	<1	-	<1	3
5 [d]	91+3 (89)	<1	1	<1	1	3

[a] Reaction conditions: 0.500 g HMF, 0.100 g catalyst, 20 mL CPME, 0.250 mL decane, H_2 (20 bar). Full HMF conversion. [b] Yields (calculated based on calibration curves and an internal standard) are reported in brackets. [c] 10 wt % HMF concentration (1.72 g HMF in 20 mL CPME) and 0.2 g catalyst were used. [d] 2.00 g HMF in 30 mL CPME) and 0.1 g catalyst were used (3 % Cu/HMF ratio).

Catalytic conversion of HMF to useful diols using various commercial catalysts

Description on main findings

The best selectivity to FDM (95%) among the tested catalyst was obtained with the CuZn nanopowder (Table 5, entry 1) showing that this is a superior catalyst for the modular conversion of HMF. As comparison, catalysts D and G, both based on copper and Ni supported on SiO_2 and SiO_2/ZrO_2, respectively, showed good selectivity to FDM (Table S5, entry 2 and 3). With $NiCu/CeO_2/ZrO_2$ and Ni Raney alloy (Table S5, entry 4 and 5) a preferential hydrogenation of the furan ring was observed (54% and 94% THFDM, respectively). Noble metal based catalyst preferably gave THFDM as major product with the exception of Pt/C, which also reduced HMF to FDM with good selectivity (82%, Table S5, entry 6). Very clean formation of THFDM (up to >99% THFDM, Table S5, entry 7) was observed with Pd supported on aluminium oxide. The hydrogenation of the furan ring by Pd catalysts has been previously reported.[1] Furthermore, Ru/C gave THFDM with high selectivity (Table S5, entry 10) while Ru/Al_2O_3, afforded an almost equimolar mixture of FDM and THFDM (Table S5, entry 9). The reduction to THFDM preferentially gave the cis isomer in all the experiments, ranging in a 5/1 to 10/1 the ratio between *cis* and *trans* isomer.

Table S5. Products and product selectivity values (determined by GC-FID) obtained in the screening of commercial catalysts for the production of diols FDM and THFDM

Entry [a]	Catalyst	Conversion (%)	FDM (%)	THFDM (%)	DMF (%)	THMFM (%)	MFM (%)	MF (%)
1[c]	CuZn	>99	95	-	-	-	<1	3
2	Cat. D	96	88	10 (8/1)	-	-	<1	2
3	Cat. G	85	84	14 (7/1)	-	-	1	1
4	$NiCu/CeO_2/ZrO_2$	>99	44	54 (9/1)	-	<1	1	1
5	Ni Raney	>99	4	94(10/1)	-	<1	<1	<1
6	Pt/C	92	89	5 (5/1)	1	1	1	3
7	Pd/Al_2O_3	>99	<1	>99 (9/1)	-	<1	-	-
8	Pd/C	>99	-	89 (5/1)	2	8	-	-
9	Ru/Al_2O_3	>99	42	55 (9/1)	-	<1	<1	2
10	Ru/C	>99	4	88 (10/1)	3	4	-	<1

[a] Reaction conditions: 0.500 g HMF, 0.100 g catalyst, 20 mL ethanol, 120 °C, 70 bars H_2, 3 h. [b] In brackets, the ratio between the *cis* and *trans* isomer is reported. [c] Unidentified products <2%.

Table S6 Detailed composition and suppliers of the commercial catalysts screened for FDM and THFDM production (used in screening shown in Table S5)

Catalyst	Composition	Supplier
Cat. D	Ni (57.9 wt %) Cu (7 wt %) on SiO_2 (35.1wt %)	BTG,* BIC
Cat. G	Ni (36.5 wt %), Cu (2.3 wt %) on SiO_2 (11.6 wt %), ZrO_2 (39 wt %)	BIC
Ni-Cu/CeO_2-ZrO_2	Ni-Cu (38.3 wt %), CeO_2-ZrO_2 (10.4 wt %)	BIC
Ni Raney	Ra-Ni(≥89 wt %) in H_2O	Sigma Aldrich
Pt/C	Pt (5 wt %) on C	Sigma Aldrich
Pd/Al_2O_3	Pd (5 wt % on Al_2O_3)	Sigma Aldrich
Pd/C	Pd (5 wt % on C)	Sigma Aldrich
Ru/Al_2O_3	Ru (5 wt % on Al_2O_3)	Fluka
Ru/C	Ru (5 wt %) on C	Sigma Aldrich

*BTG: Biomass Technology group (Enschede, The Netherlands)

XRD Characterization of nanopowders

Copper nanopowder, shows three typical peaks for the CuO phase (▲) at 2θ values of 44°, 51° and 76°[2] corresponding to the crystalline planes (111), (200) and (220), respectively, plus minor peaks attributed to CuO (△) likely due to partial oxidation upon exposure of the sample to air. These peaks are found in the diffraction pattern of the corresponding CuO nanopowder, in agreement with the phases previously reported.[3] XRD pattern of CuO nanoalloy displays predominant β-CuZn (■)[4] and CuO (▲) phases, which give rise to two overlapped peaks at around 42° for the (210) and (111) planes. The minor presence of ZnO crystallites (□) was confirmed by the diffraction pattern of pure ZnO nanopowders,[5] while no metallic Zn was detected. Both copper ferrite[6] and copper zinc ferrite[7] show a cubic structure according to previous report, the peaks at 30.5, 35.2, 57.0, 62.8 and 74.1 attributed to (220), (311), (511), (440) and (533) crystals planes of $CuFe_2O_4$ structure (●), plus a small impurity due to CuO crystallites (44°).

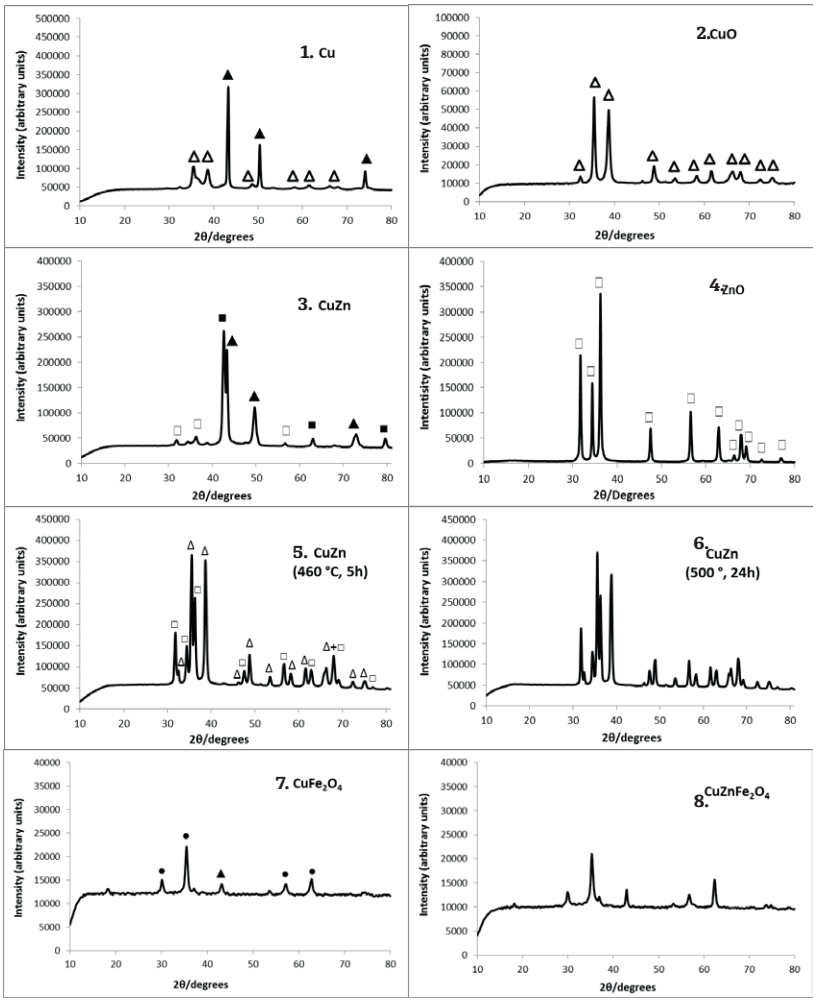

Figure S1. XRD patterns of fresh copper nanopowders: Cu nanopowder (1), CuO nanopowder (2), CuZn nanoalloy (3), ZnO nanopowder (4), copper ferrite nanopowder (5) and copper-zinc ferrite nanopowder (6)

Characterization of the spent catalyst in MIBC

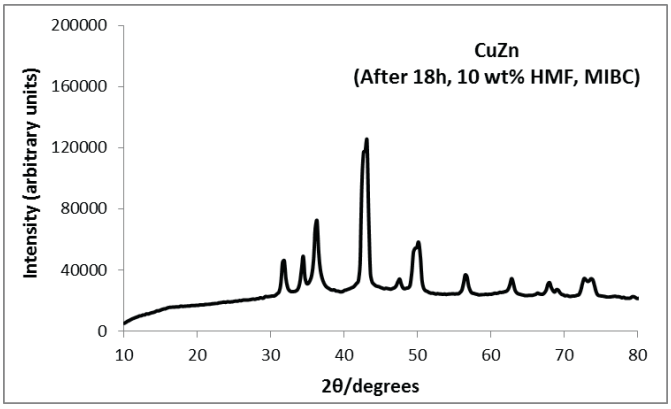

Figure S2. XRD pattern of CuZn after the run with 10 wt % HMF in MIBC (Table S4, entry 7)

The Figure shows diffraction peaks related to Cu, CuZn and ZnO phases.

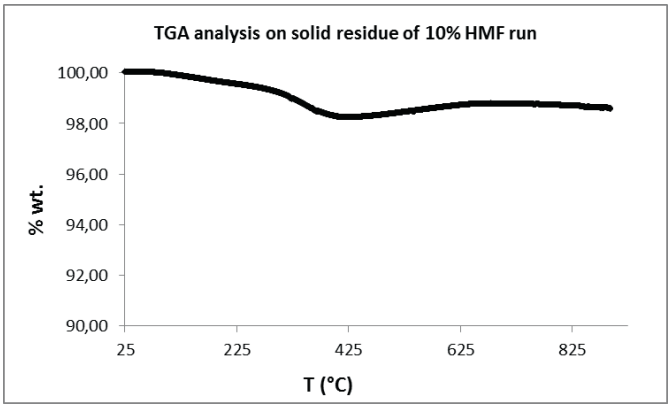

Figure S3. Thermogravimetric analysis on the spent catalyst after the run with 10 wt % HMF in MIBC

(220 °C, 18 h, more details shown in Table 3, entry 7)

Table S7. Elemental composition of the fresh and spent CuZn catalyst after the run with 10 wt % HMF in MIBC (220 °C, 18 h, more details shown in Table 3, entry 7) determined by ICP analysis of the solids

Sample	Cu	Zn	C	H
Fresh catalyst	59.9 %	33.0 %	0.1	0.1
Spent catalyst	58.9 %	32.5 %	0.6	0.1

TEM Characterization

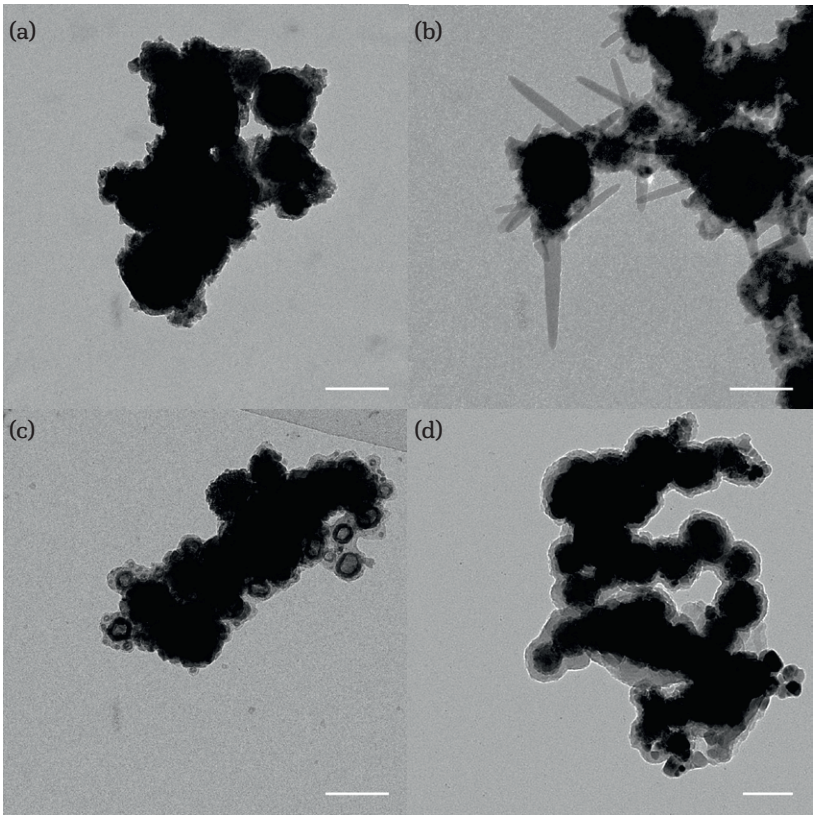

Figure S4. TEM image of the fresh CuZn nanopowder (a) and spent CuZn nanopowder after reaction with 10 wt % HMF in MIBC (220 °C, 18 h) (b), 10 wt % HMF in CPME (200 °C, 6 h) and (d) 10 wt % HMF in CPME (220 °C, 18 h). Bar scale: 50 nm.

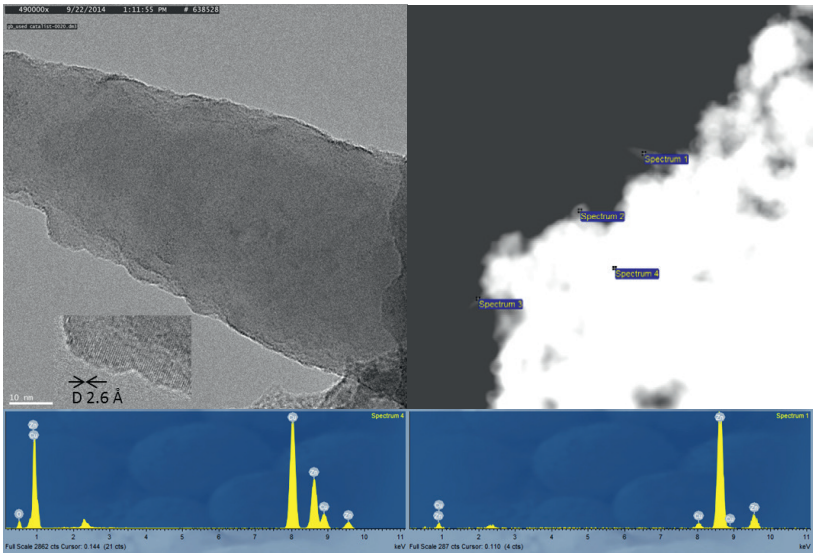

Figure S5. TEM images of the spent catalyst after the run with 10wt% HMF in MIBC (220 °C, 18 h, see Table 3, entry 7) showing a spike-like object at high magnification (on the top, left) and the corresponding STEM image (on the top, right, spectrum 1)

Elemental analysis on the spiked material (on the bottom, left) and a selected area in the bulk (on the bottom, right, spectrum 4) are also reported, showing that the spiked objects mainly comprise zinc while in the bulk the expected copper to zinc ratio (6:4) is found.

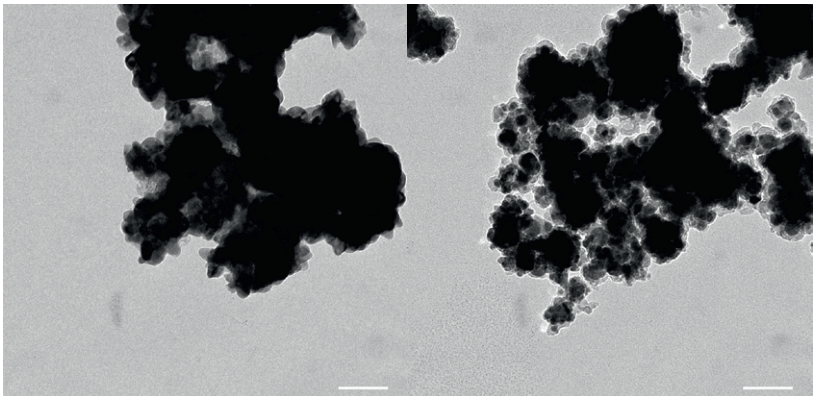

Figure S6. TEM images of spent catalyst in MIBC (after 4 recycling tests, left) and the corresponding regenerated catalyst (calcined after 4 recycling tests, right). Bar scale: 50 nm

Table S8. Comparison of catalytic activity (DMF+DMTHF yield displayed) of different batches of CuZn nanopowders (conditions: 0.500 g HMF, 0.100 g CuZn, 200 °C, 20 bar H_2, 3 h)

Nanopowder	DMF+DMTHF yield	DMF/DMTHF ratio
Sigma Aldrich (lot #04808ABV)	96	5/1
Sigma Aldrich (lot #MKBQ4035V)	90	6/1
Sigma Aldrich (lot #MKBQ4035V) calcined in air at 460 °C for 5 h	92	4/1
US Research Nanomaterials, Inc. (99.9 %, 40 nm-100 nm, Cu:Zn=6:4)	93	4/1

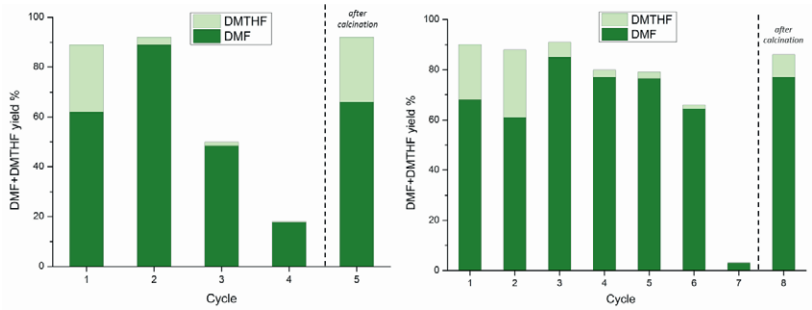

Figure S7. Left: recycling runs in MIBC (0.500 g HMF, 0.200 g CuZn, 20 mL solvent, 220 °C, 20 bar H_2, 15 h)

Right: recycling runs in CPME (0.500 g HMF, 0.200 g CuZn, 20 mL solvent, 220 °C, 20 bar H_2, 6 h; Note: a different batch of CuZn was used). Between the runs, the solid was dried at 100 °C for 3 h and used for the next run. The recalcination of the spent catalysts after the 5th (in case of MIBC) and 7th (in case of CPME) was performed at 500 °C for 6 h.

Table S9. GC-FID selectivities in the recycling tests for DMF+DMTHF production in MIBC.[a]

Cycle	CuZn (mg)	DMF+DMTHF		MFM	THMFM	FDM	1,2-HD	n.i.
		Yield	Selectivity					
1	0.200	62+27	62+27	-	2	-	4	5
2	0.188	89+3	90+3	0.5	1	-	-	5.5
3	0.181	49+1	66+2	1	0.5	-	-	30.5
4	0.177	17.7+0.3	34+0.5	11	-	10	-	44.5
5	0.170	63+24	63+26	0.2	2.5	-	0.3	8

[a] Reaction conditions: 0.5 g HMF, 20 mL MIBC, 20 bar H_2, 220 °C, 0.250 mL decane (internal standard), 15 h

Table S10. GC-FID selectivity in the recycling tests for DMF+DMTHF production in CPME [(a)]

Cycle	CuZn (mg)	HMF	DMF+DMTHF		MFM	THMFM	FDM	1,2-HD	n.i.
			Yield	Selectivity					
1	0.202	5	68+22	68+22	-	3	0.5	1	1.5
2	0.183	5	62+26	62+26	-	5	0.4	0.6	1
3	0.175	6	85+6	85+6	-	1.4	0.1	-	1.5
4	0.168	7	77+3	81+3	0.1	1.5	0.1	-	7.3
5	0.161	8	76+3	81+3	-	2	-	-	6
6	0.158	9	65+2	78+1	1	2	-	-	9
7	0.160	65	3+0.1	5+0.1	3	-	9	-	18
8	0.131	7	77+9	77+9	-	1	0.2	-	5.8

[a] Reaction conditions: 0.500 g HMF, 20 mL CPME, 20 bar H_2, 220 °C, 0.250 mL decane (internal standard), 6 h

GC traces of representative catalytic runs

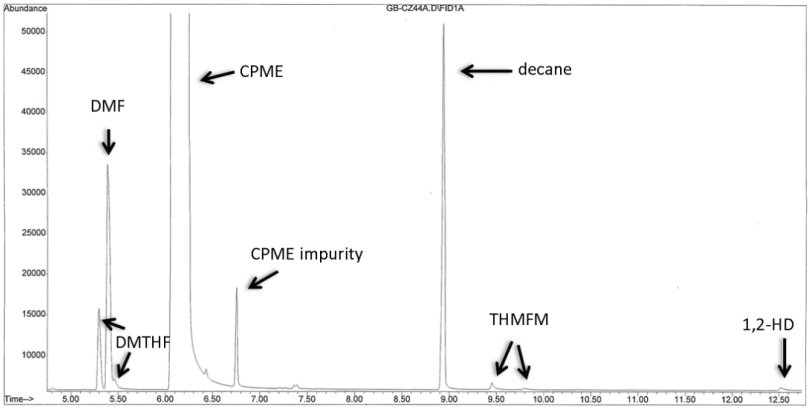

Figure S8. GC trace of a representative run for HMF conversion to DMF in CPME as a solvent (Table 3, entry 6)

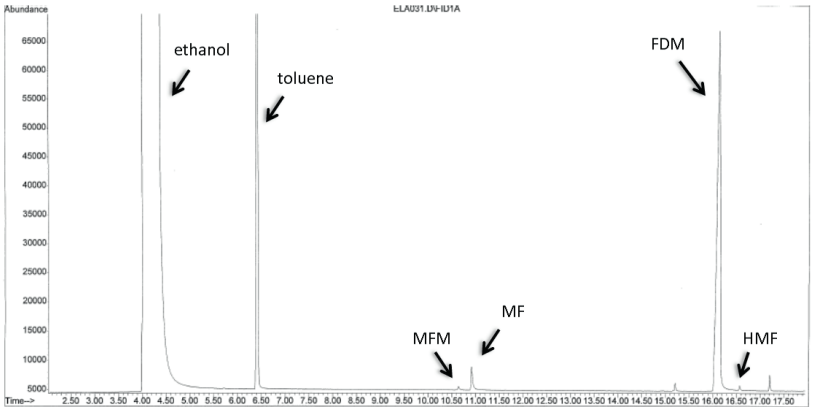

Figure S9. GC trace of a representative run for HMF conversion to FDM (120 °C, Table S5, entry 1)

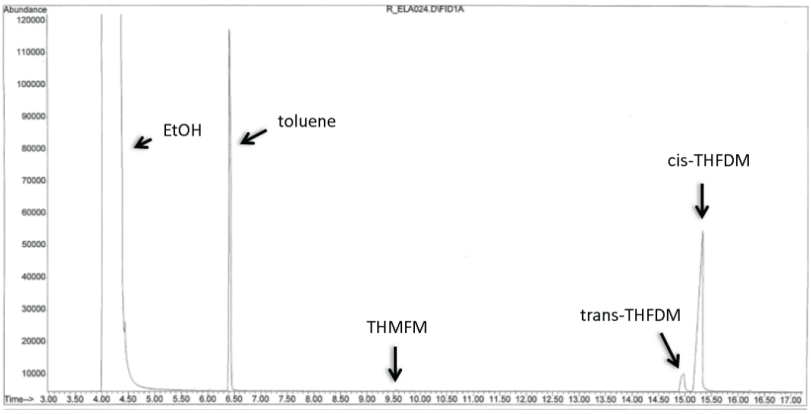

Figure S10. GC trace of a representative run for HMF conversion to THFDM (120 °C, Table S5, entry 7)

^{1}H and ^{13}C-NMR spectra of isolated products

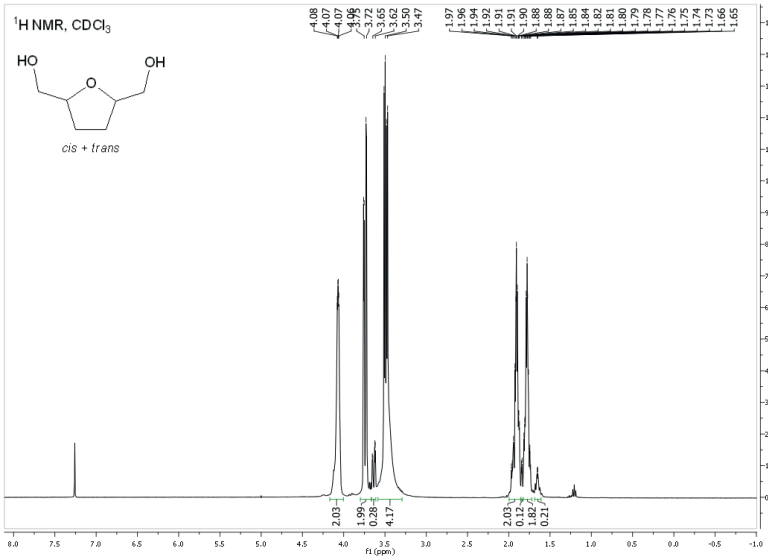

Figure S11. ^{1}H-NMR spectrum of mixture of *cis* and *trans* THFDM isomers ($CDCl_3$, 400 MHz)

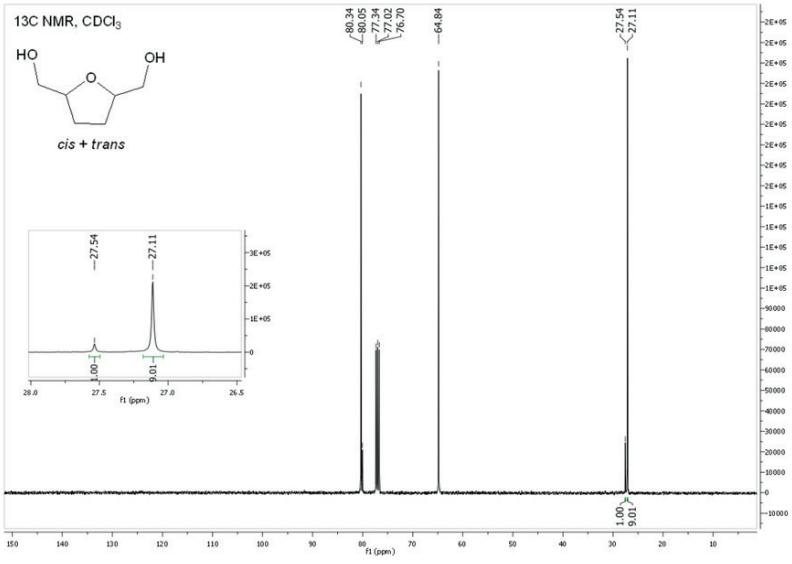

Figure S12. ^{13}C-NMR spectrum of THFDM ($CDCl_3$, 100 MHz)
Small picture shows cis/trans ratio

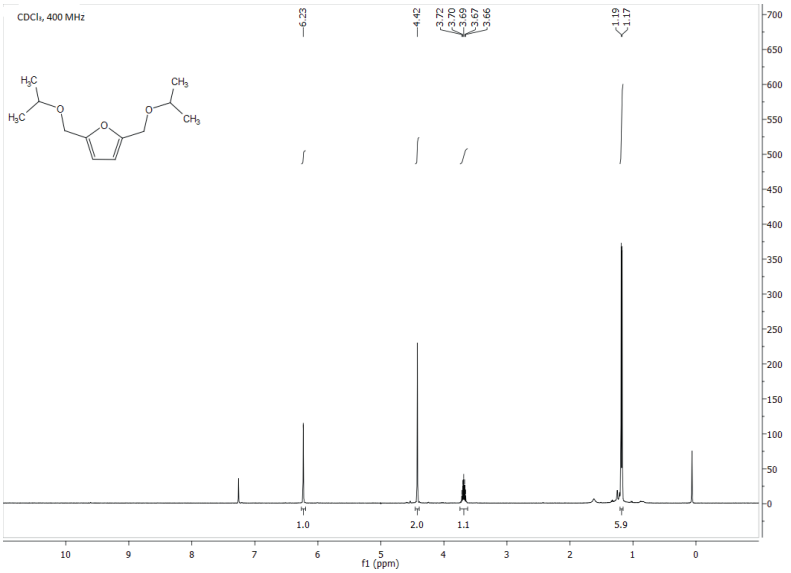

Figure S13. ^{1}H-NMR spectrum of diisopropyl ether 1 ($CDCl_3$, 400 MHz)

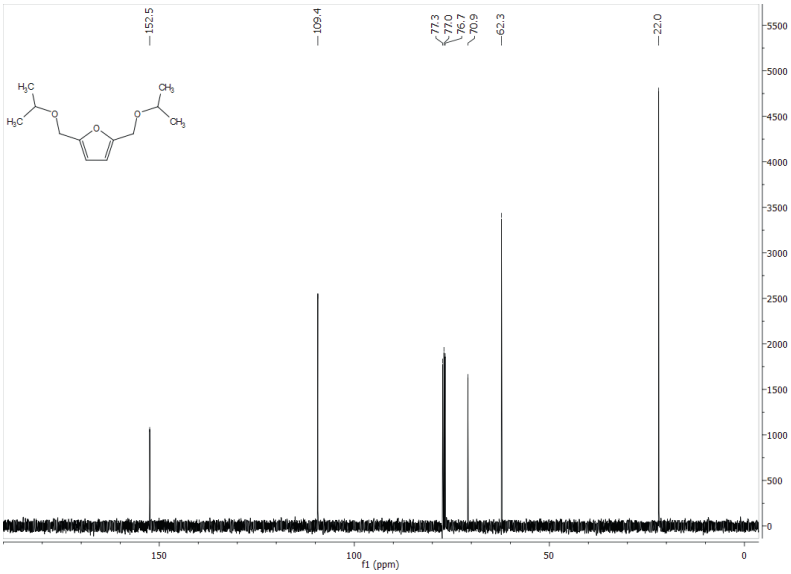

Figure S14 ^{13}C-NMR spectrum of diisopropyl ether 1 ($CDCl_3$, 100 MHz)

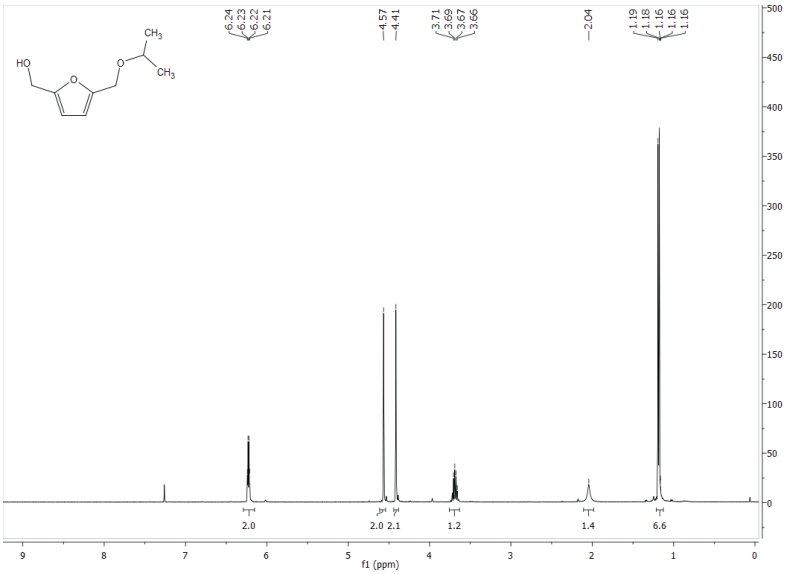

Figure S15. ^{1}H-NMR spectrum of isopropyl ether 2 ($CDCl_3$, 400 MHz)

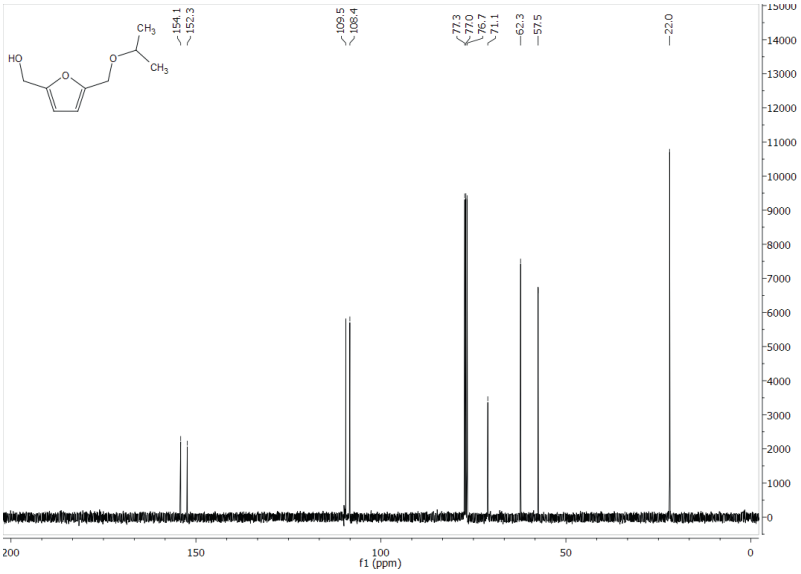

Figure S16. ^{13}C-NMR spectrum of isopropyl ether 2 ($CDCl_3$, 100 MHz).

Table S11. Dehydration of fructose in iPrOH with different acidic resins

Entry [a]	Acidic resin	Conversion (%) [b]	4 (%) [c]	5 (%) [c]	Isopropyl levulinate (%) [c]
1	Amberlyst ® 15	>99	55	24	21
2	Nafion ® SAC-13	94	83	17	-
3	Dowex ® 50WX8	99	5	81	13

(a) Conditions: fructose (0.450 g, 2.5 mmol), acidic resin (0.090 g, 20 %), iPrOH (5 mL), dioxane (0.050 mL), 120 °C, 6 h. (b) Determined by HPLC. (c) Determined by ^{1}H NMR

Table S12. Reduction of mixtures obtained in Table S11 with CuZn nanoalloy catalyst

Crude mixture (Table 11)	1 (%) [b]	2 (%) [b]	3 (%) [b]
Entry 1	1	17	2
Entry 2	7	12	5

(a) Conditions: crude mixture (entry 1 and 2, Table S11), CuZn nanopowder (0.100 g), iPrOH (15 mL), decane (0.100 mL), 120 °C, 6 h, 30 bar H_2. (b). Yield % determined by GC-FID (based on calibration curve and internal standard)

Table S13. One-pot fructose conversion to FDM and furanyl ethers

Entry	Acidic resin	Conversion (%) [b]	1 (%) [c]	2 (%) [c]	3 (%) [c]
1	Amberlyst ® 15	>99	1	49	7
2	Nafion ® SAC-13	96	1	33	-

(a). Conditions: fructose (0.450 g, 2.5 mmol), CuZn nanopowder (0.100 g), acidic resin (5 wt % Amberlyst® 15 and 20 wt % Nafion® SAC-13), iPrOH (10 mL), dioxane (0.050 mL), 120 °C, 12 h, 30 bar H_2. (b). Determined by HPLC. c Determined by GC-FID (based on calibration curve and internal standard)

References

[1] a) J. Mitra, X. Zhou, T. Rauchfuss, Pd/C-catalyzed reactions of HMF: Decarbonylation, hydrogenation, and hydrogenolysis, Green Chem. 17 (2014) 307–313;

b) Y. Nakagawa, K. Takada, M. Tamura, K. Tomishige, Total hydrogenation of furfural and 5-hydroxymethylfurfural over supported Pd–Ir alloy catalyst, ACS Catal. 4 (2014) 2718–2726;

c) H. Cai, C. Li, A. Wang, T. Zhang, Biomass into chemicals: One-pot production of furan-based diols from carbohydrates via tandem reactions, Catal. Today 234 (2014) 59–65;

d) M. H. Tucker, R. Alamillo, A. J. Crisci, G. M. Gonzalez, S. L. Scott, J. A. Dumesic, Sustainable solvent systems for use in tandem carbohydrate dehydration hydrogenation, ACS Sustainable Chem. Eng. 1 (2013) 554–560;

e) Y. Nakagawa, K. Tomishige, Total hydrogenation of furan derivatives over silica-supported Ni–Pd alloy catalyst, Catal. Comm 12 (2010) 154–156.

[2] R. A. Soomro, S. T. H. Sherazi, Sirajuddin, N. Memon, M. Raza Shah, N. H. Kalwar, K. R. Hallam, A. Shah, Synthesis of air stable copper nanoparticles and their use in catalysis, Adv. Mat. Lett. 5 (2014) 191–198.

[3] W. Wang, Y. Zhana, G. Wang, One-step, solid reaction to the synthesis of copper oxide nanorods in the presence of a suitable surfactant, Chem. Commun. (2001) 727–728.

[4] a) K. Schütte, H. Meyer, C. Gemel, J. Barthel, R. A. Fischer, C. Janiak, Synthesis of Cu, Zn and Cu/Zn brass alloy nanoparticles from metal amidinate precursors in ionic liquids or propylene carbonate with relevance to methanol synthesis, Nanoscale 6 (2014) 3116–3126;
b) J. Sun, G. Yang, Q. Ma, I. Ooki, A. Taguchi, T. Abe, Q. Xie, Y. Yoneyama, N. Tsubaki, Fabrication of active Cu–Zn nanoalloys on H-ZSM5 zeolite for enhanced dimethyl ether synthesis *via*syngas, J. Mater. Chem. A 2 (2014) 8637–8643.

[5] a) M. J. Akhtar, M. Ahamed, S. Kumar, MA M. Khan, J. Ahmad, S. A. Alrokayan, Zinc oxide nanoparticles selectively induce apoptosis in human cancer cells through reactive oxygen species, International Journal of Nanomedicine 7 (2012) 845–857;
b) S. K. Apte, S. N. Garaje, S. S. Arbuj, B. B. Kale, J. O. Baeg, U. P. Mulik, S. D. Naik, D. P. Amalnerkara, S. W. Gosavi, A novel template free, one pot large scale synthesis of cubic zinc sulfide nanotriangles and its functionality as an efficient photocatalyst for hydrogen production and dye degradation, J. Mater. Chem. 21 (2011) 19241–19248.

[6] M. Gholinejad, B. Karimi, F. Mansouri, Synthesis and characterization of magnetic copper ferrite nanoparticles and their catalytic performance in one-pot odorless carbon-sulfur bond formation reactions, Journal of molecular Catalysis A: Chemical 386 (2014) 20–27.

[7] B. K. Chatterjee, A. Dey, Ch. K. Ghosh, K. K. Chattopadhyay, Interplay of bulk and surface on the magnetic properties of low temperature synthesized nanocrystalline cubic Cu 1– x Zn x Fe 2 O 4 (x = 0.00, 0.02, 0.04 and 0.08), Journal of Magnetism and Magnetic Materials 367 (2014) 19–32.

Chapter 4

Lewis acid catalysed conversion of 5-hydroxymethylfurfural to 1,2,4 benzenetriol, an overlooked bio-based compound

Abstract

5-hydroxymethylfurfural (HMF) is a platform chemical that can be produced from renewable carbohydrate sources. HMF can be converted to 1,2,4-benzenetriol (BTO) which after catalytic hydrodeoxygenation provides a route to cyclohexanone and cyclohexanol. This mixture, known as KA-oil, is an important feedstock for polymeric products such as nylons which uses benzene as feedstock that is obtained from the BTX fraction produced in oil refineries. Therefore, the conversion of HMF to BTO provides a renewable, alternative route towards products such as nylons. However, BTO is usually considered an undesired byproduct in HMF synthesis and is only obtained in small amounts. Here, we show that Lewis acid catalysts can be utilized for the selective conversion of HMF to BTO in sub-super critical water. Overall, up to 54 mol % yield of BTO was achieved at 89 % HMF conversion using $ZnCl_2$. Lewis acids that provide limited Brønsted acidity ($ZnCl_2$, $Zn(OTf)_2$ and $Fe(OTf)_2$) displayed the highest selectivity towards BTO. Lewis acids like $Hf(OTf)_4$ and $Sc(OTf)_3$ led to aqueous solutions with higher pH and gave increased selectivity towards levulinic (up to 33 mol %) and formic acid instead of BTO. This reactivity is associated with well-known Brønsted acid mediated conversion of HMF. Catalytic hydrodeoxygenation of BTO towards cyclohexanone in water was achieved in up to 45 % yield using 5 wt % Pd on Al_2O_3 combined with $AlCl_3$ or $Al(OTf)_3$ as catalysts. Additionally, a mild selective oxygen induced dimerization pathway of BTO to 2,2',4,4',5,5'-hexahydroxybiphenyl (5,5'-BTO dimer) was identified.

Keywords: 5-hydroxymethylfurfural, HMF, platform chemicals, 1,2,4-benzenetriol, BTO, hydrodeoxygenation,cyclohexanone, cyclohexanol, lewis acid, brønsted acid catalytic, catalyst

A. J. Kumalaputri, C. Randolph, E. Otten, H. J. Heeres and P. J. Deuss, Lewis acid catalysed conversion of 5-hydroxymethylfurfural to 1,2,4-benzenetriol, an overlooked bio-based compounds (submitted)

4.1 Introduction

Due to the depletion of fossil-based feedstocks and the environmental concerns related to their use, the production of chemicals from renewable resources is of major importance for achieving a sustainable chemical industry. Aromatic compounds play an important role in the chemical industry, relying mostly on oil derived benzene-toluene-xylenes (BTX).[1,2] For example, benzene is used to produce phenol and bisphenol A as well as KA (ketone-alcohol) oil via cyclohexane, which are two processes important for industrial polymeric products such as nylons (Scheme 1).

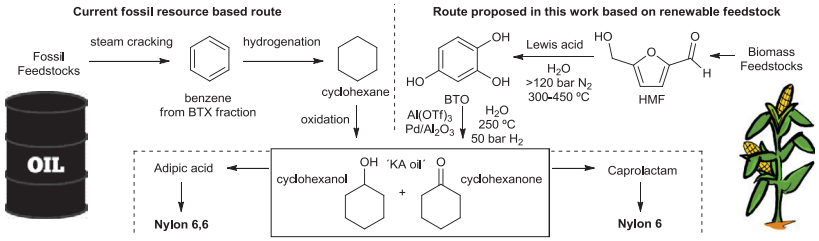

Scheme 1. Chemical routes towards KA oil and nylons, highlighting the route presented in this work relying on renewable biomass feedstocks

Biomass is an abundant and globally distributed renewable carbon resource suitable for the production of chemicals. Despite recent progress exemplified by the production of aromatics from lignin or routes from carbohydrate sources to p-xylene and mixtures of BTX, the production of aromatic chemicals from biomass is still a challenge.[1–12]

5-hydroxymethylfurfural (HMF) is a renewable platform chemical that can readily be obtained from natural carbohydrate sources and can be transformed into biofuels and valuable bio-based chemicals such as 2,5-furandimethanol (FDM), 5-methylfurfural (MF), 5-methyl-2-furanmethanol (MFM) and 2,5-dimethylfuran (DMF).[5,12] An interesting product that is often reported as a side-product in the production and conversion of HMF is 1,2,4-benzenetriol (BTO).[13,14] BTO is an antioxidant and offers a suitable platform for the production of pharmaceuticals, agrochemicals and dyes.[15,16] BTO is supposedly formed via hydrolysis of the furan ring in HMF, which is later rearranged to a hexatriene ring through an electrolytic rearrangement followed by

dehydration, which seems relatively favoured in aqueous processes at higher temperatures and with relatively long reaction times.[13,14,17–23]

In the 1990's, van Bekkum and co-workers looked at the optimization of the sub-critical reaction conditions for the conversion of HMF to BTO and achieved up to 25 mol% BTO yield in a continuous setup. The process was run with a 0.05 M aqueous HMF feed, temperatures between 330 and 350 °C, 280 bar pressure and residence times around 250 s.[13,14] Higher yields were difficult to obtain due to competing reactions such as the formation of levullinic acid as well as humin formation. Additionally, BTO itself was reported to be unstable leading to unknown degradation products. Even under ambient conditions, BTO slowly degrades in solution hampering accurate analysis.[23] In this work, for the first time the catalytic formation of BTO from HMF is presented as a method to significantly increase its rate of formation and selectivity. In particular, Lewis acids that have relatively low Brønsted acidity such as $ZnCl_2$, $Zn(OTf)_2$ and $Fe(OTf)_2$ were effective. Additionally, the main degradation pathway for BTO is identified which provides insight into how it can be suppressed and appropriately corrected for analysis. Finally, we also demonstrate the hydrodeoxygenation of BTO to cyclohexanone to provide a sustainable route to important polymeric products that avoids the use of fossil feedstocks (Scheme 1).

4.2 Results and discussion

4.2.1 Exploratory reactions including 5,5'-BTO dimer formation

An initial screening of reaction conditions in a batch reactor setup in the absence of catalyst showed that indeed 1,2,4-benzenetriol (BTO) can be obtained in significant amounts (17 mol%) from 5-hydroxymethylfurfural (HMF) at sub-critical conditions (300 °C, P_0 120 bar N_2, P_{final} up to 300 bar and 30–60 min of reaction time).[13,14] Under these conditions the HMF conversion is over 95 mol%. An initial exploratory catalyst screening showed that the addition of (Lewis acidic) salts such as $FeCl_2$ and $MgCl_2$ provided increased yields of BTO (up to 30 mol%). In addition to BTO, levulinic acid (LA) and formic acid (FA) were detected, which are products formed through the hydration of HMF as well as some minor side products and significant amounts of char that could readily be filtered from the product mixture (Scheme 2).

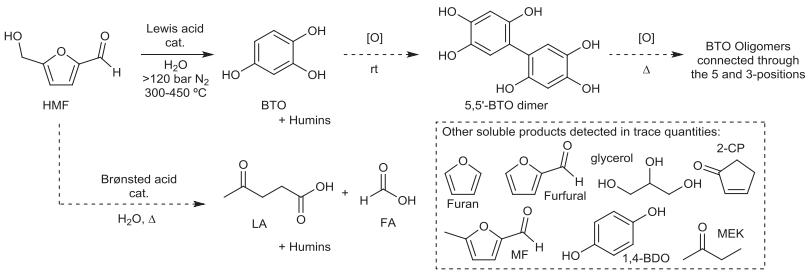

Scheme 2. Lewis acid catalysed conversion of 5-hydroxymethylfurfural (HMF) into 1,2,4-benzentriol (BTO) and detected side products formed in the reaction also showing the formation of the 5,5'-BTO dimer and further oligomers

In line with previous reports we found that the analysis of BTO can be obstructed due the degradation of BTO in solution.[18,21–22] This is typically ascribed to the formation of dimers and oligomers of unknown structure which are likely to relate to its reported air and light sensitivity.[24] To get more insight into the observed loss of BTO in our reaction samples, we made an effort in studying the degradation of BTO in solution (See SI section S5). We found that when exposed to air at room temperature, BTO selectively reacts with itself to form a 5,5' C-C bonded homodimer (5,5'-BTO dimer, Scheme 2) that could be isolated as a black powder. This material was fully characterized and crystalized from water to give the molecular structure shown in Figure 1 (Figure S1 and Table S1).

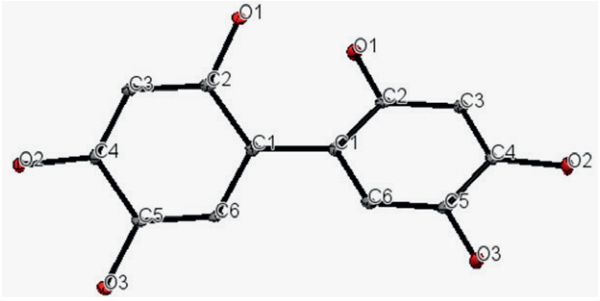

Figure 1. Molecular structure of the 5,5'-BTO dimer (2,2',4,4',5,5'-hexahydroxybiphenyl) obtained from single crystal X-ray diffraction showing 50 % probability ellipsoids. Hydrogen atoms and water solvate molecules are omitted for clarity

When a solution of BTO was heated, oligomers formed that were shown to be connected through the 3 and 5-position of BTO (Figure S2). These BTO degradation pathways could be suppressed by working under oxygen-free conditions. Long term storage of the BTO solutions could also be achieved by exclusion of air. An aqueous solution of BTO which had argon bubbled through it for an hour and which was stored under exclusion of air showed retention of BTO and no significant 5,5'-BTO dimer formation for over 10 months (as long as the experiment was run). This observation also explains why extensive degassing of the HMF to BTO reaction solutions is essential for obtaining measurable amounts of BTO. Therefore, before each experiments in which BTO was formed from HMF, the reactor was flushed three times with 120 bar of N_2. Even though this prevented dimerization of the formed BTO in the reactor some 5.5'-BTO dimer was still observed upon HPLC analysis (up to 10 mol %). This is likely caused by the formation of 5.5'-BTO dimer during the sample preparation for HPLC analysis which was not performed under exclusion of air. For this reason, we quantified the amount of 5.5'-BTO dimer by HPLC analysis and subsequently corrected the BTO yield accordingly (see SI section S3).

4.2.2 *Lewis acid catalysed formation of BTO at subcritical conditions*

Following the successful application of $FeCl_2$ and $MgCl_2$ in our first screening, a wider range of Lewis acid catalysts were applied to study the reaction in more detail. This was done by following the progress in time by a set of batch reactions at subcritical conditions (300 °C, >120 bar) and different reaction times by addition of 1.2 mM (2.4 mol %) Lewis acid catalyst (Figure 2a–c).

Figure 2d shows the error of a set of quadruplicate experiments for the reaction using $ZnCl_2$ and the non-catalysed reactions to demonstrate the reproducibility of the experiments. The rate of HMF conversion is clearly enhanced by all metal salts showing full conversion within 10 min. For several catalysts, while the reaction without catalyst takes about 40 min to reach full conversion. Overall, the HMF conversion rate showed the following order in increase for this set of metal salts: $Hf(OTf)_4 > La(OTf)_3 > Yb(OTf)_3 > Ce(OTf)_4 \approx Fe(OTf)_3 > FeCl_2 \approx Fe(OTf)_2 > HOTf > EuCl_2 > Zn(OTf)_2 > ZnCl_2 > MgCl_2$.

Additionally, the selectivity for BTO increased for all applied catalysts when compared the reaction without catalyst, however, the

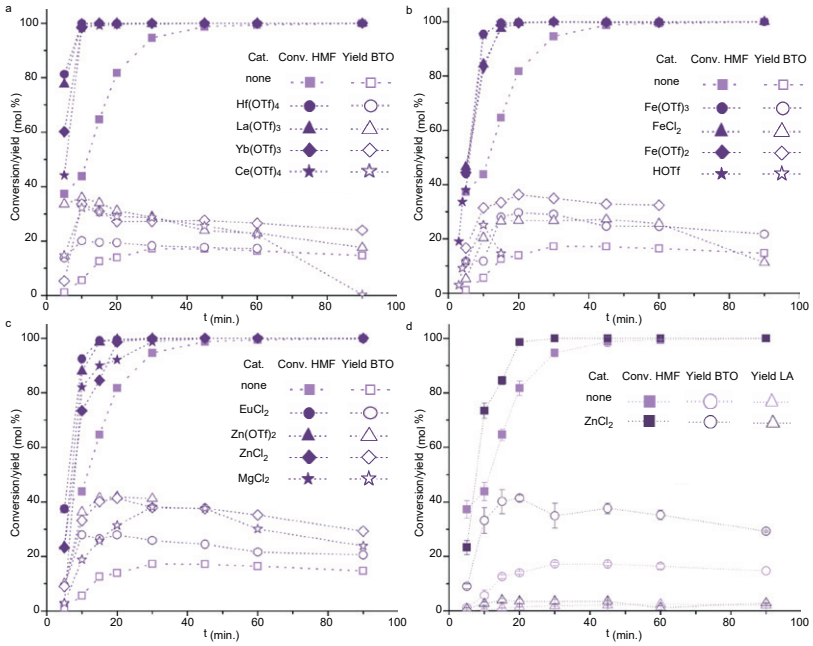

Figure 2. Lewis acid catalysed conversion of 5-hydroxymethylfurfural (HMF) into 1,2,4-benzentriol (BTO) and detected side products formed in the reaction also showing the formation of the 5,5'-BTO dimer and further oligomers

maximum yields obtained and the reaction time at which this is achieved is remarkably different. The maximum yields were increased to over 20 mol % for all catalysts and just over 40 % for $Zn(OTf)_2$ and $ZnCl_2$ (compared to 15 mol % maximum yield of BTO for the reaction without catalyst). While for the reaction without catalyst the maximum yield of BTO is achieved after 30 min, most of the catalysed reactions achieved their highest yield within 20 min. An exception was when $MgCl_2$ was used which provided a reaction progress similar to that of the reaction without catalyst nevertheless achieving a maximum BTO yield of 38 mol %. BTO appeared to be a relatively stable product under these reaction conditions as it only slowly reacted away with longer reaction times.

In order to compare the performance of the different catalysts, the reaction progress after 20 min was plotted in Figure 3a in order of the hydrolysis constants (pK_h, equations 1–3) of the different metal ions at 25 °C.[25]

$$M^{n+} + H_2O \rightarrow MOH^{n-1+} + H^+ \quad (1)$$

$$K_h = ([MOH^{n-1+}] + [H^+]) / [M^{n+}] \quad (2)$$

$$pK_h = -\log K_h \quad (3)$$

This shows that when Lewis acids are used with higher pK_h, a higher yield of BTO is obtained. On the other hand, Lewis acids with a low pK_h produced lower amounts of BTO and in general increased amounts of levulinic acid (LA) and formic acid (FA). The formation of LA and FA from HMF is known to be catalysed by Brønsted acids [22] and therefore the hydrolysis of the metal ions releasing H^+ can have a major influence on the reaction outcome. To illustrate this further, the pH of the solution before the reaction was measured. This provided an indication that more acidic media led to more LA and FA formation (Figure 3b).

However, no definite correlation was found, which is likely caused by the presence of competing reactions towards humins. Brønsted acids are known to promote the formation of humins which is the major product obtained in the reaction without catalyst or when triflic acid is added to the reaction. Lewis acid that gave the highest BTO yield (Fe and Zn) are classified as relatively soft Lewis acids compared to the others used in these reactions indicating that polarizability of the charged species might also play a role. [26,27] The use of triflate salts resulted in slightly higher BTO yields compared to chlorine salts indicating some additional influence of the counter ion.

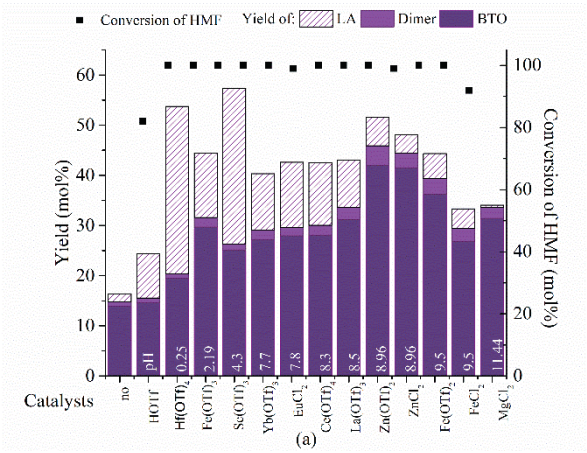

Figure 3. Lewis acid catalysed formation of BTO from HMF as well as yields of levulinic acid (LA) and comparison to the results to the pKh of the lewis acid salts to LA acid formation

(HPLC, IS = DMSO, Conditions; 5 mL 0.05 M aqueous HMF and 1.2 mM cat., T = 300 °C, P_o = 120 bar N_2, t = 20 min).

4.2.3 Further optimization of the reaction conditions

Experiments were performed for further optimization of the reaction conditions. For these experiments $Zn(OTf)_2$ and $ZnCl_2$ were selected as best performing catalysts achieving the highest yields of BTO under the reaction conditions used for catalyst screening. Of these two catalysts, $ZnCl_2$ is the cheaper option but can lead to significant corrosion of metal surfaces exposed to the reaction medium and therefore has to be handled with care. Firstly, the reaction temperature was varied from 300–450 °C (Figure 4).

As expected the HMF conversion rate increases with the increase of temperature. At higher temperature conversion rapidly increases, but seems to level off. For example at 450 °C after 10 min the HMF conversion is the same as that observed after 5 min (around 90 %). This could be due to the liquid reaching a supercritical state, which would for pure water be achieved at around 375 °C.

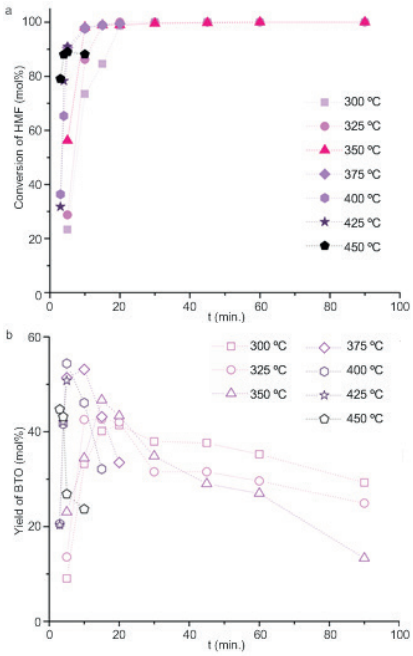

Figure 4. The reaction progress of the $ZnCl_2$ catalysed formation of BTO from HMF at different temperatures

(each t data point represents a separate experiment). a) Conversion of HMF and b) BTO yield (HPLC, IS = DMSO, Conditions; 5 mL 0.05 M aqueous HMF and 1.2 mM $ZnCl_2$, P_o = 80–120 bar N_2 depending on the final temperature)

A similar decrease in conversion was observed in reactions at temperatures above 375 °C in which no catalyst was added (Figure S4). This could be due to a change in the polarity of water heated above the critical point possibly even causing precipitation. This could indicate that the conversion of HMF is rapid under reaction conditions but does not proceed further once the critical point is reached. As for HMF conversion, the BTO yield increases with increasing temperature and seems to reach an optimum around 425 °C where a yield of 55 % is reached for $ZnCl_2$ as catalysts at 89 mol % HMF conversion and 3 min reaction time respectfully. Very similar results were obtained for $Zn(OTf)_2$ (Figure S3). At elevated temperatures the BTO yield sharply decreased in time indicating that it is not a stable product under these conditions and the reaction time has to be carefully tuned to obtain the maximum yields.

In addition to the strange effect of supercritical conditions on the HMF conversion, product selectivity seems to switch toward furan at elevated temperature (up to 22 mol %, see Table S2). Also, in reactions without catalyst furan becomes the major product. Additionally, when HMF was thermally converted in the absence of a solvent, furan is the main reaction product (Figure S5). Next, the $ZnCl_2$ concentration was varied between 0.14 and 10 mM (0.28–20 mol %) at 400 °C (Figure 5).

Only a slight increase in the rate of HMF conversion can be observed, but even with a small amount of catalyst a dramatic effect can be observed in the yield of BTO compared to a reaction without catalyst (7 mol % vs 33 mol % after a 5 min. reaction using 0 or 0.14 mM $ZnCl_2$ respectively). The BTO selectivity reaches a maximum at 1.2 mM and with higher catalyst concentrations the maximum yield of BTO seems to plateau around 50 mol %. The use of an increased catalyst concentration leads to the formation of more 2-cyclopenten-1-one and methylfurfural (2-CP and MF, Scheme 2, Table S2*). S*imilar observations were made when the HMF concentration was decreased (Figure S6 and S7). However, when the HMF concentration was increased to 0.1 and 0.25 M the selectivity for BTO dropped to around 10 %, which is likely caused by excessive char/humin formation, which is consistent with earlier reports.[22,23] Additionally, increased amounts of furan, furfural and methylfurfural are observed. Overall, in the setup used, the maximum yield of BTO was around 55 mol % using $Zn(OTf)_2$ or $ZnCl_2$ as catalyst at 400–425 °C, 80 bar initial N_2 pressure, 5 mL 0.05 M aqueous HMF and a reaction time of around 5 min.

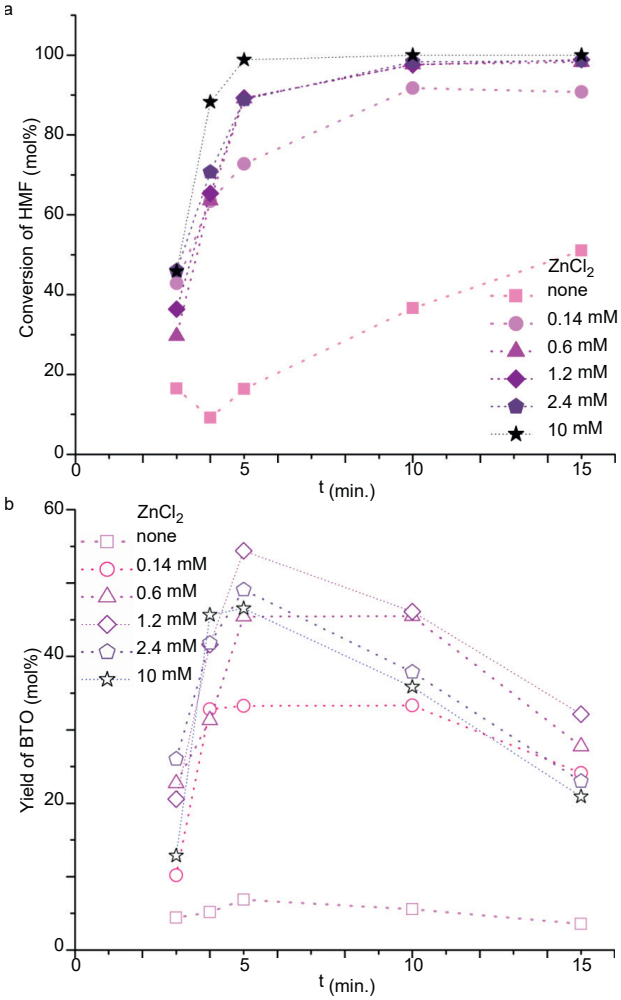

Figure 5 The reaction progress of the $ZnCl_2$ catalysed formation of BTO from HMF at different temperatures

(each t data point represents a separate experiment). a) Conversion of HMF and b) BTO yield (HPLC, IS = DMSO, Conditions; 5 mL 0.05 M aqueous HMF, T = 400 °C, P_o = 70–110 bar N_2).

4.2.4 Catalytic hydrodeoxygenation of BTO

Next, the catalytic hydrodeoxygenation of BTO to cyclohexanone was demonstrated. Cyclohexanone together with cyclohexanol is a industrial relevant compound mixture known as KA-oil, an intermediate in the production of nylons (Scheme 1). For this purpose, a mixture

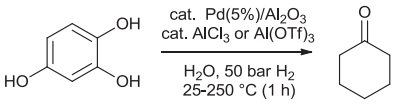

Scheme 3. Catalytic hydrodeoxygenation of BTO to cyclohexanone in water

of 2.5 mmol BTO in 25 mL water pressurized to 50 bar H_2 with 0.1 g Pd/Al_2O_3 (5 wt %) and 0.1 g $AlCl_3$ as catalysts and heating the reactor to a temperature of 250 °C followed by rapid cooling (Scheme 3). Up to 45 mol % yield of cyclohexanone (major product) could be achieved this way. $AlCl_3$ is known to be quite corrosive under the used reaction conditions. Therefore, $Al(OTf)_3$ was applied as a less corrosive alternative. At exactly the same conditions $Al(OTf)_3$ led to somewhat lower cyclohexanone yield (36 %).

The used catalytic system is inspired on a reported procedure for the catalytic hydrodeoxygenation of phenol which is achieved as milder conditions (50 °C, 10 bar H_2) but a total reaction time of 7 h and in dichloromethane as solvent.[28] Water is an excellent greener alternative solvent for such hydrodeoxygenation reactions.[29] Under these conditions no cyclohexanone formation was observed for the catalytic hydrodeoxygenation of BTO even at longer reaction times and both in water and dichloromethane as solvent. As mentioned above in water at increased temperature the reaction is successful. The required increased reaction temperature is likely the result of the additional hydrodeoxygenation steps required for the conversion of BTO to cyclohexanone compared to the same reaction from phenol. In the reaction mixture, also products such as 4-hydroxycyclohexanone, 1,2-cyclohexadiol (cis and trans), 1,4-benzenediol, furan, cyclopentene, methanol, glycerol, acetic acid and levulinic acid were detected. Some of the detected compounds (cis and trans 1,2-cyclohexadiol and 4-hydroxycyclohexanone) are likely intermediates towards cyclohexanone and hexanol, however, longer reaction times did not lead to higher yield as these appeared not to be entirely stable under the reaction conditions (Table S3).

4.3 Conclusions

This study displays the potential for the production and use of 1,2,4-benzenetriol (BTO) as a novel bio-based product that can be obtained via catalytic conversion of 5-hydroxymethylfurfural (HMF)

under supercritical conditions in water. The presented procedure for the catalytic conversion of HMF to BTO relies on the use of Lewis acid catalysts that enables the production to up to 55 mol % BTO from HMF in water under supercritical conditions. In particular, catalysts with high pK_h and low Brønsted acidity such as $ZnCl_2$, $Zn(OTf)_2$, $Fe(OTf)_2$ and $MgCl_2$ appeared suitable catalysts showing significant improvement compared to the uncatalysed reaction which yields up to 15 mol % BTO. When Brønsted acid catalysts are used HMF is converted into humins, levulinic acid and formic acid instead. Highest yields were obtained under supercritical conditions (400 °C, 280 bar). In addition, a BTO dimerization pathway as well as oligomerization was described which could lead to undesired product formation if not appropriately addressed. It was shown that these reactions can be suppressed by exclusion of air. Additionally, selective dimerization can be performed under controlled conditions leading to the isolation of 2,2',4,4',5,5'-hexahydroxybiphenyl (5,5'-BTO dimer), a compound that also has potential for use as starting material for other bio-based products. Other products that can be obtained from BTO and its dimer will be part of future investigations.

Among many synthetic possibilities BTO offers, the demonstrated catalytic hydrodeoxygenation of BTO to cyclohexanone comprises a new route towards bio-based nylons. Both reaction steps described can be performed in water as an ideal green solvent. Although the conversion of HMF to BTO requires relatively high temperatures and pressures, this conversion is atom efficient with a cheap catalyst system and therefore relatively easy to perform when suitable equipment is available. As BTO selectivity should be increased, future research will focus on further optimization of the reaction conditions, catalyst and in particular reactor set-ups. For example, implementation of a continuous flow reactor would allow for improved control over residence times, which is crucial for achieving high BTO yields and the possibility for an integrated conversion to cyclohexanone.

Acknowledgements

We would like thank the Indonesian Directorate General of Higher Education (DIKTI) for the financial sponsorship for AJK. We would also like thank Qinqing Yuan, Erwin Wilbers, Marcel de Vries, Anne Appeldoorn, Henk van de Bovenkamp, Jan Henk Marsman and Leon Rohrbach for their analytical and technical support.

References

[1] J. E. Holladay, J. J. Bozell, J. F. White, D. Johnson, Top value-added chemicals from biomass Volume II—Results of screening for potential candidates from biorefinery lignin, PNNL and NREL for the US DOE, 2007.

[2] P. C. A. Bruijnincx, B. M. Weckhuysen, Shale gas revolution: An opportunity for the production of bio-based chemicals?, Angew. Chem. Int. Ed. 52 (2013) 11980–11987.

[3] J. J. Pacheco, M. E. Davis, Synthesis of terephthalic acid via Diels-Alder reactions with ethylene and oxidized variants of 5-hydroxymethylfurfural, Proc. Natl. Acad. Sci. USA 111 (2014) 8363–8367.

[4] S. Thiyagarajan, H. C. Genuino, J. C. van der Waal, E. de Jong, B. M. Weckhuysen, J. van Haveren, P. C. A. Bruijnincx, D. S. van Es, A facile solid-phase route to renewable aromatic chemicals from bio-based furanics, Angew. Chem. Int. Ed. 55 (2016) 1368–1371.

[5] A. J. Kumalaputri, G. Bottari, P. M. Erne, H. J. Heeres, K. Barta, Tunable and selective conversion of 5-HMF to 2,5-furandimethanol and 2,5-dimethylfuran over copper-doped porous metal oxides, ChemSusChem 7 (2014) 2266–2275.

[6] C. L. Williams, C.-C. Chang, P. Do, N. Nikbin, S. Caratzoulas, D. G. Vlachos, R. F. Lobo, W. Fan, P. J. Dauenhauer, Cycloaddition of biomass-derived furans for catalytic production of renewable p-xylene, ACS Catal. 2 (2012) 935–939.

[7] P. J. Deuss, K. Barta, From models to lignin: Transition metal catalysis for selective bond cleavage reactions, Coord. Chem. Rev. 306 (2015) 510–532.

[8] H. Liu, R. Fang, Z. Li and Y. Li, Solventless hydrogenation of benzene to cyclohexane over a heterogeneous Ru–Pt bimetallic catalyst, Chem. Eng. Sci. 122 (2015) 350–359.

[9] D. Wang, C. M. Osmundsen, E. Taarning, J. A. Dumesic, Selective production of aromatics from alkylfurans over solid acid catalysts, ChemCatChem 5 (2013) 2044–2050.

[10] A. Romero, P. Yustos and A. Santos, Dehydrogenation of cyclohexanol to cyclohexanone: Influence of methylcyclopentanols on the impurities obtained in ε-caprolactam, Ind. Eng. Chem. Res. 42 (2003) 3654–3661.

[11] Y. Usui and K. Sato, A green method of adipic acid synthesis: organic solvent- and halide-free oxidation of cycloalkanones with 30% hydrogen peroxide, Green Chem. 5 (2003) 373–375.

[12] R. J. van Putten, J. C. van der Waal, E. de Jong, C. B. Rasrendra, H. J. Heeres and J. G. de Vries, Hydroxymethylfurfural, a versatile platform chemical made from renewable resources, Chem. Rev. 113 (2013) 1499–1594.

[13] G. C. A. Luijkx, F. van Rantwijk and H. van Bekkum, Formation of 1,2,4-benzenetriol by hydrothermal treatment of carbohydrates, Recueil des Travaux des Pays-Bas 110 (1991) 343–344.

[14] G. C. A. Luijkx, F. van Rantwijk and H. van Bekkum, Hydrothermal formation of 1,2,4-benzenetriol from 5-hydroxymethyl-2-furaldehyde and D-fructose, Carbohyd. Res. 242 (1993) 131–139.

[15] S. Rieble, D. K. Joshi and M. H. Gold, Purification and characterization of a 1, 2, 4-trihydroxybenzene 1, 2-dioxygenase from the basidiomycete *Phanerochaete chrysosporium*, J. Bacteriol. 176 (1994) 4838–4844.

[16] A. Suzuki, A. Fujii, H. Jokura, I. Tokimitsu, T. Hase and I. Saito, Hydroxyhydroquinone interferes with the chlorogenic acid-induced restoration of endothelial function in spontaneously hypertensive rats, Am. J. Hypertens. 21 (2008) 24–27.

[17] A. A. Rosatella, S. P. Simeonov, R. F. M. Frade and C. A. M. Afonso, 5-Hydroxymethylfurfural (HMF) as a building block platform: Biological properties, synthesis and synthetic applications, Green Chem. 13 (2011) 754–793.

[18] Z. Srokol, A. G. Bouche, A. van Estrik, R. C. J. Strik, T. Maschmeyer and J. A. Peters, Hydrothermal upgrading of biomass to biofuel: Studies on some monosaccharide model compounds, J. Carbohyd. Res. 339 (2004) 1717–1726.

[19] T. M. Aida, Y. Sato, M. Watanabe, K. Tajima, T. Nonaka, H. H. Hattori and K. Arai, Dehydration of d-glucose in high temperature water at pressures up to 80 MPa, J. Supercrit. Fluids 440 (2007) 381–388.

[20] A. Chuntanapum, T. L. K. Yong, S. Miyake and Y. Matsumura, Behaviour of 5-HMF in subcritical and supercritical water, Ind. Eng. Chem. Res. 47 (2008) 2956–2962.

[21] L. U. Huisheng, L. Xiangke and Z. Minhua, Decomposition of cellulose to produce 5-hydroxymethyl-furaldehyde in subcritical water, Trans. of Tianjin Univ. 14 (2008) 198–201.

[22] A. Chuntanapum and Y. Matsumura, Formation of tarry material from 5-HMF in subcritical and supercritical water, Ind. Eng. Chem. Res. 48 (2009) 9837–9846.

[23] A. Chuntanapum and Y. Matsumura, Char formation mechanism in supercritical water gasification process: A study of model compound, Ind. Eng. Chem. Res. 49 (2010) 4055–4062.

[24] Material Safety Data Sheet 1,2,4-Benzenetriol 99%, https://fscimage.fishersci.com/msds/56075.htm, Accessed online January 3rd 2017.

[25] S. Kobayashi, S. Nagayama and T. Busujima, Lewis acid catalysts stable in water: Correlation between catalytic activity in water and hydrolysis constants and exchange rate constants for substitution of inner-sphere water ligands, J. Am. Chem. Soc. 120 (1998) 8287–8288.

[26] S. C. Flores, J. Kherb, N. Konelick, X. Chen and P. S. Cremer, The effects of hofmeister cations at negatively charged hydrophilic surfaces, J. Phys. Chem. 116 (2012) 5730–5734.
[27] P. G. Barton, The influence of surface charge density of phosphatides on the binding of some cations, J. Biol. Chem. 243 (1968) 3884–3890.
[28] H. Liu, T. Jiang, B. Han, S. Liang and Y. Zhou, Selective phenol hydrogenation to cyclohexanone over a dual supported Pd–lewis acid catalyst, Science 326 (2009) 1250–1252.
[29] C. A. Hansen and J. W. Frost, Deoxygenation of polyhydroxybenzenes: An alternative strategy for the benzene-free synthesis of aromatic chemicals, Am. Chem. Soc. 124 (2002) 5926–5927.

Supporting Information

Materials and methods

All materials were used without further purification. HMF with a ≥99 % purity was purchased from Sigma-Aldrich. Milli-Q water was used for all experiments and analysis. The chemicals which were used as the analysis standards are: 1,2,4-benzenetriol with 99 % purity (Sigma-Aldrich), formic acid with ≥95 % purity (Sigma-Aldrich), acetic acid with 100 % purity (Merck), levulinic acid with 98 % purity (Sigma-Aldrich), glycerol with ≥99.5 % purity (Sigma-Aldrich), acetone with 99.8 % purity (Boom), 1,4-benzenediol with ≥99 % purity (Fluka), 5-methyl furfural 99 % purity (Sigma-Aldrich), furan with ≥99 % purity (Sigma-Aldrich), furfural with 77 % purity (Sigma-Aldrich), 2-butanone with ≥99 % purity (Sigma-Aldrich), 2-cyclopenten-1-one with 98 % purity (Sigma-Aldrich). Dimethyl sulfoxide which was used as the internal standard has a purity ≥99.9 % (J.T.Baker). All the catalysts which were used in this experiment are commercial catalysts, both the metal catalysts and the salt catalysts. The metal catalysts are Ru/TiO_2 (2 wt %) homemade, Ru/C (5 wt %) from Kaida, Ru/C (5 wt %) from Sigma-Aldrich, Pt/C (5 wt %) from Sigma-Aldrich, Cu/Zn alloy (np <150 nm) from Sigma-Aldrich, and $Ni/SiO_2.Al_2O_3$ (65 wt %) from Sigma-Aldrich. The salt catalysts which were used are europium (II) chloride with 99 % purity (Sigma-Aldrich), iron (II) chloride with 98 % purity (Sigma-Aldrich), anhydrous magnesium (II) chloride with ≥98 % purity (Sigma-Aldrich), zinc (II) chloride with ≥98 % purity (Sigma-Aldrich), trifluoromethanesulfonic acid with ≥99 % purity (Sigma-Aldrich), iron (II) trifluoromethanesulfonate with 98 % purity (Strem), zinc (II) trifluoromethanesulfonate with 98 % purity (Sigma-Aldrich), iron (III) trifluoromethanesulfonate with 90 % purity (Sigma-Aldrich), lanthanum (III) trifluoromethanesulfonate hydrate (Sigma-Aldrich), scandium (III) trifluoromethanesulfonate with >98 % purity (TCI), ytterbium (III) trifluoromethanesulfonate (Sigma-Aldrich), cerium (IV) trifluoromethanesulfonate hydrate (Sigma-Aldrich), hafnium (IV) trifluoromethanesulfonate with 98 % purity (Alfa Aesar).

Experimental procedure

HMF to BTO

A batch reactor made in-house from SS 316 and with a volume of 14.2 mL was used to study the conversion of HMF to BTO (see Figure S1). The maximum pressure of the reactor is 300 bar. The feed volume, setpoint temperature, and the initial pressure of N_2 determine the final pressure. The reactor was loaded with 2.5–10 mL of an aqueous feed solution of 0.01–0.25 M of HMF, with a catalyst intake of 0.14–10 mM. The reactor was closed and was flushed 3 times using 120 bar of N_2. After no leakage was detected, the reactor was pressurized with N_2, from 40–120 bar depending on the experimental conditions (reaction temperature between 300–450 °C and feed volume between 2.5–10 mL). Then the reactor was submerged in a temperature controlled fluidized sand bath. A thermocouple was placed next to the reactor to monitor the temperature. A schematic drawing is shown below.

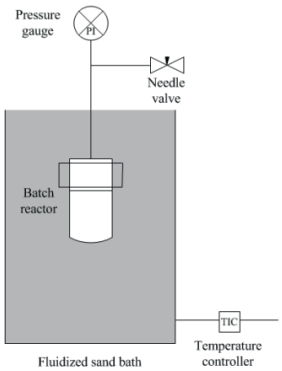

Figure S1. Experimental set up for HMF conversion to BTO

The moment the reactor was submerged was set as t_0. The reaction was performed for 3–120 min. The reactor was taken out from the fluidized sand bath and submerged in a fluidized sand bath at room temperature for about 20 min. The pressure was released by opening the valve carefully and then the reactor was opened. For analysis, 0.1 g dimethyl sulfoxide (DMSO) was added as the internal standard to the reactor before work-up. Then the solution was filtered (cellulose acetate

membrane 0.2 μm FP, Whatman) to ensure the complete removal of solids. (Part of the results are outlined in more detail in Table S2).

Analysis method for BTO

The composition of the liquid phase was determined using an Agilent 1200 HPLC consisting of a Hewlett Packard 1200 pump, a Bio-Rad organic acid column (Aminex HPX-87H), an RID and a UV detector. The mobile phase consists of an aqueous sulphuric acid (5 mM) solution which was set at a flow rate of 0.55 cm^3 per min. The column was operated at 60 °C. The analysis of a sample was complete in 80 min. The concentrations of each compound in the product mixture were determined using calibration curves obtained by analyzing standard solutions and internal standard of known concentrations. The conversion of the HMF and the yield of BTO (and others products) were calculated using equation 1–3.

$$\text{Conversion of HMF} = \frac{mmol\ HMFo - mmol\ HMF}{mmol\ HMFo} x100\% \quad (1)$$

$$\text{Yield of products} = \frac{mmol\ products}{mmol\ HMFo} x100\% \quad (2)$$

$$\text{Yield correction for BTO} = \frac{\text{mmol BTO} + (2 \text{ x mmol BTO Dimer})}{mmol\ HMFo} x100\% \quad (3)$$

The C balance numbers were calculated using equation 4–6.

$$\text{Mmol carbon in the feed} = (\text{mmol HMFo x } 6) \quad (4)$$

Where mmol HMF_o is initial mmol of HMF

$$\begin{aligned}\text{Mmol Carbon in the products} = {} & (\text{mmol HMF x } 6) + (\text{mmol BTO x } 6) + \\ & (\text{mmol Dimer x } 12) + (\text{mmol FA x } 1) + \\ & (\text{mmol Glycerol x } 3) + (\text{mmol AA x } 2) + \\ & (\text{mmol LA x } 5) + (\text{mmol MEK x } 4) + \\ & (\text{mmol 2CP x } 5) + (\text{mmol 14 BDO x } 6) + \\ & (\text{mmol Furan x } 4) + (\text{mmol Furfural x } 5) + \\ & (\text{mmol MF x } 6)\end{aligned} \quad (5)$$

$$\text{C balance} = \frac{mmol\ C\ in\ the\ products}{mmol\ C\ in\ the\ feed} x100\% \quad (6)$$

Hydrodexoygenation of BTO

A Parr batch reactor (SS 316) with a volume of 100 mL was used for the experiments (Figure S2). The maximum pressure of the reactor is 340 bar and the maximum temperature is 350 °C. The autoclave is surrounded by a heating mantle (metal block) with an electrical heater and a cooling system (air and water). A mechanical stirrer was used and was set to 600 rpm. A PRV (Pressure Release Valve) was installed for safety. This autoclave was equipped with a dip tube for sampling. A bomb vessel was installed for feed injection using N_2 gas.

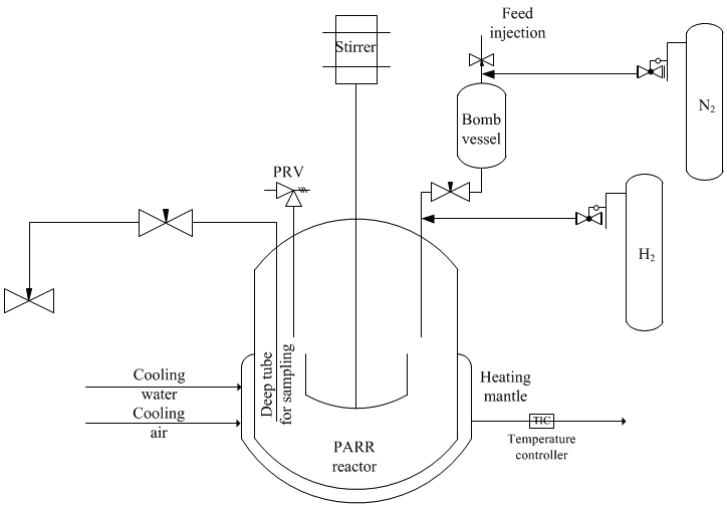

Figure S2. Experimental set up for hydrodeoxygenation of BTO

The reactor was loaded with 25 mL of mQ water containing 2.5 mmol of BTO and 0.1 g of Pd/Al_2O_3 and 0.1 g of $AlCl_3$ or $Al(OTf)_3$. The reactor was closed and flushed 3 times using 90 bar of N_2. After no leakage was detected, the reactor was filled in with 50 bar of H_2. Then the reactor was set to the desired temperature (30–250 °C).

When the temperature reached the set-point, the time was set at t_0. The reaction time was between 0–5 h. The reactor was cooled and the pressure was released by opening the valve carefully (to prevent liquid loss). Subsequently, 500 µL of a 0.1 g/10 mL dimethyl sulfoxide (DMSO) was used as the internal standard for analysis. Then the solution was filtered (cellulose acetate membrane 0.2 µm FP, Whatman) to ensure the complete removal of solids.

Furthermore, the reaction was performed in the absence of oxygen to prevent BTO dimerization and oligomerization. BTO and the catalysts (Pd/Al_2O_3 and $Al(OTf)_3$) were placed in the reactor as solids after which it was directly flushed 10 times using 60 bar of N_2. Also, the solvent (mQ water) was degassed for about 1 h before injecting to the reactor. The whole mixture was then flushed 3 times using 100 bar N_2.

Supplementary data BTO dimerization/oligomerization

5,5-BTO dimer isolation and characterization

When an aqueous solution of 1,2,4-benzenetriol (BTO), which has the appearance of a grey/beige powder (Figure S3, left picture), was left in time exposed to air the solution slowly darkened (Figure S3, middle picture), resulting in a very dark solution with a precipitate which can be isolated as a black powder after washing with water, to remove unreacted BTO, and drying (Figure S3, right picture).

Figure S3. An aqueous solution of 1,2,4-benzenetriol (BTO), which has the appearance of a grey/beige powder (left picture), was left in time exposed to air the solution slowly darkened (middle picture), resulting in a very dark solution with a precipitate which can be isolated as a black powder after washing with water, to remove unreacted BTO, and drying (right picture)

This black powder was confirmed to be the BTO dimer 2,2',4,4',5,5'-Hexahydroxybiphenyl (5,5'-BTO dimer) by NMR (see below) and X-ray diffraction of a recrystallized fraction from water yielding very brittle black needles (also below, Figure S4).

Figure S4. An aqueous solution of 1,2,4-benzenetriol (BTO), which has the appearance of a grey/beige powder (left)

^{1}H- and ^{13}C-NMR spectra of 5,5'-BTO dimer in d6-DMSO (400 MHz/100 MHz respectively) are shown below (assignment also using a APT and gHSQC experiment, see Figure S5 and S6).

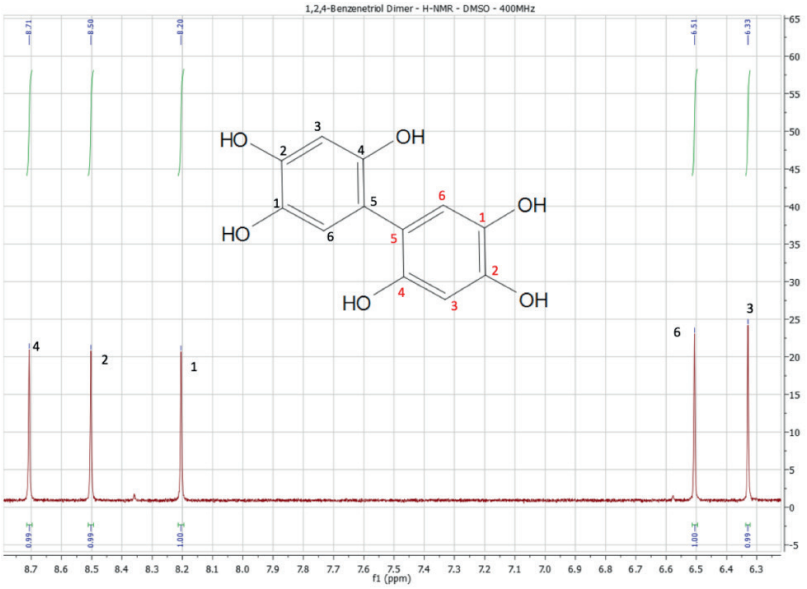

Figure S5. ^{1}H-NMR spectra of BTO dimer

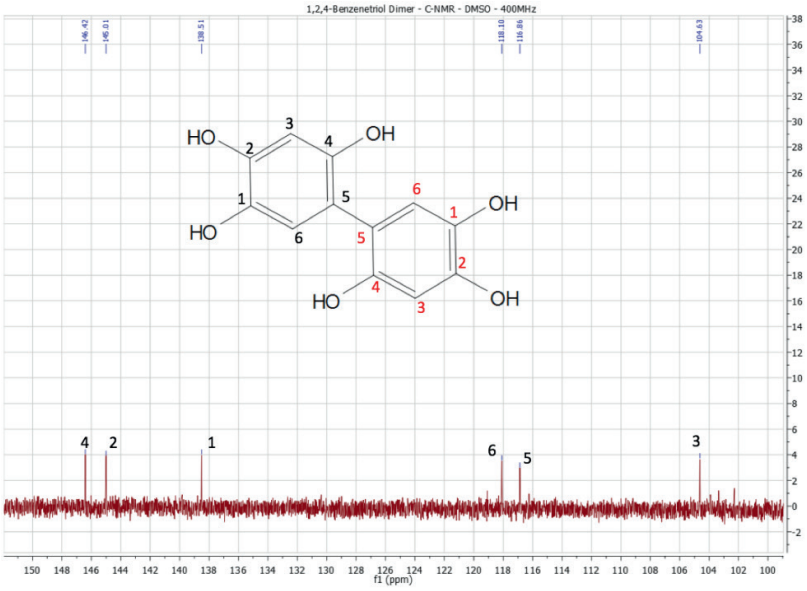

Figure S6. ^{13}C-NMR spectra of BTO dimer

X-ray crystallography

A single crystal of 2,2',4,4',5,5'-hexahydroxybiphenyl was mounted on top of a cryoloop and transferred into the cold nitrogen stream (100 K) of a Bruker-AXS D8 Venture diffractometer. Data collection and reduction was done using the Bruker software suite APEX3.[1] The final unit cell was obtained from the xyz centroids of 5785 reflections after integration. A multiscan absorption correction was applied, based on the intensities of symmetry-related reflections measured at different angular settings (*SADABS*). The structures were solved by direct methods using *SHELXT*[2] and refinement of the structure was performed using *SHLELXL*.[3] The carbon-bound hydrogen atoms were generated by geometrical considerations, constrained to idealised geometries and allowed to ride on their carrier atoms with an isotropic displacement parameter related to the equivalent displacement parameter of their carrier atoms. The oxygen-bound hydrogen atoms were tentatively located in a difference Fourier map, which indicated that those on O1 and O3 were likely disordered over two positions (in line with the expected hydrogen-bonding network). The hydrogen atom on O2 were generated by geometrical considerations, constrained to an idealised geometry and allowed to ride on O2 with an isotropic displacement parameter related to the equivalent displacement parameter of O2. The hydrogen atoms on O1 and O3 (each oxygen having a 50/50 ratio of two O-H orientations) were obtained from a difference Fourier synthesis and constrained to O-H distances of 0.84 Å, with isotropic displacement parameters related to the equivalent displacement parameters of their carrier atoms. The hydrogen atoms on the water molecule (O1W) were constrained to have O-H distances of 0.86 Å, with a H-H distance of 1.47 Å. Crystal data and details on data collection and refinement are presented in Table S1.

Table S1. Crystallographic data for 2,2',4,4',5,5'-hexahydroxybiphenyl

Chem. formula	286.23
Mr	286.23
Cryst syst	Monoclinic
Color, habit	dark brown, needle
Size (mm)	0.71 × 0.14 × 0.03
Space group	*P*2/n
a (Å)	3.8541(4)
b (Å)	6.0625(5)
c (Å)	24.554(2)
α, deg	90
β, deg	94.163(4)
γ, deg	90
V (Å^3)	572.21(9)
Z	2
ρ_{calc}, g.cm^{-3}	1.661
μ(Mo K$\bar{\alpha}$), cm^{-1}	0.142
F(000)	300
Temp. (K)	100(2)
θ range (deg)	3.328–26.372
Data collected (h,k,l)	–4:4, –7:7, –30:30
No. of rflns collected	9007
No. of indpndt reflns	1168
Observed reflns	1076 ($F_o \geq 2\,s(F_o)$)
R(F) (%)	6.68
wR(F^2) (%)	17.29
GooF	1.039
Weighting a,b	0.0640, 2.9567
Params refined	110
Restraints	7
Min, max resid dens	–0.666, 0.529

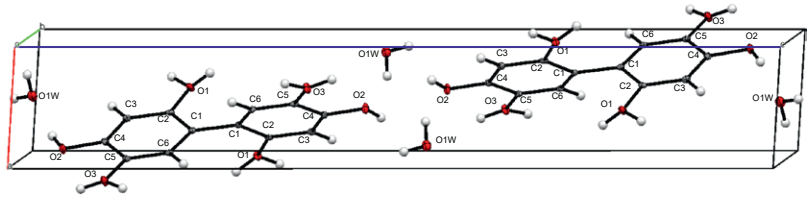

Figure S1. Molecular structure of 2,2',4,4',5,5'-hexahydroxybiphenyl (5,5'-BTO dimer), showing 50 % probability ellipsoids. The two hydrogens shown at O1 and O3 have a relative 50/50 probability ratio as described in the text above

Mechanism for BTO dimer and oligomer formation

When the aqueous solutions of BTO were exposed to base or heated to 60 °C the reaction became more complex showing the formation of trimers and higher oligomers of BTO by LCMS (ES^-). These were shown by ^{1}H-NMR to be mainly coupled through the 3 and 5 positions of BTO as relatively only the hydrogen on the 6 position can be observed in the final product (Figure S2).

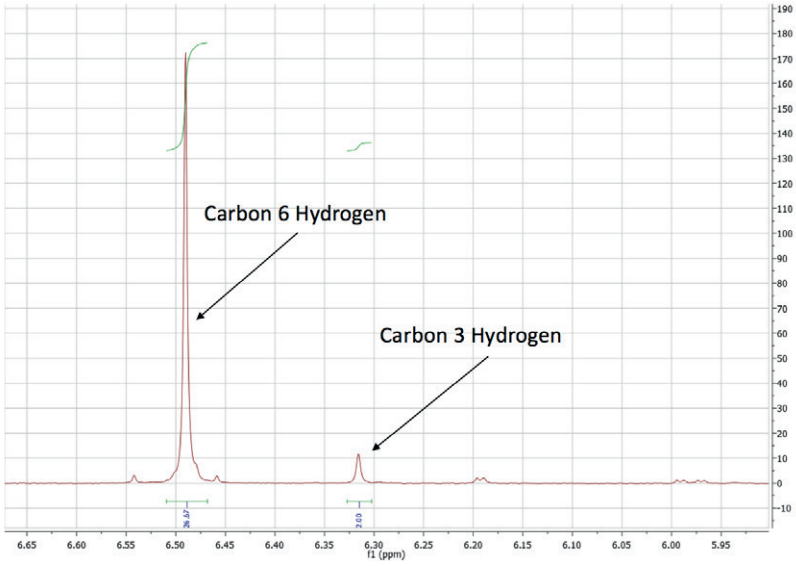

Figure S2. ^{1}H-NMR (d_6-DMSO) of the oligomeric material

An addition of a small amount of hydrogen peroxide caused complete conversion of BTO in less than a min (but unselective coupling). These observations, combined with the observed suppression of the reaction upon degassing of the reaction (see manuscript), led us to believe the reaction goes through a oxygen induced radical dimerization and oligomerization. The regioselectivity is believed the result of prefered localization of the radical on the 3 and 5 position due to resonance and preference reactivity on the 5 position due to steric hinderance of the 3 position (see scheme below).

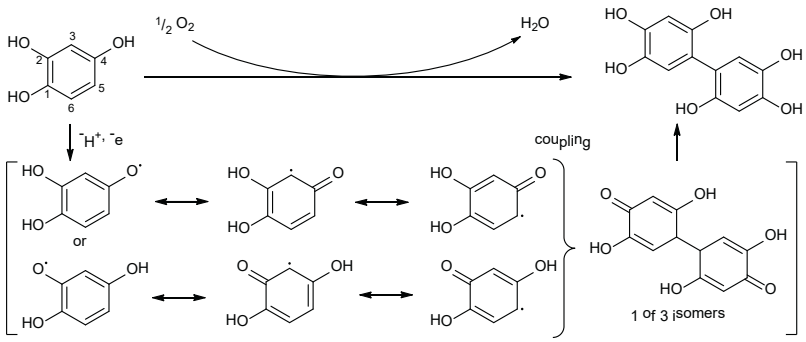

Scheme 3. The dimerization mechanism of BTO

Supplementary Data HMF to BTO reactions

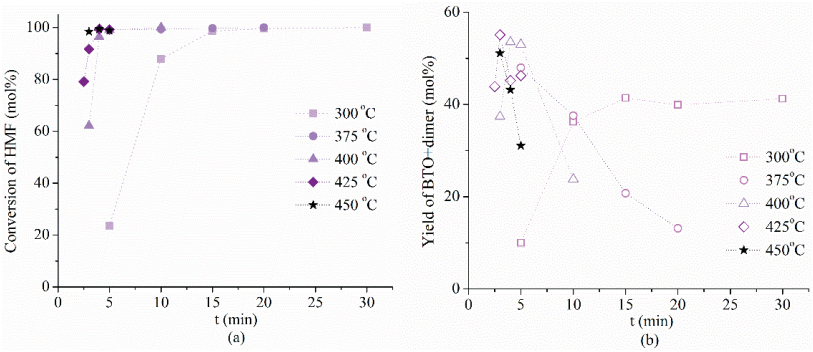

Figure S3 a) Conversion of HMF and b) BTO yield using $Zn(OTf)_2$ as catalyst at different temperatures and reaction times

(Conditions; 5 mL 0.05 M aqueous HMF and 1.2 mM $Zn(OTf)_2$, P_o = 80–120 bar N_2 depending on the final temperature, analysis by HPLC using dimethylsulfoxide as internal standard)

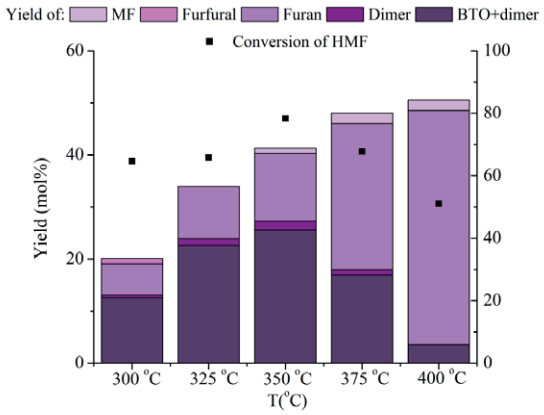

Figure S4 Blank reactions (no catalyst). Conversion of HMF and product yields

(Conditions; 5 mL 0.05 M aqueous HMF, P_o = 40–120 bar N_2 depending on the final temperature, t = 15 min)

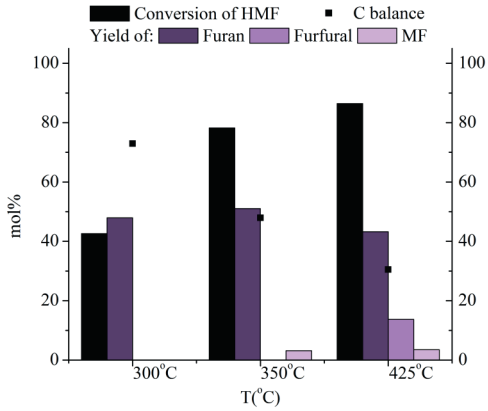

Figure S5 Thermal conversion of HMF without solvent or catalyst

(Feed = 0.0631 g HMF, T = 300–425 °C, P_o = 110 bar N_2 depending on the final temperature, t = 5 min)

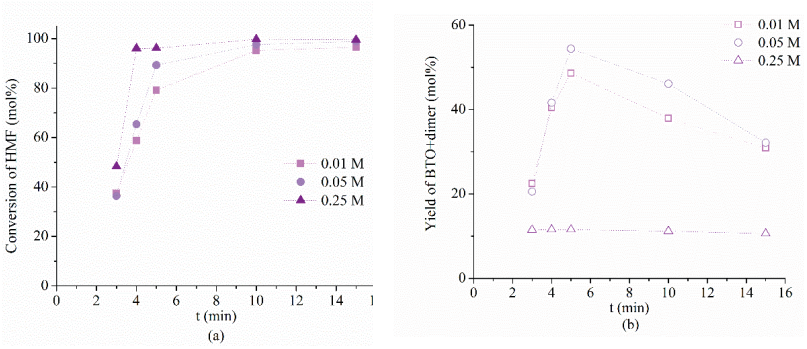

Figure S6 a) Conversion of HMF and b) BTO yield using different feed concentrations and reaction times

(Conditions; 5 mL 0.01–0.25 M aqueous HMF and 1.2 mM $ZnCl_2$, T = 400 °C, P_o = 70–120 bar N_2, analysis by HPLC using dimethylsulfoxide as internal standard)

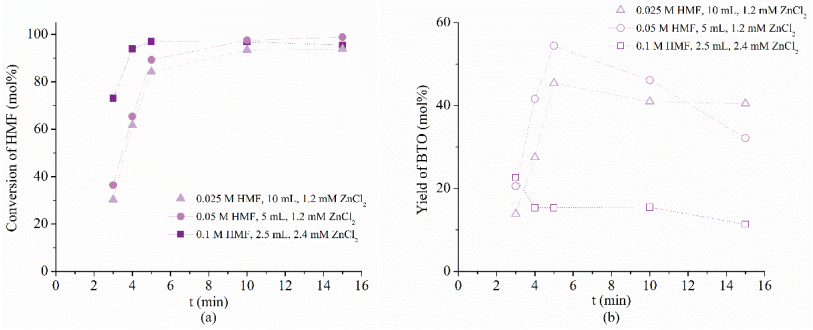

Figure S7 a) Conversion of HMF and b) BTO yield using different feed concentrations, total volume and reaction times

(Conditions; 2.5–10 mL 0.025–0.1 M aqueous HMF and 1.2–2.4 mM $ZnCl_2$, T = 400 °C, P_o = 40–120 bar N_2 depending on the final temperature, analysis by HPLC using dimethylsulfoxide as internal standard)

Table S2. Overview of data BTO production

Catalysts	T (°C)	t (min)	C HMF (M)	V feed (mL)	P_0 N_2 (bar)	P_{final} N_2 (bar)	Conversion of HMF (%)	Yield (mol %)												C balance
								BTO corr.	Dimer	FA	Glycerol	AA	LA	MEK	2CP	14BDO	Furan	Furfural	MF	(mol %)
-	300	5	0.05	5	120	285	37	1	0	0	2	0	0	0	0	0	3	0	0	68
		10				285	44	6	0	0	3	0	0	0	0	0	8	0	0	70
		15				300	65	13	0	0	4	0	1	0	0	0	5	0	0	55
		20				300	82	14	1	0	4	0	2	0	0	0	4	0	1	39
		30				300	95	17	1	1	2	0	2	0	0	0	0	1	1	31
		45				300	99	17	1	0	4	1	2	0	1	0	0	1	1	24
		60				300	99	16	1	0	3	1	2	0	1	0	2	1	0	27
		90				300	100	15	1	0	3	1	2	0	2	0	0	3	0	23
1.2 mM $ZnCl_2$	300	5	0.05	5	120	260	23	9	0	3	0	0	1	0	0	0	8	0	0	92
		10				280	73	33	3	2	0	0	3	4	0	0	7	0	0	71
		15				280	85	40	4	1	0	4	4	3	1	0	1	0	1	65
		20				280	99	41	3	0	4	1	4	2	1	0	0	0	1	41
		30				280	100	35	3	0	0	0	4	3	1	0	0	0	1	42
		45				280	100	38	4	1	0	1	4	3	2	0	0	0	0	45
		60				280	100	35	3	1	0	2	1	3	2	0	0	0	0	41
		90				280	100	29	2	1	0	1	3	2	2	0	0	0	0	35
1.2 mM $ZnCl_2$	325	5	0.05	5	120	260	29	14	0	0	3	0	2	0	0	0	6	0	0	91
		10				290	86	43	4	5	1	0	4	0	0	0	5	0	1	63
		15				300	99	43	5	5	1	1	4	5	2	0	0	0	0	54
		20				300	100	42	4	3	1	2	4	0	3	0	0	0	0	49
		30				300	100	32	2	0	0	0	3	0	4	0	0	0	0	36
		45				300	100	32	3	0	0	0	3	0	6	0	0	0	0	39
		60				300	100	30	3	0	0	0	3	0	6	0	0	0	0	37
		90				300	100	25	2	0	0	0	3	0	7	0	0	0	0	33
1.2 mM $ZnCl_2$	350	5	0.05	5	120	285	56	23	2	0	0	0	2	0	1	0	14	0	0	79
		10			120	300	98	34	4	0	5	0	4	0	3	0	6	0	0	48
		15			100	295	99	47	5	0	1	2	4	0	3	0	0	0	2	57
		20			100	285	99	43	5	0	1	2	3	0	5	0	0	0	0	52
		30			100	300	100	35	4	0	0	2	4	0	7	0	6	0	0	49
		45			100	290	100	29	3	0	0	2	3	0	10	0	6	0	0	45
		60			100	280	100	27	2	0	0	2	4	0	13	0	10	0	0	49
		90			100	290	100	13	1	0	0	2	3	0	17	0	13	0	0	39
1.2 mM $ZnCl_2$	375	5	0.05	5	90	285	91	51	6	0	3	0	2	0	3	0	8	0	2	74
		10			90	300	98	53	6	0	0	1	2	0	4	0	0	0	0	61
		15			90	300	99	43	4	0	0	1	3	0	7	0	0	0	3	56

Catalysts	T (°C)	t (min)	C HMF (M)	V feed (mL)	P_0 N_2 (bar)	P_{final} N_2 (bar)	Conversion of HMF (%)	Yield (mol %)												C balance
								BTO corr.	Dimer	FA	Glycerol	AA	LA	MEK	2CP	14BDO	Furan	Furfural	MF	(mol %)
		20			85	300	99	34	3	0	0	1	3	0	10	0	4	0	1	50
1.2 mM $ZnCl_2$	400	3	0.05	5	80	230	36	21	1	4	0	0	1	0	0	0	8	0	0	91
		4			80	260	65	42	4	5	0	0	3	0	0	0	12	0	0	87
		5			80	280	89	54	6	3	0	0	2	0	2	0	10	0	2	78
		10			80	300	98	46	5	1	0	1	2	0	6	0	0	0	3	59
		15			80	300	99	32	3	0	0	1	3	0	12	0	0	0	2	48
1.2 mM $ZnCl_2$	425	3	0.05	5	80	240	32	20	2	0	3	0	1	0	2	0	10	0	0	99
		4			80	280	78	42	4	1	2	0	1	0	2	0	9	0	2	82
		5			90	300	91	51	5	2	0	0	2	0	4	0	9	0	3	74
1.2 mM $ZnCl_2$	450	3	0.05	10	80	300	79	45	4	19	0	0	4	0	2	0	14	0	2	86
		4			80	300	88	43	4	8	0	0	3	0	2	0	12	0	2	71
		5			80	300	83	27	2	2	0	1	2	0	6	0	22	0	3	69
		10			80	300	88	24	1	2	0	2	2	0	5	0	21	0	4	70
0.14 mM $ZnCl_2$	400	3	0.05	5	110	200	43	23	1	0	1	3	1	0	1	0	18	0	2	97
		4			100	270	63	31	2	0	1	2	2	0	1	0	13	0	3	83
		5			80	295	73	33	2	0	1	2	2	0	1	0	15	0	2	77
		10			80	300	92	33	2	0	1	2	2	0	3	1	8	0	4	57
		15			70	290	91	24	1	0	1	3	3	0	6	0	13	0	5	55
0.6 mM $ZnCl_2$	400	3	0.05	5	80	210	30	10	0	5	0	1	3	0	0	0	8	0	0	89
		4			80	250	64	33	2	5	0	1	3	0	0	0	11	0	0	80
		5			80	270	89	45	4	7	0	1	3	0	2	0	11	0	2	71
		10			80	300	98	45	5	4	0	3	4	0	6	0	9	0	3	66
		15			80	300	98	28	2	3	0	3	3	0	10	0	8	0	3	50
2.4 mM $ZnCl_2$	400	3	0.05	5	80	225	46	26	2	3	0	0	2	0	0	0	9	0	0	88
		4			80	240	71	42	4	7	0	0	3	0	3	0	7	0	0	82
		5			80	260	89	49	5	5	0	0	3	0	2	0	7	0	1	71
		10			80	300	98	38	3	0	1	2	3	0	7	0	3	0	2	54
		15			80	300	99	23	2	0	0	4	3	0	16	0	11	0	2	51
10 mM $ZnCl_2$	400	3	0.05	5	80	190	46	13	1	0	1	0	1	0	0	0	6	0	0	73
		4			80	220	88	46	4	0	1	0	4	0	0	0	6	0	0	65
		5			80	260	99	46	4	0	1	0	3	0	2	0	0	0	0	52
		10			80	300	100	36	3	0	0	1	3	0	8	0	5	0	0	49
		15			70	295	100	21	1	0	0	1	3	0	16	0	9	0	0	44

*Note: BTO: 1,2,4-benzenetriol; FA: Formic acid; LA: AA: Acetic acid; Levulinic acid; MEK: Methyl ethyl ketone/butanone; 2CP: 2-cyclopenten-1-one; 14 BDO: 1,4-benzenediol; MF: 5-methylfurfural

References

[1] Bruker, (2016). *APEX3* (v2012.4-3), SAINT (Version 8.18C) and SADABS (Version 2012/1). Bruker AXS Inc., Madison, Wisconsin, USA.

[2] G. M. Sheldrick, Crystal structure refinement with *SHELXL*, Acta Cryst, A71 (2015) 3–8.

[3] G. M. Sheldrick, A short history of SHELX, Acta Cryst, A64 (2008) 112–122.

Chapter 5

Glycerol methanation in supercritical water: a systematic catalyst screening study using mono- and bimetallic supported Ru and Ni catalysts

Abstract

We here report a catalyst screening study on the methanation of glycerol in supercritical water. A number of mono-and bimetallic Ru and Ni catalysts were prepared on various supports such as TiO_2, SiO_2, ZrO_2, CeO_2, Al_2O_3, C and C nanotubes. The reactions were carried out in a batch reactor set-up using 10 wt % of glycerol in water, pressures between 200 and 300 bar at 400 °C for 20 min. Selectivity to gas phase components proved to be a strong function of the catalyst used, with the Ru catalysts giving mainly methane whereas the Ni catalysts mainly produced hydrogen. Intermediate performance was observed for the bimetallic Ru-Ni catalysts. The best results when aiming for methane were obtained using the monometallic Ru/TiO_2 catalyst (2 wt %), which gave a methane yield of 1.43 mol/mol glycerol at essential quantitative glycerol conversion. The gas phase in this case consisted of 40 mol % of methane, which is 4 % below the calculated equilibrium value. Stability of this catalyst was investigated by performing several recycle experiments, showing a significant reduction in catalytic activity after 5 runs. Regeneration of the catalyst proved possible by an oxidative treatment. Catalyst characterization studies of fresh and spent catalyst reveal that coke formation on the catalyst is the main source for deactivation, in line with the recycle/regeneration studies.

Keywords: glycerol, methanation, supercritical water gasification, scwg, methane, green gas, Ru catalyst, Ni catalyst, Ni-Ru catalyst, titania support.

A. J. Kumalaputri, H. J. Heeres, Glycerol methanation in supercritical water: a systematic catalyst screening study using mono- and bimetallic supported Ru and Ni catalysts *(to be submitted)*

5.1 Introduction

The production of biodiesel inevitably leads to the formation of glycerol. The amount of glycerol is expected to grow substantially in the future due to the anticipated growth in the biodiesel industry.[1,2] As such, novel outlets for glycerol need to be developed, for instance for the generation of bio-based chemicals, syngas, to be used for biofuel generation (Fischer-Tropsch/FT, dimethyl ether/DME) or for green gas.[3] Supercritical water gasification (SCWG) of biomass, using both of solids (wood, straw) or liquids (e.g. glycerol) is an emerging technology that has received considerable attention over the last decade.[4–6]

SCWG is typically performed at severe reaction conditions with pressures exceeding 200 bar and temperatures up to 800 °C. The technology is particularly suited for wet feeds.[7–11] The raw product gas contains mainly H_2, CO_2, CO and CH_4, of which the exact composition can be steered by process conditions and the catalyst type.[1]

Thermodynamic calculations dictate that CH_4 is preferably formed at low temperatures (<500 °C) whereas CO and H_2 rich gases are favoured at elevated temperatures (>500 °C). An advantage of the process is that the gas products become available at high pressures (>200 bar), which eliminates the use of an expensive compression step.[12,13] In addition, the gas is relatively clean and most of the contaminants remain in the water phase.[14]

The maximum amount of methane is obtained when the biomass source is quantitatively converted to methane and CO_2 without the formation of CO and hydrogen. For glycerol, the overall stoichiometry is given in eq 1.

$$C_3H_8O_3 \rightarrow 1.75\ CH_4 + 1.25\ CO_2 + 0.5\ H_2O \qquad (1)$$

Thus, a maximum methane yield of 1.75 mol per mol of glycerol converted is attainable, giving a dry gas composition of at maximum 58 mol % methane and 42 mol % CO_2. When aiming for methane, thermodynamics dictate that operation at low temperature is required. Thus, to obtain high glycerol conversions and high amounts of methane in the gas phase, the use of catalysts is essential. The catalysts need to be active for different reactions in the network *viz.* (i) the initial decomposition of glycerol into water-soluble intermediate products (e.g. acrolein); (ii) the conversion of these intermediate products to gas phase components; and (iii) gas phase reactions like the water shift reaction and methanation of CO and CO_2.

Well known catalysts for SCWG are homogeneous catalysts such as metal salts ($NaHSO_4$, $ZnSO_4$), supported noble metal catalysts (Ru, Pd, Pt, Ir) and non-noble metal catalysts (e.g. Ni, Co, Cu) on several supports as CeO_2, Al_2O_3 and La_2O_3. An overview of catalyst studies using heterogeneous catalysts for glycerol gasification is given in Table S1 and S2.[15–28]

Ru and Ni based catalysts have shown significant activity for methane production when using glycerol as the feed.[29] We recently reported an exploratory catalyst screening study with a number of Ni catalysts (i.e. Ni/ZrO_2, Ni/CaO–6Al_2O_3 and NiCu/$CeZrO_2$) at a wide range of temperature (375–700 °C) and pressures (255–270 bar). A continuous flow reactor made from Incoloy 825 was used with residence times between 8–87 s. Quantitative glycerol conversion could be achieved. For these Ni catalysts, the gas phase was enriched in hydrogen (44–67 mol % H_2, 1–21 mol % CO and 16–34 mol %).[30] The observation that Ni catalysts are better for hydrogen production was also confirmed by Iriondo et al. for a Ni/Al_2O_3-La_2O_3 catalyst. In a continuous fixed-bed reactor operated at a WHSV (Weight Hourly Space Velocity) of 1.25 h^{-1}, glycerol conversions of at least 37 mol % were obtained at relatively low temperatures (225 °C) and pressures (30 bar). The gas phase contained 32 mol % of hydrogen, 28 mol % of CH_4 and CO_2 (40 mol %).[31]

The use of a bimetallic Ni-Pt catalyst supported on alumina for glycerol reforming in supercritical water in a continuous fixed bed reactor was reported by Brilman et al. (15 wt % of glycerol, 2 mL/min flowrate, WHSV of 17.86 h^{-1}) at a temperature of 450 °C and a pressure of 250 bar. Quantitative glycerol conversion was observed at these conditions, giving a gas phase consisting of 46 mol % of H_2 and 20 mol % of CH_4. Catalyst deactivation was not a major issue and runtimes of 85 h were possible.[32]

Particularly Ru catalysts have shown to be active catalysts for the methanation of glycerol. For instance, Kersten et al. reported the use of Ru/TiO_2 at 600 °C and a pressure of 300 bar. The reactions were performed in quartz capillaries for 1 min and gave 20 mol % of methane in the gas phase at 52–60 mol % glycerol conversion (17 wt % glycerol as the feed with addition of 1–3 wt % NaOH).[16] Byrd et al. reported the use of Ru/γ-Al_2O_3 at high temperature (800 °C) and pressure (241 bar) in a fixed-bed flow reactor using residence times between 1–4 s. Almost full glycerol conversion (>99 %) was observed and the gas phase contained up to 20 mol % of CH_4.[21] The use of a Ru/ZrO_2 catalyst for glycerol gasification was reported by May et al. at temperatures between 510–550 °C and 350 bar pressure. Higher gasification efficiencies were observed when prolonging the residence

time (up to 8.5 s) and at higher temperatures. However, carbon balance closure was limited until a maximum of 80 %. [20]

Recently, the use of a bimetallic Ni-Ru catalyst on an alumina support was reported for the gasification in supercritical water at 500–700 °C and pressure of 275 bar in a continuous set-up. In this case, the aqueous fraction of a pyrolysis liquid was used as the feed. Carbon-to-gas efficiencies of 0.91 mol/mol C and a methane yield of 0.26 mol/mol C were reported. The catalyst was stable for runtimes of 6 h (WHSV = 3 h^{-1}). [33]

We here report a systematic screening study on the use of heterogeneous catalysts for the catalytic gasification of glycerol in supercritical water with the objective of obtaining a methane-rich gas phase at high glycerol conversion and high carbon-to-gas efficiencies (limited coke formation). Such screening studies at well-defined conditions are lacking in the literature, particularly in the low temperature regime (<500 °C) where methane formation is thermodynamically favoured. A number of monometallic Ru and Ni and bimetallic Ru-Ni catalysts were prepared. Several supports tested *viz*. TiO_2, ZrO_2, CeO_2, Al_2O_3, carbon, carbon nanotubes (multi-walled) and SiO_2. Reactions were carried out in a batch set-up using 10 wt % glycerol in water was used as the feed at 400 °C for 20 min batch time. The best catalysts on the titania support were characterized in detail. Stability of this catalyst was investigated by performing several recycle experiments. Characterization of fresh and spent catalysts reveal was performed to study possible catalyst deactivation pathways.

5.2 Materials and methods

All chemicals were used as received. Glycerol with a purity ≥99.5 % was purchased from Sigma Aldrich. Ru (III) nitrosyl nitrate [$Ru(NO)(NO_3)_x(OH)_y$] with 31.3 wt % Ru was obtained from Alfa Aesar. Ni (II) nitrate hexahydrate [$Ni(NO_3)_2.6H_2O$] with 99.999 % purity was from Sigma Aldrich. n-butanol (99 %) was purchased from Across Organic, polyethylene glycol (PEG) with an average Mw of 950–1050 was from Sigma Aldrich. Activated carbon (particle size <100 μm) was bought from Merck. Titanium dioxide (TiO_2, pure anatase, average particle size 21 nm, ≥99.5 %), silicon dioxide (SiO_2, average particle size 5–15 nm, 99.5 % purity), zirconium (IV) dioxide (ZrO_2, particle size <100 nm), aluminium oxide (Al_2O_3, ≥98 % purity), cerium (IV) oxide (CeO_2, 99.995 % purity), multi walled carbon nanotubes (OD L 6–9 nm

with 5 μm particle size, ≥95 % purity) were obtained from Sigma Aldrich. Milli-Q water was used for all experiments.

5.3 Experimental procedure

5.3.1 Catalyst preparation

A. Monometallic Ru-catalysts (2 wt % Ru)

Ru (III) nitrosyl nitrate (0.2134 g) and PEG (1.76 g) were added to a solvent mixture of water-*n*-butanol (75–25 vol %, 120 mL) and heated till reflux for 2 h. The support (3 g), which was pre-calcined at 600 °C for 16 h (except for carbon and carbon nanotubes, which were pre-calcined at 120 °C for 4 h) was added under vigorous stirring for 3 h. The solvent was distilled off and the resulting solid was calcined at 400 °C for 5 h in ambient air. The sample was heated up with a rate of 10 °C/min. The catalysts were used for the experiments without a reduction step and as such it is assumed that *in-situ* activation by molecular hydrogen occurs.

B. Monometallic Ni catalysts (2 wt % Ni)

A similar procedure as given above for Ru was followed except that Ni (II) nitrate-hexahydrate (0.313 g) was used.

C. Bimetallic Ni-Ru catalysts (2 wt % Ni, 0.3 wt % Ru)

A similar procedure as given above for Ru was followed except that 0.313 g of Ni (II) nitrate-hexahydrate and 0.032 g of Ru (III) nitrosyl nitrate were used as the precursors.

5.3.2 Description of the batch set-up

A homemade SS-316 reactor (14.2 mL) equipped with a pressure indicator was used for the batch experiments (Figure 1). The maximum allowable pressure of the reactor is 300 bar. Typically, the reactor was loaded with 5 mL of an aqueous feed solution consisting of 10 wt % glycerol in water and catalyst (10 wt % on glycerol). The reactor was

closed and submerged in a temperature controlled fluidized sand bath (Figure 1).

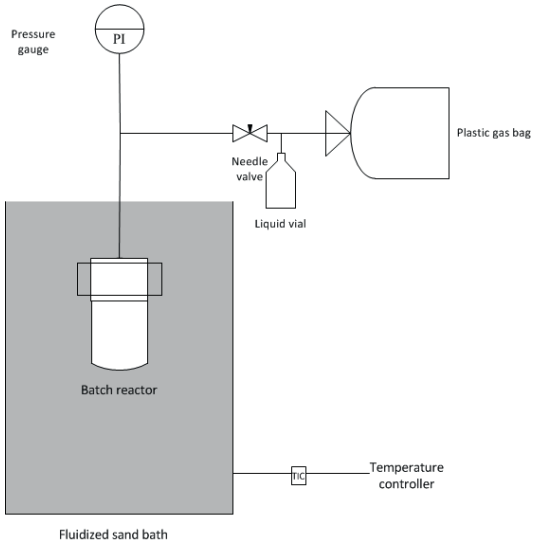

Figure 1. Schematic representation of the batch reactor set-up used in this study

The reaction time was set at zero when the reactor was placed in the sand bath. A typical reaction time is 20 min. After reaction, the reactor was taken out from the hot fluidized sand bath and rapidly cooled by placing it in another fluidized sand bath at room temperature for about 20 min. The final pressure after cooling the reactor to room temperature was recorded. The weight of the gas phase was determined by taken the difference of the weight of the reactor before and after gas release. Subsequently, the reactor was depressurized and the gas phase was collected in a gas bag (SKC Tedlar 1-2 L sample bag with a polypropylene septum fitting) for further analysis by GC.

5.3.3 Analysis

A. Gas phase analysis

The composition of the gas phase was determined by GC-TCD using a Hewlett Packard 5890 Series II GC equipped with an Porablot Q

Al_2O_3/Na_2SO_4 column and a molecular sieve (5 Å) column. The injector temperature was set at 150 °C, the detector temperature at 90 °C. The oven temperature was kept at 40 °C for 2 min then heated up to 90 °C at 20 °C/min and kept at this temperature for 2 min. The columns were flushed for 30 seconds with gas sample before starting a measurement. A reference gas from Westfalen AG with known composition (55.19 % H_2, 19.70 % CH_4, 3 % CO, 18.1 % CO_2, 0.51 % ethylene, 1.49 % ethane, 0.51 % propylene and 1.50 % propane) was used for quantification of the individual components.

B. Liquid phase analysis

The total organic carbon (TOC) content of the liquid phase was analyzed using a TOC analyzer (TOC-$V_{CSH,}$ Shimadzu). Before analysis, the sample was filtered to ensure the complete removal of solids. The samples were diluted with water to be in the measuring range of the apparatus.

5.3.4 Catalyst characterization

Transmission Electronic Microscopy (TEM) analyses were performed to determine the average metal nanoparticle size of the catalysts. Samples were dispersed in ethanol using ultrasound and deposited on a mica grid with a carbon coating. The samples were measured using a Philips CM12 at an acceleration voltage of 120 kV.

The actual metal composition of the Ru/TiO_2 catalyst (2 wt % of Ru) and the liquid phase composition after a representative catalytic experiment were determined using ICP (Inductively Coupled Plasma). Solid samples were digested in a mixture of HNO_3 (7 mL), HCL (1 mL) and HF (2 mL) at 200 °C for 2 h in a CEM Mars 5 microwave and then diluted to 50 mL with double-distilled water, while liquid samples were directly dissolved in a HNO_3 solution and then diluted. ICP analyses were carried on a Perkin Elmer Optima 7000 DV ICP-OES.

Thermo Gravimetric Analyses (TGA) were used to quantify coke formation after a representative catalytic experiment. The TGA test was done on a Perkin Elmer thermogravimetric analyzer TGA7 in an inert atmosphere (N_2). The samples (approximately 10 mg) were placed in the device and heated from 20 to 900 °C with a heating rate of 10 °C/min.

Nitrogen physisorption experiments were performed using a Micromeritics ASAP 2020 at –196.2 °C. Prior to analysis, samples (in the range of 0.15–0.20 g) were degassed at 200 °C for 10 h in vacuum conditions. Surface area was calculated using the BET (Brunauer-Emmett-Teller) method, and the micropore volume (V_m) was quantified using the t-plot method. Pore size distributions (PSD) and mean values were obtained from the desorption branch data. The BET surface area was determined by considering the amount of gas adsorbed at a relative pressure of 0.98 in the desorption branch. The adsorption branch of the isotherms were used to determine the pore size distributions (PSD). The PSD maximum was taken as the mean pore size.

The equilibrium gas phase compositions at different temperatures, pressures and glycerol intakes were determined according to a published procedure by our group,[30] with equilibrium correlations for the methanation reaction taken from the Catalyst Handbook.[34] Non ideality was introduced using the Redlich-Kwong-Soave equation.[35] Critical properties and acentric factors were taken from literature sources.[36]

The equilibrium composition of gas phase components in case of full glycerol conversion was calculated by using the software package Matlab. The results of these calculations are shown in the following Figures S1 and S2 (see Supporting Information).

The carbon-to-gas efficiency (CGE) is defined as the ratio of the total carbon (g) present in the product gas (Øc, gas) and the carbon in the feed (Øc, feed, eq. 2).

$$\mathrm{CGE} = \frac{\text{Øc,gas}}{\text{Øc,feed}} \cdot 100 \text{ wt \%} \qquad (2)$$

The carbon in the feed (Øc, feed) was calculated from the intake of glycerol. The carbon in the product gas (Øc, gas) was determined from the amount of gas formed and the gas phase composition. The carbon conversion (Ç) was calculated from the amount (g) of carbon in the feed (Øc, feed) and the amount of carbon (g) in the water phase after reaction as measured by TOC (Øc, effluent) (eq. 3).

$$Ç = \frac{\text{Øc,feed} - \text{Øc,effluent}}{\text{Øc,feed}} \cdot 100 \text{ wt \%} \qquad (3)$$

The difference between Ç and CGE is the amount of coke formed. In case the difference is zero, coke formation is negligible.

The methane yield is defined as the mols of methane formed divided by the mols of glycerol in the feed (eq 4). The amount of methane

formed during reaction was calculated from the amount of gas phase formed, as determined gravimetrically, and the composition of gas phase (GC).

$$CH_4\ yield = \frac{\text{amount of } CH_4 \text{ formed (mol)}}{\text{amount of glycerol feed (mol)}} \quad (4)$$

5.4 Results and discussion

5.4.1 Blank experiments

Reactions in the absence of a catalyst were performed with 10 wt % glycerol in water at 400 °C for 20 min batch times. Significant amounts of gas phase components were not formed for these reactions (CGE <1 wt %). However, considerable amounts of black solids were present after reaction, indicative for glycerol conversion to coke. As such, a catalyst seems required to gasify the glycerol at these conditions.

5.4.2 Catalyst screening using the monometallic catalysts

A total of 14 monometallic catalysts were tested with Ru or Ni as the active metal (2 wt %) on various supports (Al_2O_3, active carbon, carbon nanotubes, CeO_2, SiO_2, TiO_2 and ZrO_2). Experiments were performed in batch at 400 °C for 20 min with 10 wt % glycerol in water and 10 wt % catalyst on glycerol. The maximum pressure was between 180–285 bar, the exact value depending on the catalyst used. The catalysts were used in the oxidised form without a pre-reduction, thus assuming that reduction occurs *in situ*. The occurrence of an in-situ reduction to active Ru(0) species has recently been proven by using operando X-ray absorption spectroscopy. [37,38]

All experiments were performed at least in triplicate and showed good reproducibility with a standard deviation lower than 3 %. Typically, the gas phase after reaction consisted of CO, CO_2, CH_4 and some higher hydrocarbons, the exact amount being a function of the catalyst. Char formation was also depending on the type of catalyst and ranged from 2 wt % for the best and 27 wt % for the worst catalyst.

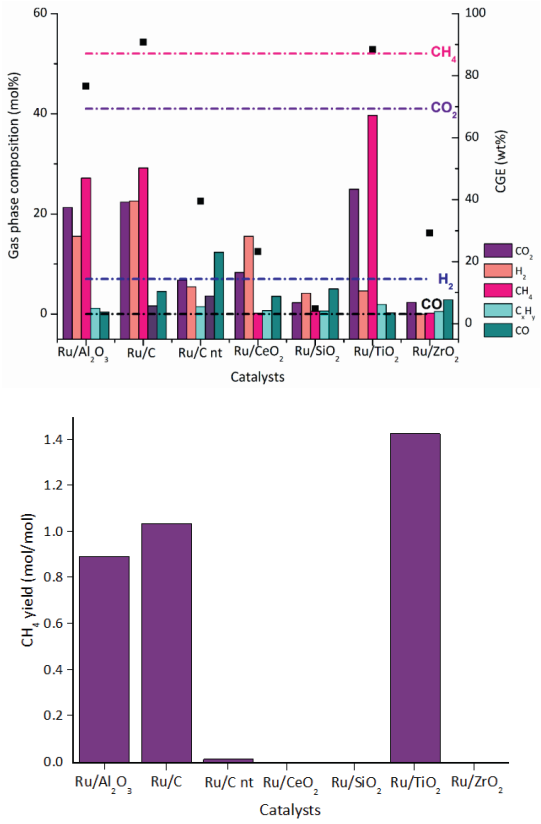

Figure 4. Results for glycerol gasification using monometallic Ru catalysts

Top: gas phase composition and CGE; Bottom: CH_4 yields as a function of catalyst type. Horizontal lines: calculated gas phase equilibrium compositions

A. Results for the monometallic Ru catalysts

The results for the catalyst screening experiments with the monometallic Ru catalysts are provided in Figure 4. Considerable differences in catalyst performance were observed, with CGE values between 5 and up to 90 %. Best results when considering CGE were obtained for the titania (88 %) and carbon support (91 %), the worst results were obtained using silica (5 %).

The most abundant gas phase component is CH_4, with amounts ranging from <1 to 40 mol %. Highest amounts of methane in the gas phase were found for Ru/TiO_2 (40 mol %), which is 12 % below the calculated equilibrium value at these conditions (52 mol %).

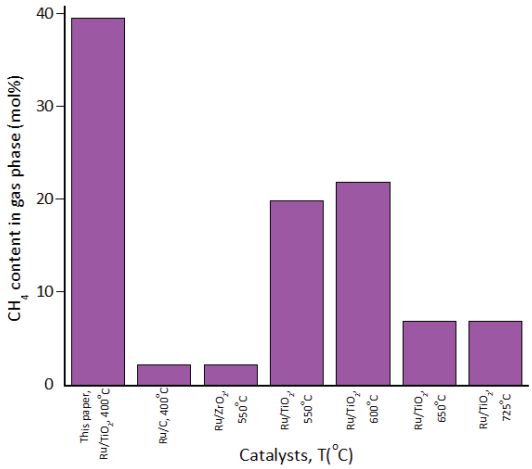

Figure 5. CH_4 contents in the gas phase for glycerol reforming in water using Ru based catalysts

Methane yields were between 1.43 mol/mol for Ru/TiO_2 and less than <0.001 mol/mol for Ru/SiO_2. Thus, we can conclude that support effects play a major role and that the best catalyst performance was obtained for Ru/TiO_2.

A comparison between the amount of methane in the gas phase (mol %) and data reported in the literature for various Ru catalysts and process conditions for glycerol reforming in supercritical water is given in Figure 5. It shows that the amount of methane in the gas phase is highest for the Ru/TiO_2 catalyst used in this study. These good results are likely due to the relatively low temperature in combination with a relatively long batch time.

B. *Results for the monometallic Ni catalysts*

Results for the experiments with the monometallic Ni catalysts are given in Figure 6. The catalysts are by far less active than the corresponding Ru complexes and the carbon-to-gas efficiencies (CGE) were all below 40 %. Best results regarding CGE were again found for the titania support (38 %), with up to 4 mol % of CH_4 in the gas phase, though this value is significantly lower than for Ru (88 %). In addition, a considerable change in the gas phase composition was observed when compared to Ru, with H_2 being favored in all cases. This change

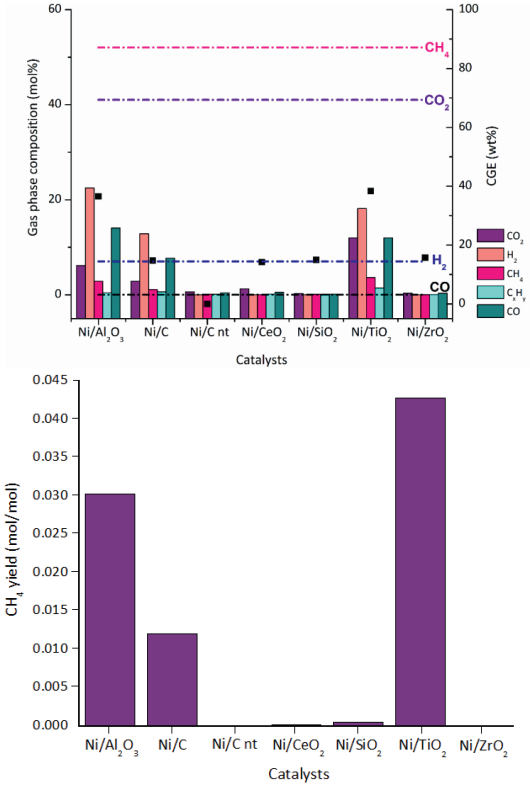

Figure 6. Results for glycerol gasification using monometallic Ni catalysts

Top: gas phase composition and CGE; Bottom: methane yields as a function of catalyst type. Horizontal lines: calculated gas phase equilibrium compositions

in selectivity is in line with literature data, showing that Ni catalysts are more efficient for hydrogen generation.[39]

5.4.3 *Catalyst screening using bimetallic Ni-Ru catalysts*

For comparison, a number of bimetallic Ni-Ru catalysts on different supports were prepared with 2 wt % Ni and 0.3 wt % Ru loading and tested for the gasification of glycerol (Figure 7). Compared to both the monometallic Ru and Ni catalysts (Figure 5 and 6), the CGE is in general higher and between 70 % and 90 %. As such, the bimetallic catalyst are more active for gasification than the monometallic ones. Best results were observed carbon and silica, whereas the performance

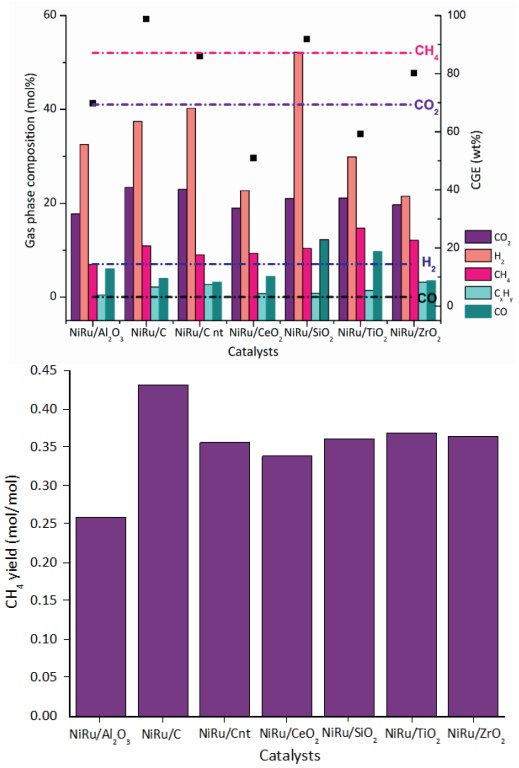

Figure 7. Results for glycerol gasification using bimetallic Ni-Ru catalysts

Top: gas phase composition and CGE; Bottom: methane yields as a function of catalyst type. Horizontal lines: calculated gas phase equilibrium compositions

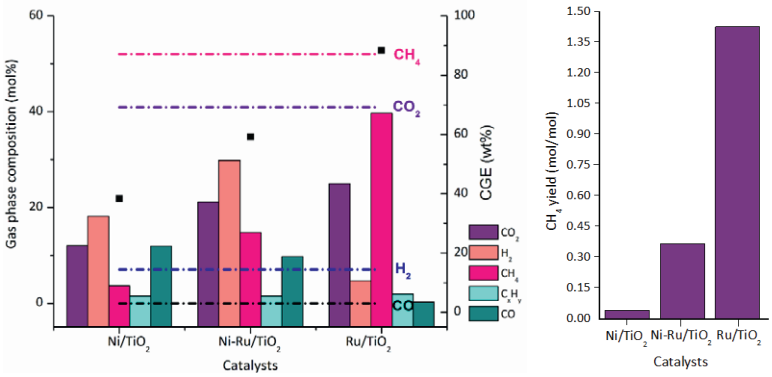

Figure 8. Comparison of the performance of the various catalysts on the TiO_2 support. Left: gas phase composition and CGE; Right: methane yields as a function of catalyst type. Horizontal lines: calculated gas phase equilibrium compositions

of the titania support was at the low end. Of interest is the gas phase composition for the bimetallic catalyst, which contains mainly hydrogen (23–52 mol %) and limited amounts of methane (<15 mol %). The amount of hydrogen is higher than predicted based on equilibrium considerations (7 %, Figure 6), indicative for kinetic control. It is well possible that primary liquid phase reactions occur to a significant extent with the formation of hydrogen (e.g. dehydrogenations) and that the rate of gas phase reactions (water gas shift, CO and CO_2 hydrogenation to methane) is low when using these bimetallic catalysts.

As such, we can conclude that bimetallic catalysts are very promising catalysts for the conversion of glycerol to hydrogen at relatively low temperatures with rates, as expressed by the CGE, which are by far higher than for the monometallic catalyst. Apparently, the presence of Ru in the catalyst increases the reaction rates considerably (even at the low amounts of 0.3 wt %), though methanation is suppressed and hydrogen is the main product gas.

5.4.4 Catalyst selection for dedicated experiments

The primary aim of this study was to obtain a product gas with a high amount of methane in combination with a high methane yield, which was realized when using Ru as the catalyst and TiO_2 as the support (see Figure 5). Titania was selected instead of active carbon, which also showed good performance, as catalyst regeneration by an oxidative treatments in case of catalyst deactivation (*vide infra*) is more facile for TiO_2 than for activated carbon. In addition, TiO_2 has shown good hydrothermal stability compared to other inorganic supports, which is also preferred when considering catalyst stability. [40]

A comparison between the performance of the Ru, Ni and Ni-Ru catalyst on the TiO_2 support is given in Figure 8, showing that the monometallic Ru catalyst is the best choice for methanation.

5.4.5 Optimization of catalyst intake and catalyst metal loading

To increase the CGE and the methane yield for the Ru/TiO_2, the preferred methanation catalyst in this study, the catalyst intake and the metal loading of the catalysts were varied. Experiments were carried out at 400 °C for 20 min batch times with 10 wt % of glycerol in water.

A. Effect of catalysts intake

The catalyst (2 wt % Ru) intake was varied between 10 wt %, 20 wt % and 30 wt % on glycerol and the results are given in Figure 9. The composition of the gas phase did not change dramatically, with methane being the main component. The main difference is the observation of a reduction of the amount of hydrogen at higher catalyst intakes. Remarkably, the carbon-to-gas efficiency was reduced considerably at higher catalyst intakes. So far, we do not have a sound explanation for these findings. As such, a catalyst intake of more than 10 wt % does not lead to improvements regarding methane yields.

B. Effect of metal loading of the catalyst

In all screening experiments, 2 wt % of Ru/TiO_2 was used. A number of catalysts was prepared with lower (0.3, 1 wt %) and higher metal loadings (5 wt %) and were tested for glycerol gasification. The catalyst intake for each experiment was constant (10 wt % on glycerol). The results are given in Figure 10. The CGE efficiency increased from 0.3 to 2 wt % and then leveled off. In addition, the amount of methane in the gas phase also increased steadily at higher catalyst intakes and reached a maximum value of 48 % for a catalyst with 5 wt % of Ru. As a result, the methane yields increase with metal loading and reach a value of 1.5 mol methane/mol glycerol for the highest catalyst loading. These findings indicate that higher leading lead to improved results. In addition, it implies that equilibrium gas phase compositions are not yet attained when using 2 wt % of Ru as in the catalyst screening study (*vide supra*) and that higher methane yields and amounts of methane in the gas phase are possible by increasing the metal loading of the catalyst.

5.4.6 Catalyst stability

The stability of the monometallic Ru/TiO_2 catalyst was investigated by performing a series of batch recycle experiments. For this purpose, a typical batch experiment was performed (10 wt % glycerol, 10 wt % Ru/TiO_2 (5 wt % Ru) on glycerol, 400 °C, 20 min batch time). The spent catalyst after an experiment was dried overnight in an oven (at 40 °C) and used without any further treatment for another experiment. The

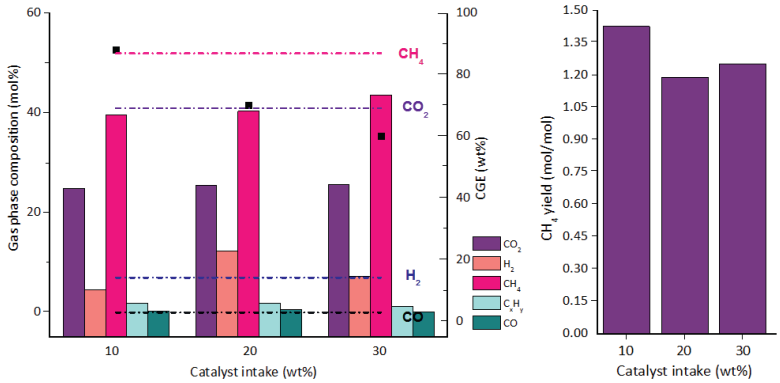

Figure 9 Effect of catalysts intake on glycerol gasification (10 wt % glycerol in water, 400 °C, 20 min batch time)

Left: gas phase composition and CGE; Right: methane yields as a function of catalyst type. Horizontal lines: calculated gas phase equilibrium compositions

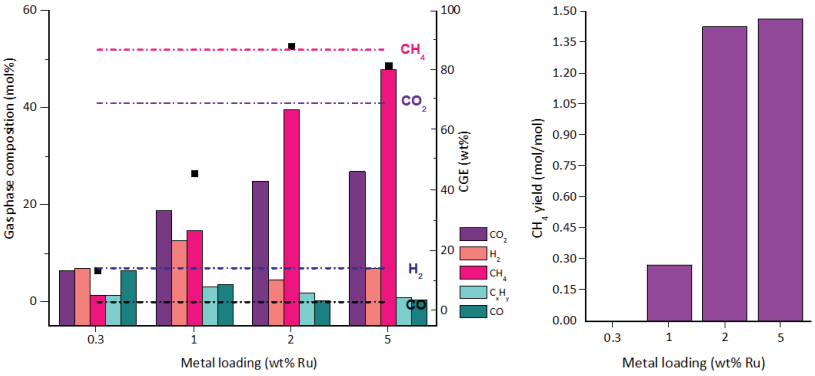

Figure 10. Effect of metal loading on glycerol gasification (10 wt % glycerol in water, 400 °C, 20 min batch time, 10 wt % of catalyst)

Left: gas phase composition and CGE; Right: methane yields as a function of catalyst type. Horizontal lines: calculated gas phase equilibrium compositions

results are given in Figure 11 and show that the catalyst is still active after 4 recycles. However, the CGE dropped slightly and less CH_4 in the gas phase was present, which is indicative for some catalyst deactivation. A possible reason for catalyst deactivation is coke formation on the catalyst, leading to reduced availability of active sites (*vide infra*). To test this hypothesis, the catalyst was calcined after the 4th cycle at 400 °C for 5 h in air before using it for another experiment. After

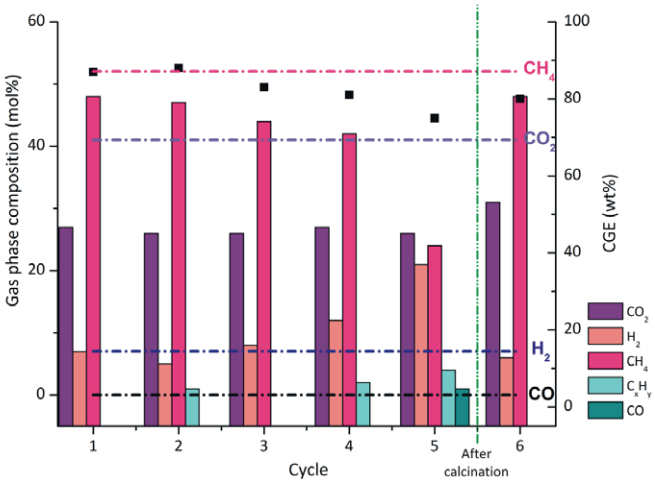

Figure 11. Recycling/regeneration tests using 10 wt % of Ru/TiO_2 (5 wt %) catalyst

this treatment, the activity was improved, eventhough it was lower than the value obtained for the first batch experiment (see Figure 11).

As such, we can conclude that some catalyst deactivation occurs but that an oxidative treatment is sufficient to regain at least part of the original activity. This suggests that coke formation is the main pathway for catalyst deactivation, which was supported by catalyst characterization studies for both the fresh and spent catalysts (*vide infra*).

5.4.7 Catalyst characterization

A. Characterization of the fresh TiO_2 based catalysts

For the Ru/TiO_2 (2 wt % Ru) catalyst, the actual Ru loading was determined by ICP analysis and shown to be 2.2 wt %. TEM measurements were carried out for the fresh TiO_2 based catalysts (Ni/TiO_2, $Ni\text{-}Ru/TiO_2$ and Ru/TiO_2, 2 wt % metal loading), see Figure 12 for details. The average metal nanoparticle size varies considerably for the samples. The Ni catalyst shows the largest particles (18.2 ± 1 nm), the Ru catalyst the smallest (5.9 ± 0.2 nm). As such, the low activity of the Ni catalyst (as expressed by the CGE and glycerol conversion) compared to the Ru one may be (partly) due to the larger average Ni nanoparticle size. The particle size of the bimetallic catalyst, Ni-Ru (12.2 ± 0.5 nm), is in between the particle size of Ni/TiO_2 and Ru/TiO_2.

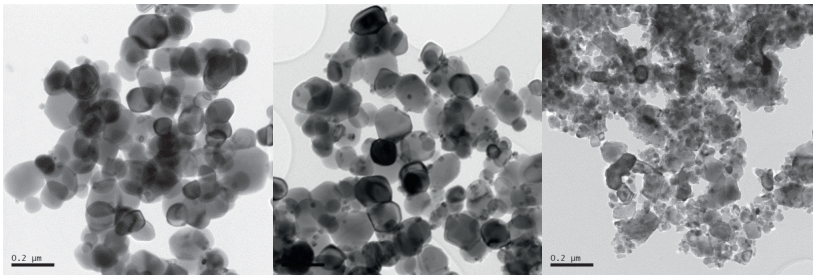

(a) (b) (c)

Figure 12. TEM images for (a) Ni/TiO_2 (18.2 ± 1 nm), (b) Ni-Ru/TiO_2 (12.2 ± 0.5 nm), and (c) Ru/TiO_2 (5.9 ± 0.2 nm)

Nitrogen physisorption experiments were performed for Ru/TiO_2, the best methanation catalyst in the series. The BET surface area was determined and found to be 30 m^2/g, which is higher than reported by Piskun *et al.* for similar anatase based TiO_2 catalysts (ca. 13 m^2/g).[41] However, the average TiO_2 particle size for the support used in this study is much smaller than for the support used by Piskun *et al.* (21 nm compared to 156 nm)[41] and this is a possible reason for the differences in values. The BET surface area for the Ru/TiO_2 catalyst used in this study is slightly lower than for P25 TiO_2 (40–60 m^2/g, a mixture of anatase and rutile).[42]

B. Characterization of spent Ru/TiO_2 catalyst

The spent Ru/TiO_2 catalyst after one batch experiment was characterized by TEM, TGA and nitrogen physisorption to gain insight in the possible catalyst deactivation pathways. TEM measurements (Figure 13) show that the average Ru nanoparticle size increased after reaction, from 5.9 ± 0.2 nm for the fresh to 7.4 ± 0.1 nm for the spent catalyst.

This is indicative for some Ru sintering which is expected to have a negative effect on catalyst activity and may be partly responsible for the experimentally observed slight drop in activity after recycling of the catalyst. TGA measurements on spent catalyst (Figure S3, Supporting Information) show a mass loss of about 2.6 wt % in the 150–400 °C range. This is indicative for the presence of some coke on the catalyst after reaction. The temperature range for weight loss implies that the coke can be classified as soft coke.[43]

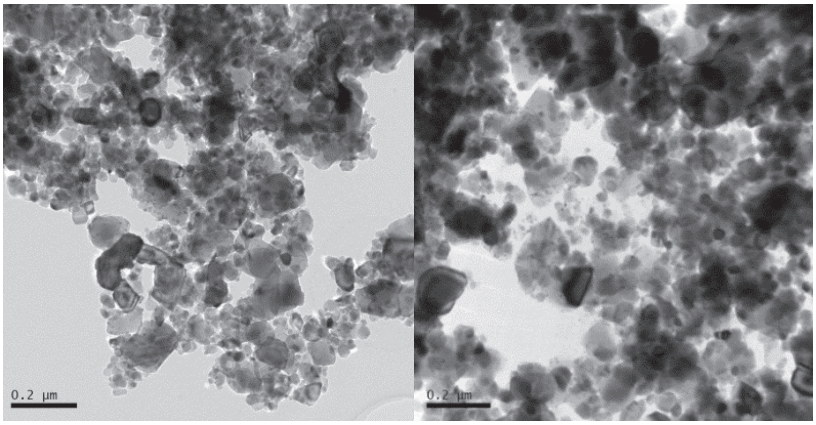

Figure 13. TEM images for Ru/TiO_2 (2 wt %)
Left: before reaction and right: after 1 batch reaction

The BET surface area of the spent catalyst after 1 batch experiment was also determined and shown to be reduced from 30 m^2/g to 19 m^2/g. This is likely due to coke formation (as seen in the TGA analysis).

To gain insights in metal leaching to the liquid phase during an experiment, the aqueous phase after reaction was also analyzed using ICP (Table 1).

Table 1 Compositional analyses (ICP) of the aqueous phase after a reaction with Ru/TiO_2

Element	Concentration (µg/L)
Ni	0.09
Cr	0.11
Mo	<0.01
Fe	1.42
Ru	0.03

The liquid phase contained mainly Fe, some Cr, Ni and Ru. The former three are due to some metal leaching from the reactor wall (SS-316, 12 % Ni, 17 % Cr, 2.5 % Mo, the remaining being Fe). The amount of Ru leaching from the catalyst was calculated from the catalyst intake and the ICP data and shown to be less than 0.02 %. Thus, we can conclude that Ru leaching is very limited for a batch experiment and not a major source for catalyst deactivation.

Thus, based on the catalyst characterization studies on fresh and spent Ru/TiO_2 supported by ICP analyses of the liquid phase after reaction, we can conclude that the main catalyst deactivation pathways are coke formation (TGA, nitrogen physisorption) and Ru nanoparticle sintering (TEM). Coke deposits may be removed by performing an oxidative treatment, though the experimentally observed lower activity of this regenerated catalyst compared to the original one likely due to some metal nanoparticle sintering.

5.5 Conclusions

We here reported a systematic catalyst screening study on glycerol gasification in supercritical water using supported monometallic Ru, Ni and bimetallic Ni-Ru catalysts. The best results when aiming for methanation were obtained with Ru/TiO_2, giving a methane yield of 1.43 mol/mol glycerol at 400 °C, 20 min batch time. The amount of methane in the gas phase was up to 40 mol %, which is close to the limit set by thermodynamics. The corresponding Ni catalysts were by far less active and mainly resulted in hydrogen formation. Surprisingly, the bimetallic catalysts showed high activity as expressed by the CGE and gave a hydrogen rich product gas. As such, these bimetallic catalysts have high potential to be used as catalysts for hydrogen formation from glycerol at relatively low temperatures. Catalyst stability for the Ru on TiO_2 catalyst was probed by performing catalyst recycle studies. Catalyst activity slightly dropped after 4 recycles. Catalyst characterization studies on fresh and spent Ru/TiO_2 supported by ICP analyses of the liquid phase after reaction, show that the main catalyst deactivation pathways are coke formation (TGA, nitrogen physisorption) and Ru nanoparticle sintering (TEM). Coke deposits may be removed by performing an oxidative treatment, though the experimentally observed lower activity of this regenerated catalyst compared to the original one is likely due to some metal nanoparticle sintering. Further experimental studies in a dedicated continuous set-up at prolonged runtimes will be required to assess catalyst stability is more detail.

Acknowledgements

This research was part of AGATE (Advanced Green Gas Technology) project from EDGAR research program (Energy Delta Gas Research).

The Northern Netherlands Provinces (SNN), European Union, European Fund for RegionalDevelopment, Ministry of Economic Affairs, and the Province of Groningen partly contributed the fund for the project. We would like to thank H. van der Velde for the ICP analysis, G.H. ten Brink for the TEM measurements, G.O.R. Alberda van Ekenstein for TGA analyses and E. Wilbers, M. de Vries, and A. Appeldoorn for technical support. Finally, we would like to thank the Indonesian Directorate General of Higher Education (DIKTI) for providing a scholarship to AJK.

References

[1] M. Pagliaro, R. Ciriminna, H. Kimura, M. Rossi, C. D. Pina, From glycerol to value-added products, Angewandte Chemie International 46 (2007) 4434–4440.

[2] Team of ENI (Ente Nazionale Idrocarburi), World oil & gas review 2012, https://www.eni.com/docs/en_IT/enicom/publicationsarchive/publications/wogr/2012/wogr-2012_completo.pdf, Accessed online at May 24th, 2017.

[3] T. Werpy and G. Petersen, Top value added chemicals from biomass Volume I: Results of screening for potential candidates from sugars and synthesis gas, U. S. Department of Energy (DOE) by the Pacific Northwest National Laboratory (PNNL) and National Renewable Energy Laboratory (NREL) a DOE National Laboratory, Oak Ridge, TN, 2004.

[4] P. Basu, Biomass gasification and pyrolysis practical design and theory, Elsevier, U. S., 2009.

[5] H. Balat and E. Kırtay, Hydrogen from biomass-Present scenario and future prospects, Int. J. Hydrogen Energy 35 (2010) 7416–7426.

[6] M. Naqvia, J. Yana, E. Dahlquistb, S. R. Naqvi, Waste biomass gasification based off-grid electricity generation: A case study in Pakistan, Energy Procedia 103 (2016) 406–412.

[7] L. Ott, M. Bicker and H. Vogel, Catalytic dehydration of glycerol in sub- and supercritical water: a new chemical process for acrolein production, Green Chem. 8 (2006) 214–220.

[8] V. Sricharoenchaikul, Assessment of black liquor gasification in supercritical water, Bioresource Technology 100 (2009) 638–643.

[9] G. V. Rossum, B. Potic, S. R. A. Kersten, W. P. M. Van Swaaij, Catalytic gasification of dry and wet biomass, Catalysis Today 145 (2009) 10–18.
[10] D. L. King, L. Zhang, G. Xia, A. M. Karim, D. J. Heldebrant, X. Wang, T. Peterson, Y. Wang, Aqueous phase reforming of glycerol for hydrogen production over Pt–Re supported on carbon, Applied Catalysis B: Environmental 99 (2010) 206–213.
[11] C. Cao, L. Guo, Y. Chen, S. Guo, Y. Lu, Hydrogen production from supercritical water gasification of alkaline wheat straw pulping black liquor in continuous flow system, International Journal of Hydrogen Energy 36 (2011) 13528–13535.
[12] W. Bühler, E. Dinjus, H. J. Ederer, A. Kruse, C. Mas, Ionic reactions and pyrolysis of glycerol as competing reaction pathways in near- and supercritical water, Journal of Supercritical Fluids 22 (2002) 37–53.
[13] Y. J. Lu, H. Jin, L. J. Guo, X. M. Zhang, C. Q. Cao, X. Guo, Hydrogen production by biomass gasification in supercritical water with a fluidized bed reactor, International Journal of Hydrogen Energy 33 (2008) 6066–6075.
[14] B. F. Tapah, R. C. D. Santos, G. A. Leeke, Processing of glycerol under sub and supercritical water conditions, Renewable Energy 62 (2014) 353–361.
[15] X. Xu, D. Yukihiko, M. Jonny, Carbon-catalyzed gasification of organic feedstocks in supercritical water, Industrial and Engineering Chemistry Research 35 (1996) 2522–2530.
[16] S. R. A. Kersten, B. Potic, W. Prins, W. P. M. Van Swaaij, Gasification of model compounds and wood in hot compressed water, Industrial and Engineering Chemistry Research 45 (2006) 4169–4177.
[17] E. Afif, P. Azadi, R. Farnood, Catalytic gasification of model compounds of activated sludge and their mixtures in supercritical water, Unpublished results.
[18] E. Supp, How to produce methanol from coal, Springer-Verlag, Berlin, 1990.
[19] M. Schubert, Catalytic hydrothermal gasification of biomass – salt recovery and continuous gasification of glycerol solutions, PhD Thesis, ETH, Zürich, 2010.
[20] A. May, J. Salvadó, C. Torras, D. Montané, Catalytic gasification of glycerol in supercritical water, Chemical Engineering Journal 160 (2010) 751–759.
[21] A. J. Byrd, K. K. Pant, R. B. Gupta, Hydrogen production from glycerol by reforming in supercritical water over Ru/Al_2O_3 catalyst, Fuel 87 (2008) 2956–2960.
[22] K. Lehnert and P. Claus, Influence of Pt particle size and support type on the aqueous-phase reforming of glycerol, Catalysis Communication 9 (2008) 2543–2546.

[23] G. D. Wen, Y. P. Xu, H. J. Ma, Z. S. Xu, Z. J. Tian, Production of hydrogen by aqueous-phase reforming of glycerol, International Journal Hydro Energy 33 (2008) 6657–6666.

[24] V. Nichele, M. Signoretto, F. Menegazzo, A. Gallo, V. Dal Santo, G. Cruciani, G. Cerrato, Glycerol steam reforming for hydrogen production: Design of Ni supported catalyst, Applied Catalysis B: Environmental 111–112 (2012) 225–232.

[25] I. Rosetti, A. Gallo, V. Dal Santo, C. L. Bianchi, V. Nichele, M. Signoretto, E. Finocchio, G. Ramis, A. Di Michele, Ni catalysts supported over TiO_2, SiO_2 and ZrO_2 for the steam reforming of glycerol, ChemCatChem 5 (2013) 294–306.

[26] J. G. van Bennekom, R. H. Venderbosch, D. Assink, K. P. J. Lemmens, H. J. Heeres, Bench scale demonstration of the supermethanol concept: The synthesis of methanol from glycerol derived syngas, Chemical Engineering Journal 207 (2012) 245–253.

[27] M. Akizuki and Y. Oshima, Kinetics of glycerol dehydration with WO_3/TiO_2 in supercritical water, Industrial and Engineering Chemistry Research 51 (2012) 12253–12257.

[28] E. Markocic, B. Kramberger, J. G. van Bennekom, H. J. Heeres, J. Vos, Z. Knze, Glycerol reforming in supercritical water: A short review, Renewable and Sustainable Energy Reviews 23 (2013) 40–48.

[29] A. Pei, L. Zhang, B. Jiang, L. Guo, X. Zhang, Y. Lv, H. Jin, Hydrogen production by biomass gasification in supercritical or subcritical water with Raney-Ni and other catalysts, Front. Energy Power Engineering China 3 (2009) 456–464.

[30] J. G. van Bennekom, V. A. Kirillov, Y. I. Amosov, T. Krieger, R. H. Venderbosch, D. Assink, K. P. J. Lemmens, H. J. Heeres, Explorative catalyst screening studies on reforming of glycerol in supercritical water, Journal of Supercritical Fluids 70 (2012) 171–181.

[31] A. Iriondo, V. L. Barrio, J. F. Cambra, P. L. Arias, M. B. Güemez, R. M. Navarro, Hydrogen production from glycerol over Ni catalysts supported on Al_2O_3 modified by Mg, Zr, Ce or La, Top Catalysis 49 (2008) 46–58.

[32] A. G. Chakinala, W. P. M. van Swaaij, S. R. A. Kersten, D. de Vlieger, K. Seshan, and D. W. F. (Wim) Brilman, Catalytic reforming of glycerol in supercritical water over bimetallic Pt–Ni catalyst, Ind. Eng. Chem. Res. 52 (2013) 5302–5312.

[33] I. Behnia, Z. Yuan, P. Charpentier and C. Xu, Supercritical water gasification of aqueous fraction of pyrolysis oil in the presence of a Ni-Ru catalyst, AIChE Journal 62 (2016) 2786–2793.

[34] M. V. Twigg, Catalyst handbook, 2nd ed., Wolfe Publishing Ltd., 1989.

[35] G. Soave, Equilibrium constants from a modified Redlich-Kwong equation of state, Chem. Eng. Sci. 27 (1972) 1197–1203.
[36] R. C. Reid, J. M. Prausnitz and B. E. Poling, The properties of gases and liquids, 4th ed., McGraw-Hill *Inc.,* New York, 1987.
[37] S. Rabe, M. Nachtegaal, T. Ulrich and Frédéric Vogel, Towards understanding the catalytic reforming of biomass in supercritical water, Angew. Chem. Int. Ed. 49 (2010) 6434–6437.
[38] M. Dreher, B. Johnson, A. A. Peterson, M. Nachtegaal, J. Wambach, F. Vogel, Catalysis in supercritical water: Pathway of the methanation reaction and sulfur poisoning over a Ru/C catalyst during the reforming of biomolecules, Journal of Catalysis 301 (2013) 38–45.
[39] M. Osada, O. Sato, M. Watanabe, K. Arai, M. Shirai, Water density effect on lignin gasification over supported noble metal catalysts in supercritical water, Energy & Fuels 20 (2006) 930–935.
[40] J. P. Lange, Renewable feedstocks: The problem of catalyst deactivation and its mitigation, Angew. Chem. Int. Ed. 54 (2015) 13186–13197.
[41] A. S. Piskun, J. G. M. Winkelman, Z. Tang, H. J. Heeres, Support screening studies on the hydrogenation of levulinic acid to γ-valerolactone in water using Ru catalysts, Catalysts 6 (2016) 131–151.
[42] J. Okal, Characterization and thermal stability of Ru nanoparticles supported on γ-alumina, Cat. Commun. 11 (2010) 508–512.
[43] J. Shi, J. Guan, D. Guo, J. Zhang, L. J. France, L. Wang and X. Li, Nitrogen chemistry and coke transformation of FCC coked catalyst during the regeneration process, Sci Rep. 6 (2016) 1–10.

Supporting Information

Table S1 Overview of studies on glycerol reforming in SCWG in batch mode

Catalyst	Glycerol (wt %)	Temp. (°C)	P (bar)	Reaction time (s)	Results (mol %)	Ref.
Heterogenous catalysts						
Ru/TiO_2-R	10	600		n.d.	Conversion: n.d. Gas composition: H_2:22; CH_4: 12	1
Ru/TiO_2	17–19	550–700	250	60	Conversion: 45–90%. Gas composition: H_2: 8–15; CO_2:8–16; CO: 30–65; CH_4:7–20	2
Raney Ni	3	380	n.d	900	Conversion: n.d. Gas composition: H_2:27; CH_4: 15; CO_2:13	3
C	18	600	345	44	Conversion: n.d. Gas composition: H_2:54; CO:2; CO_2:29; CH_4:13	4
Catalytical wall effects						
Inconel 625	5	600	300	60	Conversion: n.d. Gas composition: H_2:25–38; CO:34–40; CO_2:13–14; CH_4:10–11.	1

Table S2 Overview of studies on glycerol reforming in SCWG in continuous mode

Catalyst	Glycerol (wt %)	Temp. (°C)	P (bar)	Residence time (s)	Results (mol %)	Ref.
Heterogenous catalysts						
Ru/C	20	400	300	7–20	Conversion: n.d. Gas composition: H_2:0–2; CO: 0; CO_2:40–42 CH_4:56–58	5
Ru/ZrO_2	5	510–550	350	8.5	Conversion: 100%. Gas composition: H_2:4–55, CO: ≤21 ;CO_2: ≤40, CH_4: ≤2	6
Ru/γ-Al_2O_3	2.5–40	700–800	241	1–4	Conversion: 93–98 %. Gas composition: H_2:42–70 CO:0–4 CO_2:25–35 CH_4:4–20	7
Pt/Al_2O_3	10	250	20	3600–14400	Conversion: 45%; Gas composition: H_2: 85	8
Pt/Al_2O_3 Co/Al_2O_3 Cu/Al_2O_3 Ni/Al_2O_3	10	230	32	2400–14400	Conversion: n.d. Gas composition: H_2: 41–95; CO_2:6–24; CO: ≤0.05; CH_4: ≤16	9
Ni/TiO_2 Ni-SBA/15 Ni/ZrO_2	10	500–650	n.d.	18000–72000	Conversion: <10–72%. Gas composition: H_2: <5–65%	10
Ni/TiO_2 Ni/SiO_2 Ni/ZrO_2	n.d.	650		18000–72000	Conversion: 71–100%. Gas composition: CO:7–44; CO_2:53–94; CH_4: ≤3	11
Ni/CaO-6Al_2O_3	3–10	675–725	240–270	30–35	Conversion: 95–100%. Gas composition: H_2:44–67 CO:1–21, CO_2:16–34.	12
TiO_2, WO_3/TiO_2	0.46	400	330	n.d.	Conversion: >99% Gas composition: n.d. (focus on liquid products)	13
Coconut shell activated carbon	18.72	550–725	280	4752–19728	Conversion: n.d. Gas composition: H_2:38–51; CO:2–3, CO_2:31–35; CH_4:11–20.	14
Coconut shell activated carbon	18.4	600	345	n.d.	Conversion: n.d. Gas composition: H_2:3; CO: <1 CO_2:2; CH_4: <1	14
Catalytical wall effects						
Hastelloy C276	18.71	748–758	280	4212–10872	Conversion: 45–90%. Gas composition: H_2: 8–15; CO_2:8–16; CO: 30–65; CH_4:7–20	2

[a]n.d. = not determined or not reported

Equilibrium gas compositions

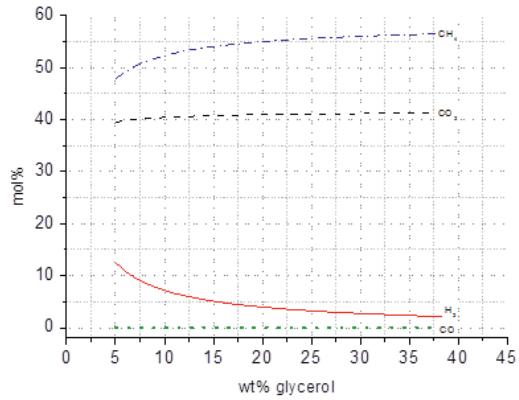

Figure S1 Thermodynamic equilibrium gas composition of the SCWG versus different feed concentrations at 400 °C and average pressure of 250 bar

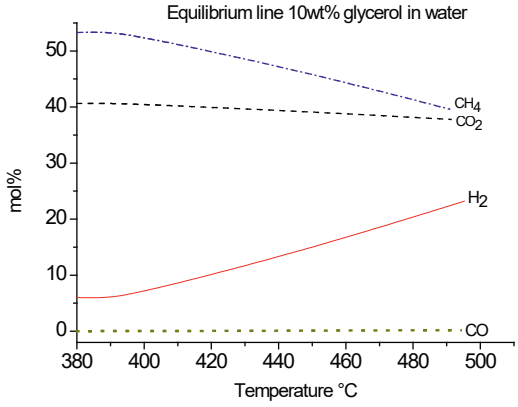

Figure S2 Equilibrium gas phase composition for the SCWG of glycerol versus the temperature (10 wt % of glycerol, pressure 250 bar)

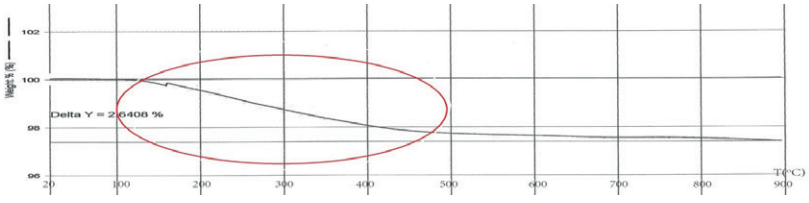

Figure S3 TGA image for spent Ru/TiO_2 (2 wt % Ru)

References

[1] G. V. Rossum, B. Potic, S. R. A. Kersten, W. P. M. Van Swaaij, Catalytic gasification of dry and wet biomass, Catalysis Today 145 (2009) 10–18.

[2] S. R. A. Kersten, B. Potic, W. Prins, W. P. M. Van Swaaij, Gasification of model compounds and wood in hot compressed water, Industrial and Engineering Chemistry Research, 45 (2006) 4169–4177.

[3] E. Afif, P. Azadi, R. Farnood, Catalytic gasification of model compounds of activated sludge and their mixtures in supercritical water, Unpublished results.

[4] E. Supp, How to produce methanol from coal, Springer-Verlag, Berlin (1990), ISBN 3-540-51923-8.

[5] M. Schubert, Catalytic hydrothermal gasification of biomass–salt recovery and continuous gasification of glycerol solutions, PhD Thesis, ETH, Zürich (2010).

[6] A. May, J. Salvadó, C. Torras, D. Montané, Catalytic gasification of glycerol in supercritical water, Chemical Engineering Journal 160 (2010) 751–759.

[7] A. J. Byrd, K. K. Pant, R. B. Gupta, Hydrogen production from glycerol by reforming in supercritical water over Ru/Al_2O_3 catalyst, Fuel 87 (2008) 2956–2960.

[8] K. Lehnert and P. Claus, Influence of Pt particle size and support type on the aqueous-phase reforming of glycerol, Catalysis Communication 9 (2008) 2543–2546.

[9] G. D. Wen, Y. P. Xu, H. J. Ma, Z. S. Xu, Z. J. Tian, Production of hydrogen by aqueous-phase reforming of glycerol, International Journal Hydro Energy 33 (2008) 6657–6666.

[10] V. Nichele, M. Signoretto, F. Menegazzo, A. Gallo, V. Dal Santo, G. Cruciani, G. Cerrato, Glycerol steam reforming for hydrogen production: Design of Ni supported catalyst, Catalysis B: Environmental 111–112 (2012) 225–232.

[11] I. Rosetti, A. Gallo, V. Dal Santo, C. L. Bianchi, V. Nichele, M. Signoretto, E. Finocchio, G. Ramis, A. Di Michele, Ni catalysts supported over TiO_2, SiO_2 and ZrO_2 for the steam reforming of glycerol, ChemCatChem 5 (2013) 294–306.

[12] J. G. van Bennekom, R. H. Venderbosch, D. Assink, K. P. J. Lemmens, H. J. Heeres, Bench scale demonstration of the supermethanol concept: The synthesis of methanol from glycerol derived syngas, Chemical Engineering Journal 207 (2012) 245–253.

[13] M. Akizuki and Y. Oshima, Kinetics of glycerol dehydration with WO_3/TiO_2 in supercritical water, Industrial and Engineering Chemistry Research 51 (2012) 12253–12257.

[14] X. Xu, D. Yukihiko, M. Jonny, Carbon-catalyzed gasification of organic feedstocks in supercritical water, Industrial and Engineering Chemistry Research 35 (1996) 2522–25.

Summary

The production of biofuels and biobased chemicals from lignocellulosic biomass is high on the international research agenda. A number of prospective molecules (platform chemicals) have been identified. Of high interest are biobased alcohols such as glycerol, and alcohol/aldehydes such as 5-hydroxymethylfurfural (HMF), which have shown to be very versatile precursors for a wide variety of derivatives. In this thesis, experimental studies are reported on two platform chemicals from biomass, HMF and glycerol, with the objective to convert them to interesting derivatives using catalytic methodology. In the case of 5-hydroxymethylfurfural (HMF), the emphasis will be on the synthesis of reduced components like 2,5-furandimethanol (FDM), 2,5-dimethylfuran (DMF) as well as on the formation of 1,2,4-benzenetriol (BTO). For the glycerol, the efficient conversion to green gas is aimed for. The overall objectives were to improve the product yields by selection and screening of suitable catalysts and to optimize process conditions. In addition, the conversions were preferably carried out using environmentally benign solvents like water and ethanol.

In **Chapter 2**, experimental studies are reported on the conversion of HMF to two important building blocks, *viz.* 2,5-furandimethanol (FDM) and 2,5-dimethylfuran (DMF). Noble-metal-free-catalysts and novel copper doped porous metal oxides (PMOs) with a very low ruthenium loading were prepared, characterized and tested in a batch reactor set-up. Process conditions like temperature (80–220 °C), and reaction time (1–18 h) and type of solvent (methanol, ethanol, isopropanol, and methyl isobutyl carbinol (MIBC)) were explored to maximize HMF conversion and FDM or DMF yield. A reaction network is proposed based on identification of intermediate products, such as 2,5-dimethyl-tetrahydrofuran (DMTHF), 2,5-tetrahydrofuran dimethanol (THFDM), 5-methyl-2-furanmethanol (MFM), 5-methylfurfural (MF), 5-methyl-2-tetrahydrofuranmethanol (THMFM), 1,2-hexanediol (1,2-HD), 1,2,6-hexanetriol (1,2,6-HT) and 2-(ethoxymethyl)-5-methylfuran (EMMF). Catalyst recycling experiments were performed to determine the stability of the catalysts. It was shown that catalyst activity is slowly reduced after multiple recycles. Catalyst activity was regained after a recalcination step. Further investigations on catalyst stability were performed in a flow set-up, and these confirmed the batch recycle experiments.

In **Chapter 3,** experimental studies on the hydro(deoxy)genation of HMF to DMF using a number of commercial copper-containing nanopowders with different elemental compositions are described. The

catalysts were characterized by elemental analysis and XRD and these revealed that the CuZn nanoalloys contain predominantly β-CuZn and Cu0 phases. Ethanol was used as the solvent and the reactions were carried out at a temperature of 220 °C using 30 bar H_2 pressure for 6 h. A catalyst screening study showed that CuZn was the best catalyst, with 95 % yield of FDM at >99 % conversion. This catalyst was used for further optimization studies by investigating a range of process conditions such as H_2 pressure and the type of solvent (isopropanol, MIBC, 2-methyltetrahydrofuran and cyclopentyl-methyl-ether (CPME)). Recycling experiments for DMF synthesis showed that catalyst stability is good. Transmission electron microscopy (TEM) measurements gave more insight into morphological changes of this intriguing class of materials during catalysis. The one-pot conversion of fructose to valuable furan-ethers was also explored.

When using the CuZn catalyst in combination with Amberlyst 15, full fructose conversion was obtained and 7 % of FDM was formed.

In **Chapter 4,** experimental studies on the synthesis of 1,2,4-benzenetriol (BTO), a 'forgotten' biobased aromatic chemical, from HMF using Lewis and Brønsted acid catalysts in a batch set-up with water as the solvent are reported. Screening studies using a range of Lewis acid catalysts (300 °C, >120 bar, 1.2 mM catalyst) were performed. In particular, catalysts with a high pKh and low Brønsted acidity such as $ZnCl_2$, $Zn(OTf)_2$, $Fe(OTf)_2$ and $MgCl_2$ appeared suitable catalysts, showing a significant BTO yield improvement compared to the uncatalysed reaction (15 mol % BTO). Best results were obtained using $ZnCl_2$ giving a BTO yield of 54 % at 89 % HMF conversion. When Brønsted acid catalysts are used, HMF is converted into humins, levulinic acid and formic acid instead of BTO. BTO was shown to be slowly converted into a 5,5' C-C bonded homodimer (2,2',4,4',5,5'-hexahydroxybiphenyl) at ambient conditions in air. The molecular structure was confirmed by X-ray diffraction. Catalytic hydrodeoxygenation of BTO towards cyclohexanone in water was achieved in yields up to 45 % using 5 wt % Pd on Al_2O_3 combined with $AlCl_3$ or $Al(OTf)_3$ as catalysts. This demonstrated catalytic hydrodeoxygenation of BTO to cyclohexanone comprises a new route towards biobased nylons.

A catalyst screening study on the methanation of glycerol in supercritical water is reported in **Chapter 5**. A number of mono-and bimetallic Ru and Ni catalysts were prepared on various supports such as TiO_2, SiO_2, ZrO_2, CeO_2, Al_2O_3, C and C nanotubes. The reactions were carried out in a batch reactor set-up using 10 wt % of glycerol in water, pressures between 200 and 300 bar at 400 °C for 20 minutes.

Selectivity to gas phase components proved to be a strong function of the catalyst used, with the Ru catalysts giving mainly methane whereas the Ni catalysts mainly produced hydrogen. Intermediate performance was observed for the bimetallic Ru-Ni catalysts. The best results when aiming for methane were obtained using the monometallic Ru/TiO_2 catalyst (2 wt %), which gave a methane yield of 1.43 mol/mol glycerol at essential quantitative glycerol conversion. The gas phase in this case consisted of 40 mol % of methane, which is 4 % below the calculated equilibrium value. Stability of this catalyst was investigated by performing several recycle experiments, showing a significant reduction in catalytic activity after 5 runs. Regeneration of the catalyst proved possible by an oxidative treatment. Catalyst characterization studies on fresh and spent catalyst revealed that coke formation on the catalyst is the major source for deactivation, in line with the recycle/regeneration studies.

Samenvatting

De productie van biobrandstoffen en biobased chemicaliën uit lignocellulose biomassa staat hoog op de internationale onderzoeksagenda. Er zijn een aantal potentiële moleculen (platformchemicaliën) geïdentificeerd. Van groot belang zijn biobased alcoholen zoals glycerol en gecombineerde alcohol/ aldehyden zoals 5-hydroxymethylfurfural (HMF), die zeer veelzijdige start materialen voor een grote verscheidenheid aan derivaten zijn. In dit proefschrift worden experimentele studies gerapporteerd over twee platformchemicaliën uit biomassa, te weten HMF en glycerol, met als doel ze om te zetten in interessante derivaten met behulp van katalytische methodologie. In het geval van 5-hydroxymethylfurfural (HMF) de nadruk op de synthese van gereduceerde componenten zoals 2,5-furandimethanol (FDM), 2,5-dimethylfuran (DMF) en op de vorming van 1,2,4-benzeentriol (BTO). Voor glycerol is gekeken naar de efficiënte omzetting naar groen gas. De algemene doelstellingen waren het verbeteren van de productopbrengsten door selectie en screening van geschikte katalysatoren en om de procesomstandigheden te optimaliseren. Daarnaast werden de omzettingen bij voorkeur uitgevoerd in milieuvriendelijke oplosmiddelen zoals water en ethanol.

In hoofdstuk 2 worden experimentele studies beschreven naar de omzetting van HMF to twee belangrijke bouwstenen, namelijk. 2,5-furandimethanol (FDM) en 2,5-dimethylfuran (DMF). Edelmetaalvrije metaal katalysatoren en nieuwe koper gebaseerde poreuze metaaloxiden (PMO's) met een zeer lage rutheniumbelading werden bereid, gekarakteriseerd en getest in een batch reactoropstelling. Procesomstandigheden zoals temperatuur (80–220 °C) en reactietijd (1–18 uur) en type oplosmiddel (methanol, ethanol, isopropanol en methylisobutylcarbinol (MIBC) werden onderzocht om de HMF omzetting en de FDM of DMF opbrengsten te maximaliseren. Daarnaast is een reactie netwerk op gesteld op basis van identificatie van intermediaire producten, zoals 2,5-dimethyl tetrahydrofuran (DMTHF), 2,5-tetrahydrofuran dimethanol (THFDM), 5-methyl-2-furan methanol (MFM), 5-methylfurfural MF), 5-methyl-2-tetrahydrofuranmethanol (THMFM), 1,2-hexaandiol (1,2-HD), 1,2,6-hexaantriol (1,2,6-HT) en 2-(ethoxymethyl) 5-methylfuran (EMMF). Katalysator recycling experimenten werden uitgevoerd om de stabiliteit van de katalysatoren te bepalen. Er werd aangetoond dat de katalysator activiteit langzaam verminderd na een aantal recylces. De katalysator kon worden gereactiveerd met een calcinerings stap. Verdere onderzoek naar

katalysator stabiliteit werd uitgevoerd in een continue opstelling, en deze bevestigden de batch recycle experimenten.

In hoofdstuk 3 worden experimentele studies naar de hydro-(deoxy)genering van HMF naar DMF met behulp van een aantal commerciële koperhoudende nanopoedermiddelen met verschillende elementaire samenstellingen beschreven. De katalysatoren werden gekarakteriseerd met element analyse en XRD en tonen aan dat de CuZn nanoalloy overwegend β-CuZn en Cu0 fases bevat. Ethanol werd gebruikt als het oplosmiddel en de reacties werden uitgevoerd bij een temperatuur van 220 °C onder gebruikmaking van 30 bar H_2 druk gedurende 6 uur. Een katalysator screenings studie toonde aan dat CuZn de beste katalysator is , met 95 % opbrengst aan FDM bij >99 % HMF conversie. Deze katalysator werd gebruikt voor verdere optimalisatie studies waarbij procesomstandigheden zoals H_2 druk en het type oplosmiddel (isopropanol, MIBC, 2-methyltetrahydrofuran en cyclopentylmethylether (CPME) bestuurd zijn. Recycling experimenten voor DMF synthese toonden aan dat de katalysator stabiliteit goed is. Transmissie elektronenmicroscopie (TEM) metingen leverden meer inzicht in morfologische veranderingen tijdens de katalyse. De één-pot conversie van fructose naar waardevolle furanethers werd ook onderzocht. Bij gebruik van de CuZn-katalysator in combinatie bij Amberlyst 15 werd een volledige fructose conversie verkregen en 7 % FDM gevormd.

In hoofdstuk 4 wordt een experimentele studie beschreven naar de synthese van 1,2,4 benzeentriol (BTO), een 'vergeten' biobased aromatische verbinding, uit HMF met Lewis- en Brønsted-zur, katalysatoren in een batch opstelling met water als oplosmiddel. Screening studies met een reeks Lewis-zure katalysatoren (300 °C, >120 bar, 1,2 mM katalysator) werden uitgevoerd. In het bijzonder bleken katalysatoren met een hoge pKh en lage Brønsted-zuurgraad zoals $ZnCl_2$, $Zn(OTf)_2$, $MgCl_2$ geschikte katalysatoren, die een significante BTO opbrengst verbetering vertonen in vergelijking met de niet-gekatalyseerde reactie (15 mol % BTO). De beste resultaten werden verkregen met behulp van $ZnCl_2$ met een BTO-opbrengst van 54 % bij 89 % HMF omzetting. Waneer Brønsted-zure katalysatoren worden gebruikt, wordt HMF omgezet in humines, levulinezuur en mierenzuur in plaats van BTO. BTO wordt langzaam omgezet in een 5,5 'C-C gebonden homodimeer (2,2', 4,4 ', 5,5'-hexahydroxybifenyl) bij kamer temperatuur in lucht. De moleculaire structuur werd bevestigd met röntgendiffractie. De katalytische hydrodeoxygenering van BTO met 5 gew. % Pd op Al_2O_3 gecombineerd met $AlCl_3$ of $Al(OTf)_3$ in water gaf cyclohexanon

in opbrengsten tot 45 %. Cyclohexanon is met bestaande technologie om te zetten in caprolactam, een bouwsteen voor nylon kunststoffen. Deze route dus een mogelijke interesant groen alternatief voor bio-based nylons.

In **hoofdstuk 5** wordt een katalysator screenings studie beschreven naar de methanering van glycerol in superkritisch water. Een aantal mono- en bimetallischee, Ru en Ni katalysatoren op verschillende dragers zoals TiO_2, SiO_2, ZrO_2, CeO_2, Al_2O_3, C en C nanotubes zijn gesynthetiseerd en gekarakteriseerd. Met deze katalyzatoren zijn reacties uitgevoerd in een batch reactor opstelling met 10 gew. % glycerol in water, drukken tussen 200 en 300 bar, 400 °C gedurende 20 minuten. Selectiviteit voor gasfase componenten bleek een sterke functie te zijn van de gebruikte katalysator, waarbij de Ru katalysatoren voornamelijk methaan en de Ni katalysatoren voornamelijk waterstof gaven. Intermediaire gas samenstellingen werden waargenomen voor de bimetallische Ru-Ni katalysatoren. De beste resultaten voor methaan werden gevonden met de monometallische Ru/TiO_2 katalysator (2 gew. %), met een methaanopbrengst van 1.43 mol/mol glycerol bij volledige glycerol conversie. De gasfase in dit geval bestond uit 40 mol % methaan, wat 4 % lager is dan de berekende evenwichtswaarde. Stabiliteit van deze katalysator werd onderzocht door het uitvoeren van recycle-experimenten. Er werd een significante vermindering van de katalytische activiteit waargenomen na 5 recycles. Regeneratie van de katalysator bleek mogelijk door middel van een oxidatieve behandeling bij verhoogde temperatuur. Katalysator karakterisering studies laten zien dat coke vorming op de katalysator de belangrijkste bron voor deactivering is, in lijn met de recycle/regeneratie studies.

Acknowledgements

14 years ago, in the second year of my Bachelor degree program, I was dispirited. I realized that Chemical Engineering was far from my childhood dream to become a (medical) doctor. The same experience happened again during the last year of my Master degree program. Surprisingly, exactly the same feeling came again during the first 2 years of my PhD period, since my dream to go to Europe was to be a musician. But, I believe that everything that happens is not a coincidence, eventhough may start by mistake. It happens for a reason, so I need to be responsible to finish it with a victory. Without abundant love and support from people surrounding me, I could not have finalized my PhD thesis. I would like to sincerely express my deepest gratitude to them.

My most gratitude belongs to my promotor, **Prof. H. J. Heeres**, who patiently guided me and made this 5 years become fruitful. I learnt a lot from our discussions. Thanks for believing in me, even when I did not believe in myself. Erik, thank you for inspiring me a lot. Your words, even the little world changed me in many ways. Even in your busy schedule, you always tried to find time to help me whenever I faced difficulties. Thanks for always asking: *"How's life?"* and always saying: *"Nothing is too difficult, there will be a solution for everything"*. My (co-) promotors, Prof. Katalin Barta and Dr. Peter J. Deuss, I feel so blessed that I could work with you. **Katalin**, if not because of you, I would not have any confidence in my work. Thanks for our collaboration and our long discussions which delivered my first two publications. **Peter**, thank you for helping me with the BTO project. You are the one who understood my struggles and tears: my long days and nights in the laboratory, bunch of 'unfinished' and technical problems, my fights with the HPLC and with other users of the HPLC. Your support, patience and kindness to guide and help me brought very nice results and made me feel relieved and gave me the faith that I could leave Groningen and finish my PhD thesis soon.

My PhD thesis would not have been materialized without financial support from the Indonesian Directorate General of Higher Education (**DIKTI**) (thanks to Mba Anis and Mba Erlin for your patience and kind help), the **EDGAR** research program (Energy Delta Gas Research), The Northern Netherlands Provinces (SNN), European Union, European Fund for Regional Development, Ministry of Economic Affairs, and the Province of Groningen.

To the reading committee, **Prof. A. A. Broekhuis**, **Prof. F. Picchioni** and **Prof. K. Seshan**, thank you for your willingness to read, give input and asses my thesis. I do hope that you enjoyed reading it.

Leon Jansen, Inge, **Joost**, **Paolo** and **Jun**, thanks a lot for your comments and inputs, especially during lunch meeting. **Leon**, thanks for your promise to give me a great & unforgettable PhD defense! **Inge**, I enjoyed our light talk about nice spots around Europe. **Patrizio**, thanks for our lost time together in the canoe during a *labuitje.* 2 Indonesian women + 1 Italian man = lost!!

I could not have done any experiments without abundant help and advice from **Anne**, **Erwin**, **Marcel**, **Jan Henk** and **Leon**. Sorry for disturbing you all the time, even for a small problem. **Tim Zwaagstra**, **Alphons Navest**, **Annette Korringa** and Marya, thank you for helping and organizing the financial and administration things I need. **Marya**, thank you for our '*10 minuten*' time to help me to improve my Dutch. *Eindelijk*, I found someone someone who also hates summer and sun! Thank you guys for arranging the great *'lab uitje'* and *'kerst lunch'* every year. **Maarten** (thanks for always providing me nice quartz cappilaries and other glass materials), **H. van der Velde** (thanks for the ICP analysis), **Gert H. ten Brink** (thanks for the TEM analysis), **Alberda** (thanks for the TGA analysis).

Prof. **Ben** Feringa, **Luc** Rabou (ECN), Giovanni and Valentine, thank you for our nice collaboration. I enjoyed our discussions. **Gio**, muchas gracias for everything! Thanks for your patience and your clear explanation whenever I ask for something. I owe you a lot! Thanks for the great 'Italian lunch together' with Peter, Marzia and Allesia. **Valentine**, we did a lot of silly things together during our collaboration. Thank you for the nano catalyst, please don't break again *'that metal thing'*! Gracias!

My dear paranymphs, Sanne and Idoia, thank you for our friendship. We met only for a short time, but I believe that it will be *'amigos para siempre, friends for life not just a summer or spring'*. **Sanne**, we met for the first time during the EDGAR annual meeting in Nunspeet. We started with small talk since we realized that we both came from Groningen, and later we realized that we were in the same AGATE project. We planned to have a collaboration, although at the end, we did not have enough time to finalize it. The project ended, but our friendship grew stronger. Thanks for your sincere support during my difficult time, you really tried to help me with some real solutions. Thank you for taking care of me whenever I got a surgery or I was sick. I did enjoy our quality time together, with the cute seals. **Idoiiiaaaa**,

gracias! Thanks for being my officemate. We only met during my last year in Groningen, when I was in the 'critical and desperate time' to finish my PhD. Thank you for being there, right in front of my desk. We shared a lot (from chemicals, knowledge, private stories and gossips, until drinks and foods!!). Thanks for accommodating me in your cozy apartment during my 'half-illegal' time in Groningen.

Zheng 'jie-jie', Martijn, Erik and Tim, thanks for being my great officemates. **Zheng 'jie-jie'**, thank you for being my 'jie-jie' (*sister) and sharing everything (especially gossip and food!). **Martijn**, **Erik**, **Tim** and **Douwe** sorry for being 'invisible' and 'very quiet' in our office, but I did enjoy our office time together.

My beloved students, Marte, Lais and Anzhelika. Thank you for your hardwork and our discussion time. **Marte**, thank you for being my first student. **Lais**, sorry that I could not even say goodbye when you went back to Brazil. **Anzhelika**, I enjoyed our time together, especially when you stayed in my home. We enjoyed our foods while watching Korean dramas together. **Caelan**, thanks for the dimer and oligomer for our BTO project.

I also acknowledge my ex lecturer, **Ko Verdi**, for he challenged me to stay in chemical engineering when I almost gave up during my bachelor. *Nuhun pisan, Koko dosen wali!*

Member of Chemical Engineering department: **Ci Jenny**, you are the one who introduced me to Erik, thank you for that. Thank you for choosing me to be your bridesmaid. **Louis**, thank you to accompany me during my first visit to Groningen (also for the visa application process) and for teaching me a lot of things during my first stay in Groningen (church, Babylon, Pathe, etc.). **Arjan**, you are the first person Erik introduced me to, thanks for guiding and teaching me a lot during my first year. **Andrew Phua** and **Joost van Bennekom**, thanks for sharing your knowledge and experience about SCWG to me. **Henk**, thank you for helping me a lot, both with technical and analysis problems. **Mba Agnes**, **Erna**, **Ria**, **Iqbal & Eryth**, **Mas Ilmi**, **Dian**, **Sasa**, **Keisia** and **Caecilia**, thank you for our togetherness, our 'chit chat time' (and food!). **Iqbal**, thank you for supplying me bunch of chips. **Yusuf + kak Ili** and Susan, thank you for letting me play with **Abang**, **Zulaikha** and Anika whenever I felt bored or stressed. Yusuf, thank you for helping me with the proof reading of this thesis. **Susan & Mas Bino & Anika**, *nuhun pisan nya!* Thank you for the bunch of *'tombo kangen'* food you prepared. **Pak Henky**, *hatur bedankt*, Beh! Thank you for always being there for me and guiding me, since my bachelor until the end of my PhD time, from academic and life problems. You

came back to Groningen in the very right time, you helped me a lot to overcome my '*kegalauan*'. Thank you for always welcoming me in your home, together with **Ci Dita**, **Clairine** and **Ailey. Pak CB**, thanks for your idea and input. I always enjoy our discussion, especially the one in Bali. **Mba Frita**, thank you for letting me always stay in your office, while I was waiting for the reaction, or while I was just simply bored. I already miss play monopoli with **Muti**. **Mas Boy**, thank you for choosing me as your paranymph! **Bu Ima***, semangaaaatttt, tot ziens in* Unpar! **Anna Piskun**, I will not forget our 'food poisoning' experience while following an external course together with Henk. Thank you for your catalyst and for sharing about the catalyst synthesis with me. People from the high pressure lab: **Inouk** (thank you for sharing the thermocouple and sand bath), **Yin** and **Wang** (thanks for helping me to open my reactor, didi and gege!), **Shilpa** (thank you for your recommendation for using image-j), **Laurens** (thanks for helping me with the samenvatting), **Lidia**, **Ignacio** (thanks for letting me used the BET machine), **Bilal**, **Ionela** (thanks for your advice about Rumania!), **Ibbie**, **Monique (**thanks for arranging my farewell dinner!), **Alessandra** and **Feng**, thanks for our time together in the 'most noisy' lab. **Arne**, **Maria Jesus**, **Ko Teddy** & Ci **Yenni** Urip (thanks for the discussion about HMF hydrogenation, Ko Teddy!), **Yifei** & **wife**, thanks for always smiling and call me! **Lihe**, **Zhenchen** (thanks for the TEM analysis & the chicken Szechuan), **Qingqing** (thanks for helping me with the HPLC calibration curve while I was already back in Indonesia), **Kevin**, **Luigi** (sorry for the sand bath fighting), **Patrick**, **Ricardo**, **Juan**, **Jan Willem**, **Valeriya**, **Arjen**, **Albert**, **Rajeesh**, **Ramesh**, **Bhawan**, **Lorena**, **Raymond**, **Frank**, **Giovanni**, **Pablo**, **Esteban**, **Diego**, **Rodrigo**, **Cyntia**, **Albert**, **Nicole**, **Jurjen** and **Minke**. To some of them, my deepest apologize for fighting a lot for the HPLC. **Bernoulli board**, thank you for choosing me to be your photographer. I am glad that our picture was positioned at a good position. That was one of my great last memories in the department! **Hary**, thanks for cleaning my room and my desk with a lot of chat.

Trio kwak-kwik-kwek, Han Han and Widi. Thank you for our togetherness, during good and bad times, especially food! We shared a lot, especially our worries in our 'last year' and in our future, eventhough at the end the trio changed to become a duo. **Han Han**, you inspired me a lot: your spirit, enthusiasm and sincerity. I learnt a lot from you. I enjoyed (and will always enjoy) your music. Thanks for always helping me whenever I needed a hand. Thanks for accompanying me during my first surgery in Amsterdam. It such a strange coincidence

that we were neighbours for years in Bandung without knowing each other and only got into contact with each other in Groningen. I will always be your fan, Han! **Widi**, thanks for our 'curhat time', 'choir time', newest Indonesian songs references, travelling together and for choosing me to be your paranymph. I learned a lot about persistency from you, guys! Thanks for always enjoy the foods & drinks which I made without any complaints! You know so well that I released my stress through that way.

Ko Christian, thanks for being there for me during my first two years, eventhough we were apart thousand miles. Thanks a lot for your time in the middle of your busy time. Thanks for sharing a lot of dreams with me.

Doctors in AMC and UMCG, *bedankt voor uw hulp*. Thank you for our consultation time and always encourage me that everything will be okay. **Nurses** in the AMC, thank you for taking care of me patiently during the surgery. **Sahieda**, thanks for always hold my hand during the surgery.

KVS 98, Putri and **Doti**, thanks for being great housemates for my first 2 years. Your little notes whenever I faced a problem made me even cry more. I will miss our *'tjurtjol'* time until morning. Teteh **Putri**, thank you for insisting to accompany me to Amsterdam for my surgery, thank you for bringing me bandages and food when I got an infection after the surgery. I did enjoy our time in Luxembourg. Keep being creative, Teteh *arteis*! **Amirah**, thanks for our deep conversations about life! **Mba Inung**, I enjoyed our KFC time (with chit chat) and travelling time together, Mba!

Kenzieeee, thanks for inspiring me and sharing a lot about travelling! Hopefully we get other chances to travel together and to multiply our jinx to become lucky, like the upgrading to a 'business class'Emirates tickets!

GBI Groningen's member: **Mba Ika** & **Paul**, thank you for welcoming and accommodating me during my first week in Groningen. **Tante Tini** & **Om Fred**, **Tante Hanna**, thanks for being my parents while I was in Groningen, taking care of me and preparing me bunch of delicious food. **Kak Roga** and **oCha**, thank you for our crazy time and a lot of overnight time we spent together in the laboratory, Zernike and UMCG. Ocha, thanks for always being with me in every circumstances, *saranghae*!! **Tante** 'schaatje' **Ray**, **Opa Henry**, **Janiz** family: Tante Sri, Liza+Edwin+Ryu+Lintang. **Stella** (thank you for accommodating me during my 'half illegal' time in Groningen), **Mba Elva+Bert+Keizia**, **Mba Meita+Om Max+Andrew**, **Mba Ria**, **Mba Hennie**, **ci Fia**, **Mas**

Win, **Inang Sahat**, **John**, **Laura**, **Claudya**, **Leidya**, **Ko Jeffry** praise & worship team & all the officers of the GBI Groningen church and all members of the GBI Groningen. Pastors in GBI Europe: **Pdt. Ivan** & **Pdt. Wakano**, your sermons always encourage me!

Tante Indah & **Om Yon**, **Mba Ari** & **Om Herman**, **Om Rudi** & **Tante Sylvi**, thanks for taking care about me a lot. Thanks for treating me as your daughter.

My 'musical' friends: **Ko Dody**, **Satriya**, **Deasy**, **Dea**, **Felix**, thanks for making me jealous and made me re-think again about my PhD for several times! Indeed, everyone has their own calling. As time goes by, spending time with you and attending your concerts made me able to accept the fact that I will not be like you. To be part of the audience is enough.

Sint Jozef Church: David van Laar, Mas Ronny, Rieza & **Geby**, Ita and Kuba, Retha, **Mba Elsa** and **Bang Lucas**, **Vino**, **Mba Erna+Mas Buyung+Tana+Naris**, **Anita** thanks for our togetherness in mass. **David**, thanks for being my orgel teacher for a while, sorry that I was a lazy student. **Mas Ronny**, thanks for being a great brother for me. I will definitely miss our *'curhat time'*. You are one of the kindest persons I ever met. **Rieza**, thanks for introducing me to Bragi and the Saturday's choir. **Ita**, **Kuba**, and **Marcia** plus **Tante 'Ungu'** and **Oma** thanks for sharing time, together also with **Fani**, **Bartex**, and **Bibik** also **Zofia**'s family in Aarhus and Lodz. **Retha**: 'Kamsiah, *Maaaaak*!', we became very close just in the moment when I was about to leave Groningen. Thanks for helping me pack and clean my bunch of stuffs.

Dutch student choir, **Bragi**, thanks for letting me get a great experience, especially in the event 4∞ RUG. I could sing in front of the King of the Netherlands, it was such an enchanted experience. **Kak Yoke** and **Fos**, bedankt for teaching me Dutch nicely.

Indonesian friends in NL: **Ci Poppy** & fam, **Ci Connie** & fam, **Ci Fesia** & fam, **Ci Yuli**-**Ko Wisnu** & fam, **Mba Agne**s, **Agnes** & **Ko Canggih** (plus cute **Lionel** & **Darian**), **Ko Steve** & **Ci Nike**, **Angel** & fam, **Ci Iyang** & koko 'bule' **Edwin** (plus si ganteng **Marvin & Cici**), **Wilda**, **Jilly**, having you made me realize that I was not alone in the Netherlands.

Mba Astri & **Arqi** (looking at you inspired and taught me a lot of things about life), **Pak Asmoro & Bu Rini+Mas Adi+Iva+Riffat**, **Desti** & **Iging+Danish**, **Aulia** & **Ysbrand**, **Cyndy**, **Yvan**, **Mba Tiur**, **Yosi** & **Ali+Fatih**, **Ali** & **Liana+Cici**, **Ida**, **Ucon**, **Mas Fean**, **Renren**, **Guntur**, **Niar**, **Auliya** & **Neily+ Almira**, **Mba Laksmi** & **Bli Kadek** (plus **Vina** and **Dita**), **Mas Yayok & Mba Lia+Keyzia+Katya Rully+Intan+Kinan**, Kakak **Linggar**, **Ema+Yani+Eta+SS'ers**, we played, laughed, and ate

together a lot! I feel blessed that I meet you. Members of PPI Groningen, Patrimonium Patri (**Theo**, **Yaya**, **Kanya**, **Andro**, **Meme**, **Tesa**, **Glenn**, **Marry**, **Gita**, **Tyo**, **Nia**, **Yordan**, **Jennifer**, **Vanessa**), the PPIG choir (esp. **Radhit** and *kakak+adik angsa*), thanks for welcoming and letting me involved in a lot of events! I learnt a lot from you guys! Thanks for letting me become an artist. LoL. My stay in Groningen became very colorful. Indonesian - Planetenlaan flat's friend: Mba Ira, Mba Nur, **Koh Tjie**, **Adjie**, **Mas Adhyat**, **Mas Urry**, **Mas Tri**, thanks for our meeting time in the '*RT Planetenlaan*'. **Mba Ira** and **Mba Nur** thanks for sharing food (& some ingredients) with me. All my Indonesian friends in Groningen which I cannot mention one by one, thank you for everything! '*Terima kasih banyak dan semoga tali silaturahmi kita bisa tetap berlanjut di Indonesia*'.

Vania Widyaya, thanks for sharing all about travelling with me. You have been my best travel mate so far! Angels whom I met during 'harsh' and full of drama travelling: **Daniela**, **Siwon**, **Yoan**, **Floriana**, **Veselina**, **Nathalie** and **Johan**, **Rob**, **Ingrid**, **김윤지**, **Hyang Seong Kim**, **Mas Dicky**, **Akif**, **Agustine**, **William**, **Jure Čulić**, **Damian**, **Cohlene**, **Tunia**, **Zofia**, **Sabrina**, **Sara**, **Ksenya** and **Chinedu**. That is what I like about being a solo traveler!

Victor, we reunite again in the NL after our high school. I enjoyed our 'hunting time' together. I hope that we can hunt more pictures together, I hope in NY!

Shierli, because of your brother's recital, I got to know you. We became close and shared a lot of things. **Fiona**, we didn't have much time to get along while I was your *'responser'*, but when I was in the Netherland, by coincidence, we became close. Shierli & Fiona, your existence blessed me! To be honest, our chat time, & waiting for your messages was one of my favourite things during my PhD time!

Anna & **Fahad**, **Abi**, **Sophie**, **Tante Rosita** & **Om Paul**, thanks for your hospitality when I was attending the conference in Melbourne. Thanks for inviting & sponsoring me to come to Auckland. I feel so blessed to have Anna as my very first best friend (and will always!).

Rector, **vice rectors**, **ex rector**, **ex vice rectors** of the Parahyangan Catholic University, **Pak Kapto** (vice rector), **Pak Thedy** (dean), **Bu Jo** (ex. vice dean) and **Bu Santi** (head of department), thank you for your support and trust in me, so I could finish my PhD. **Bu Judy**, thanks for being my mother and guiding me, my gratitude also for **Pak Witono**, **Oma** and **Dina** for treating me as a family member and accommodating me during my first two months in Bandung. Thanks for coming all the way to Tangerang for accompanying

me and praying for my mom when my mom passed away. **Ci Susi**, **Ko Ade** & **Mikei**), thanks for cheering me up and encouraging me, please help me to find 'papi Tezu'. **Hans** and Linda, thanks for sharing everything, please do not be *'petjah kongsi'*. **Linda**, we first met as opponent during the chemistry Olympiad, but later we became best friends, thank you for accompanying me for my defense, all the way to Groningen. **Pak Harto**, **Pak Asaf**, **Pak Tony** & **Ci Maria**, thanks for helping me find a house), **Pak Tedi** & **Ci Jenna** (I admire you a lot, Pak! Every single word from your lecture and our discussion always important and enlightening), **Pak Yos** (thanks for a lot of fruitful and deep conversation, Pak!), **Bu Arry** (thanks for always providing us *emping* & other *tjemilan*), **Pak Herry**, **Pak Budi**, ***Pak Arenst*** (I hope that I could still do a lot of travelling combined with conferences, just like you) **Bu Maria**, **Pak Andy** & **Nia**, **Ci Arlene**, **Pandega**, 'sedulur' **Yansen**, **Nana**, **Kevin**, **Putri** (thanks for our time, Put!, eventhough we just got to known each other, but surprisingly we became close in no time. Thanks for letting me borrow your PC and install origin to finish my thesis). All of **my students** (research proposal, internship, plant design and 2016ers) & **ex students**, being your lecturer successfully refreshed my 'superheated' condition.

Gcom church's member (& ex member): **Ko Cahyo** & **ci Ola**, thank you for your discipleship, thank you for supporting me when I doubted going for PhD. **Ci Ben** & **Ko Ben**, (**Nathan** &**Federick)**, thank youuuu fooor everything. For me, you are like a real brother and sister. Ci Ben, thanks for sharing your '*racun*' with me. **Ci Moo**, we laughed, we cried, we fought together a lot! But, I changed a lot because of you. Thanks for your patience and kindness. Ex. **Efata** & **Nard** LG & DG (Fen2, **Dhytha**, **Like**). **Fen2**, from student to best friends, thanks for that! **Vania 'dede'** thanks for supplying me bunch of *'ratjuns'* and picked me from the airport whenever I came back to Indonesia, **Ci Luci** & **ko Yohan** thanks for taking care of *'suamiku'*, **Ecil**, **Della** & **Eko**, **Cella**, **Bona** & **Friska**, **Felix** & **Ninot**, thank you guys for not forgetting me while I was away! Hope our friendship will last forever.

Pastor Tedjo, thank you for welcoming me back to the '*right path*'. Indeed, there is no place like home. Thank you for making me feel 'at home' and believing in me. I will not turn back. To be your 'student'is such a blessing for me. Because of music, I got the courage and spirit to finish my PhD thesis. I found myself back through it. Thank you for introducing me to the Sacrum Canticum choir and offering me to join the Taize-Nias. Thanks for always pray for me & my deceased parents. **Tante Dede**, you are the first person I knew in SC and we got along

well in no time. Keep being *maceuh*, Tan! (**goyang-goyang*). Pastor Tedjo & Tante Dede, thanks for always caring & sharing a lot of things with me. All members of the **SC choir**, thank you for letting me join the choir as your organist! Our music made me alive and supported me to finish my thesis.

Last but not least, I want to acknowledge the most important person in my PhD life. "***Papi**, see? I fulfilled your dream to study in the Netherlands, I also fulfilled your dreams to travel around Europe and did some pilgrimages*". **Mami**, thanks for waiting for me until your last breath. You waited for me until I 'finished' my PhD & went back to Indonesia. Papi & Mami, I believe that my achievements will make you smile in heaven. *Ela kangen Papi & Mami.* **Oh Toni** & **Engso Maria**, **Ci Anne** & **Cihu William**, **Patricia**, **Vania**, **Nathan**, **Farrel**, **Ben**, thanks for taking care of Mami while I was in the Netherlands. Thanks for supporting me and understanding my decision to go for PhD in the Netherlands. Poei's big family: **Ik Oen** & **Om Ho**, **Ik Giok** & **Om Enghong**, **Ku Khoen** & **Engkim Ing**, **Om Sugeng** & **Ik Lan** (+), **Ik Lian** & **Om Tjeng Gie**, thanks for being my parents after Papi & Mami passed away, thanks for supporting me during my PhD & taking care of my family. **Cik Joan**, **Ko Aau**, **Nicole** & **Ethan**, thank you for being my best cousin ever! Eventhough we have just met, but I felt lots of love from you! **Ci Melda** & **Engkim**, thanks for visiting my mom frequently while I was away. All of my **cousins** (from **Poei's** and **Khoe's** big family), thank youuu so much cuzzo for your love!

Praise to the Lord, to whom belong glory and power, forever and ever!
Dr. Angela Justina Kumalaputri

List of Publications

1. A. J. Kumalaputri, G. Bottari, P. M. Erne, H. J. Heeres and K. Barta, Tunable and Selective Conversion of 5-HMF to 2,5-Furandimethanol and 2,5-Dimethylfuran over Copper-Doped Porous Metal Oxides, ChemSusChem 7 (2014) 2266 – 2275.
2. G. Bottari, A. J. Kumalaputri, K. K. Krawczyk, B. L. Feringa, H. J. Heeres and K. Barta, Copper-zinc alloy nanopowder: A robust precious-metal-free catalyst for the conversion of 5-hydroxymethylfurfural, ChemSusChem 2015, 8, 1323 – 1327
3. A. J. Kumalaputri, H. J. Heeres, Green gas by gasification of wet biomass in supercritical water, Asian Pacific Confederation of Chemical Engineering (APCChE) Conference, Melbourne, Australia, 2015 (Oral presentation).
4. A. J. Kumalaputri, V. Hornillos, L. Carnaúba, K. Krawczyk, A. Kloekhorst, B. L. Feringa, H. J. Heeres, Green gas reforming by wet biomass supercritical water, 2nd International Conference on Renewable Energy Gas Technology (REGATEC), Barcelona, Spain, 2015 (Poster presentation).
5. A. J. Kumalaputri, V. Hornillos, L. Carnaúba, K. Krawczyk, A. Kloekhorst, B. L. Feringa, H. J. Heeres, Green gas reforming by wet biomass supercritical water, Energy Delta Gas Research (EDGAR) Closing Project Conference, Amsterdam, The Netherlands, 2015 (Poster presentation).
6. A. J. Kumalaputri, G. Bottari, K. Barta, H. J. Heeres, From biomass to biobased products: Catalytic hydrogenation studies on the 5-hydroxymethylfurfural platform using supported Cu catalysts, NPS 14 (Netherlands Process Technology Symposium), Utrecht, The Netherlands, 2014 (Oral presentation)